Development of a Time Projection Chamber for a linear collider experiment; Optimization of the readout electronics

Ted Lind

Supervisor: Anders Oskarsson

Master of Science Thesis

Department of Physics
Division of Particle Physics

Table of contents

Abstract

The field of particle physics is ever evolving. With the recent advent of the Large Hadron Collider (LHC) it is possible that the long sought for Higgs boson is detected. While this is not certain even if it is found it is likely that it will need more precise methods of investigation. For this and other reasons, a new collider called the International Linear Collider (ILC) is being planned. This collider will be used to collide leptons which will enable more precise measurements compared to a hadron collider. In order to benefit from this, improvements to the current detectors, such as the Time Projection Chamber (TPC), are also needed.

The TPC is placed inside a solenoid shaped magnet with a field strength usually ranging up to a few Teslas. In the bore of the magnet the TPC contains a mixture and an electric field applied between a central cathode and the anode at the signal readout plane. When a particle enters the gas mixture it ionizes the gas thus releasing electrons which will drift towards the anode where they will undergo an avalanche process in a high E-field region. The signal is then read out by small pads. The TPC is a 3D particle detector capable of momentum measurements, energy loss measurements and particle identification.

This thesis is based on the improvement of the current TPCs. Both a novel amplification technique, called Gas Electron Multiplier (GEM) as well as new amplifier chip PCA16 is tested. The ALTRO chip is an Analog to Digital converter with, among other characteristics, a resolution of 10 bits and a sampling frequency of 20 MHz.

The measurements dealt with in this thesis were done at DESY in 2009 and 2010. Unfortunately they both suffer from distortions caused by an inhomogeneous electric field. The 2009 data appear to be a little less affected and that is why the analysis is focused on that data.

The results seem to indicate that the GEMs are likely to enable good enough momentum and energy loss measurements of a future TPC. The results also point towards the fact that a 6 bit ADC should be sufficient while still retaining a good enough resolution in a future TPC. The sampling frequency however should not be set lower than 20 MHz.

1. Introduction

Ever since the dawn of man one has been looking for ways to explain and understand the surroundings. Why is the sky blue? Does Earth orbit the Sun? What is everything made up of? This thesis will focus on how we nowadays try to find the answers to the latter of those questions.

The ancient Greeks believed that everything consisted of four elements; earth, water, air and fire but they also conceived the idea of something being so small that it could not be further divided. Such an indivisible object was called atomos in ancient Greek and that is from where the word atom is derived. When the particles that we now call the atoms were discovered in the 19^{th} century, it was believed that these particles were indivisible, hence the name.

For over one hundred years we have known this to be false. While the existence of the electron had been known for some time it was Rutherford who discovered the nucleus of an atom in his famous experiment where he studied the deflection angles of alpha particles that penetrated a gold foil. Further experiments proved that the nucleus itself was made up of two different types of particles, the positively charged proton and the uncharged neutron. Since the discovery of the proton and neutron not only have other particles been discovered, two fundamental forces, the weak and the strong force, have also been described and studied in detail. Before the 20^{th} century only the electromagnetic force and the force of gravity were known. Currently four fundamental forces are sufficient to describe the world around us. The electromagnetic force and the force of gravity have an infinite range, whereas the weak and the strong force have sub atomic ranges.

2 The building blocks of matter according to the Standard Model

The discovery of the proton and the neutron was thus not the end of particle physics and the subsequent search for even smaller particles, it was merely the beginning. At the time of the discovery most scientists considered the proton and the neutron to be the smallest conceivable particles, however, further studies once again baffled scientists. As more fundamental particles were found and theoretical models were refined these particles and models combined to form the Standard Model (SM). Although not perfect, this model accurately describes the vast majority of particles and interactions occurring on a subatomic level.

2.1 The Quarks

As it turned out the protons and the neutrons are made up out of a family of particles called quarks. The quarks making up the proton and neutron are the up and down quark, with two up quarks and one down quark making up the proton and one up quark and two down quarks making up the neutron. Any particles consisting of quarks are called hadrons. Particles consisting of three quarks are called baryons and have non integer spin and thus obey Fermi-Dirac statistics; particles with this behavior are aptly named Fermions. Particles containing only a quark and an anti-quark are called mesons and have integer spin which makes them obey Bose-Einstein statistics and are called Bosons. Scientists have proposed the existence of both tetra-quarks, a pair of meson, and penta-quarkstates, a meson and a baryon. However, the existence of these exotic particles has not been confirmed. Further studies have revealed that there exists a second and third generation of quarks and also that every quark has a corresponding anti-quark with opposite charge. The properties of the quarks are shown in **Table 1**.

	Spin	**Electric Charge** (e)	**Baryon number**	**Isospin**	**Charm**	**Strangeness**	**Topness**	**Bottomness**	**Mass***
Generation 1									
Up quark	*1/2*	*2/3*	*1/3*	*1/2*	*0*	*0*	*0*	*0*	*2.4 MeV*
Down quark	*1/2*	*-1/3*	*1/3*	*-1/2*	*0*	*0*	*0*	*0*	*4.8 MeV*
Generation II									
Charm quark	*1/2*	*2/3*	*1/3*	*0*	*1*	*0*	*0*	*0*	*1.27 GeV*
Strange quark	*1/2*	*-1/3*	*1/3*	*0*	*0*	*-1*	*0*	*0*	*104 MeV*
Generation III									
Top quark	*1/2*	*2/3*	*1/3*	*0*	*0*	*0*	*1*	*0*	*171.2 GeV*
Bottom quark	*1/2*	*-1/3*	*1/3*	*0*	*0*	*0*	*0*	*-1*	*4.2 GeV*

Table 1: General properties of the known quarks.
***The masses of the quarks are only estimations, they have as of yet never been detected freely.**

Since the quarks have half integer spin they behave according to Fermi-Dirac statistics and obey the Pauli exclusion principle. All quarks interact via the electric, weak and strong force. These forces are described by the Standard model (SM).

Another distinct and rather peculiar characteristic of quarks is the fact that they carry color charge. It should be noted that despite the fact that the property is called color charge it has nothing to do with what we in everyday life call colors. The fact that the quarks contain color charge is what enables interaction trough the strong force.

2.2 The Leptons

According to SM there exists a second family of fundamental particles with half integer spin. Unlike the quarks these particles, called Leptons, have integer electric charge and no color charge. Since they do not have color charge they do not interact via the strong force. In the case of Leptons with non zero electric charge they interact via the electric force. The properties of the Leptons are given below in **Table 2:**

Generation I	**Spin**	**Electric Charge** (e)	**Mass**
Electron	*1/2*	*-1*	*0.511 MeV*
Electron neutrino	*1/2*	*0*	*
Generation II			
Muon	*1/2*	*-1*	*105.7 MeV*
Muon neutrino	*1/2*	*0*	*
Generation III			
Tau	*1/2*	*-1*	*1.777 MeV*
Tau neutrino	*1/2*	*0*	*

Table 2: The general properties of the known Leptons. It is believed that the neutrinos carry mass but the masses are as of yet unknown but they do have an upper limit.

2.3 The Gauge Bosons

According to the SM the forces are mediated by their corresponding gauge bosons. Since gauge bosons are described by quantum field theory one has not yet been able to incorporate the force of gravity into the SM. It is still possible to understand high energy physics experiments without an exact knowledge of the force of gravity. This is possible since the force of gravity is many orders of magnitudes weaker than any of the other fundamental forces, so it can simply be neglected.

According to the SM there exists only one more particle to be detected and that is the Higgs boson. The properties of the known bosons are given in **Table 3**.

Mediator	**Force**	**Relative strength**	**Spin**	**Charge** (e)
Photon	*Electromagnetic*	*1/137*	*1*	*0*
Gluon	*Strong*	*1*	*1*	*0*
Z^0	*Weak*	10^{-6}	*1*	*0*
W^-, W^+	*Weak*	10^{-6}	*1*	*-1,+1*

Table 3: The known force mediators and their properties of the forces described by the SM.

It is the Higgs mechanism that gives the interacting vector bosons their mass. While the photon and the gluons are vector bosons they do not interact with the Higgs field and are thus massless. The range of the forces are generally said to be determined by the Heisenberg uncertainty principle. This is because the mediated forces interact with the particles by creating a virtual force mediating particle that alters the state of the real particles. Since energy must be conserved it comes naturally that such virtual particle must not be allowed to exist longer than Heisenberg uncertainty principle permits.

$$\Delta t \sim \frac{h}{2\pi \cdot \Delta E} \qquad (1)$$

Since the photon is massless, the electromagnetic force has an infinite range according to the Heisenberg uncertainty principle.

The weak force is the only fundamental interaction that can change the flavor of a quark. It is also the only boson that does not follow parity conservation. What this means is that the bosons that mediate the weak force do not behave like the other vector bosons when undergoing mirror reflection. The spatial distribution does not look the same as if one were to study the boson in a mirror. This type of symmetry violation is called Parity violation or P violation for short. The weak force mediating bosons also exhibit a charge violation. Reversing the magnetic and electric fields as well as the replacing a W^+ with a W^- would not result in the same behavior for the system. This type of symmetry violation is called C violation. It has also been shown that violation of both symmetries is possible, so called CP violation. CP violation is the most plausible explanation as to why the Universe is filled with matter and not just as sea of radiation. However, CP violation of only the weak force mediating bosons do not explain the abundance of all matter in the universe, merely a tiny fraction of it. Thus future studies are needed. It is also these spontaneous symmetry violations that give the weak force bosons their mass. It's the reason why they can couple to the Higgs field. The mass of the W^+, W^- and Z^0 bosons are 80.4, 80.4 and 91.2 GeV respectively which then corresponds to a range of $\sim 10^{-18}$ m.

The massless gluons do not have an infinite range, the strong force is in fact the force with the next shortest range. The reason for this behavior is because of the fact that gluons carry color charge. Each gluon carries a color and anti-color charge. This causes gluons to couple to other gluons, preventing its field from spreading radially outwards. This instead causes the gluon to create a so called color string between the quarks. This string is what gives the strong force its characteristic behavior. The strong force acts almost like a rubber band between the quarks. When they are close to each other the tension

between them is very small and they can move quite freely. However, if one quark is moved further away from the other, then the tension in the string increases forcing the quark back in place. Just like a rubber band can break so can a color string. If there is enough energy deposited into the string it will become energetically favorable to break the string. This does not lead to the formation of a free quark but instead it creates a quark anti-quark pair. Such a process is called hadronization.

2.4 Discrepancies in the Standard Model

While the SM is truly one of the best theories to date it is not without shortcomings. The most obvious would be that gravity is not incorporated. It is also believed that all the fundamental forces share a common origin, at high enough energies they would behave identically. Currently a theory uniting the electromagnetic and weak force have been proposed and it was experimentally confirmed in 1983 [1]. This unified force is called the electroweak force. A plausible next step is to formulate a theory which unifies the electroweak and strong force, such a theory is called a Grand Unified Theory (GUT) and a theory uniting all the four fundamental forces is called a Theory of Everything and would be able to not only describe everything around us but also predict the outcome of every event.

Another problem with the SM is neutrino oscillations. The SM predicts that all the neutrinos should have zero mass. However, experiments have shown that neutrinos can undergo a change in flavor, for example, a tau neutrino can be transformed into an electron neutrino. This is possible only for a particle with non zero mass.

Recently scientists at the Tevatron accelerator at Fermilab have discovered a behavior of the top quark that is not in accordance with the SM. It appears as if the behavior is influenced by some, as of yet, unknown force. The force mediator of this force is thought to be something called a top gluon. The interaction between a top quark and the anti top quark could, according to some theorists, function as a version of the aforementioned Higgs boson thus giving particles their mass [2].

Astronomic observations of the rotational speed of galaxies are inconsistent with the theory of gravity when based on the observed matter. The most common and accepted explanation to this is the existence of Dark matter. What exactly this Dark matter consists of is however a topic of much debate. One possible candidate are SUper-SYmmetric (SUSY) particles. Some theories suggest that all the fundamental particles predicted by the SM have a super-symmetric partner. The most characteristic difference between the SM particle and the SUSY particle is that the spin differs by ½. As such a fermion in the SM would have a boson partner in SUSY. If symmetry otherwise was followed then the SUSY particle or “sparticle” would have the same mass as the SM particle. No such particles have been detected which indicates that SUSY, if existing, is a broken symmetry and as such the sparticles could be much heavier than their SM counterpart.

These are just some of the discrepancies of the SM and much more research is needed to be able to explain some of the problems discussed in this sub chapter. In order to have a fair chance of achieving this, research has to be conducted at higher energies and with better resolution. As such even bigger accelerators are needed and some of the current detector systems will need to be further refined and optimized.

3 Accelerators

There exist several types of accelerators but they all have two things in common, they increase the kinetic energy of the particles and they do this with the use of electric fields in various forms, often generated from Radio Frequency (RF) cavities. There are two distinct groups of accelerators, the linear accelerators and the circular accelerators. Among these two groups there exist several slightly varied types. The circular family of accelerators consists of accelerators such as the Cyclotron and the Synchrotron, whereas the linear family contains accelerators like the LINAC (LINear ACcellerator) and the Van der Graff.

		B-Field	***Radius***
Linear Machines	*Accelerates particles in a straight line:* *LINAC* *Electron gun* *Electrostatic generators*	$B = 0$	
Circular spiraling machines for heavier particles	*Used for both relativistic and non-relativistic particles:* *Synchrocyclotrons*	$dB/dt = 0$	$dr/dt \neq 0$
Circular machines	*Relativistic Particles:* *Lepton Synchrotron* *Hadron Synchrotron* *Storage ring* *Collider rings*	$dB/dt \neq 0$	$dr/dt = 0$

Table 4: Various types of accelerators and their basic properties [3].

Nowadays the accelerators used for particle physics are of either Synchrotron or LINAC design. They both have their advantages and drawbacks.

3.1 Synchrotron accelerators

The fundamental principle behind a synchrotron is the same as for any circular accelerator, a particle will travel in a circular path according to:

$$r = \frac{mv}{qB} \qquad (2)$$

In eq 2, r is the radius of the path of the particle, m the relativistic mass and v is the velocity of the particle. B is the magnetic flux density and q the charge of the particle. Thus, assuming a stable circular path, can be rewritten to give the time of one revolution according to:

$$T = \frac{2\pi \cdot m}{qB} \qquad (3)$$

As can be seen from eq 2 the radius of the particles' path will increase with increased kinetic energy. This unwanted feature is remedied in a Synchrotron. By increasing the B-field one can compensate for the increase of energy. The relationship employed in a synchrotron is given by:

$$r = \frac{mv}{qB} = \frac{1}{qB} m_0 c\gamma \sqrt{1 - \frac{1}{\gamma^2}} \qquad (4)$$

As such, the time of a revolution of a particle, when $v \approx c$, in a synchrotron is approximately constant and given by :

$$T = \frac{2\pi \langle R \rangle}{c} \qquad (5)$$

Where $\langle R \rangle$ is the radius of a perfectly aligned particle, the particle in a synchrotron is thus kept on the same path at all time. The main advantage of circular accelerator is that the same particle can be accelerated by the same RF cavity several thousand times per second. This allows relatively weak RF cavities to be used. However, as the charged particle undergoes acceleration perpendicular to its velocity in order to stay on the circular path it will emit energy in the form of synchrotron radiation. The energy radiated due to synchrotron radiation during a single revolution of a charged particle is found by eq 6.

$$\Delta E = \frac{q^2 \beta^3 \gamma^4}{3\varepsilon_0 R} \qquad (6)$$

Here q is the charge of the particle, β is the velocity of the particle in fractions of the speed of light and γ the gamma factor which using natural units is given by E/m. As such it can be seen that as $\beta \rightarrow 1$ the radiated power lost due to synchrotron radiation will be dominated by the energy of the particle and the mass of the particle. So a lighter particle will suffer more from synchrotron radiation losses compared to a heavier particle with the same energy. This makes the current top of the line circular accelerators unsuitable for electron-positron collisions; the energy losses will simply be too severe at those high energies [3].

3.2 The Large Hadron Collider

The circular accelerator with the highest energy is built in the CERN laboratory outside of Geneva. It is called Large Hadron Collider, or LHC for short. It is used to accelerate protons and nuclei. Hadrons are relatively heavy particles compared to the electron, which is a lepton, and are thus not as susceptible to synchrotron radiation. The LHC accelerator is just one part of the whole Cern accelerator complex which consists of several different accelerators. They are used to accelerate the particles in successive steps. While experiments are conducted at all the various accelerator steps the main focus is now on the LHC accelerator. The first acceleration of the protons is achieved by the use of a linear accelerator LINAC2 where they are accelerated up to 50 MeV. From there they are injected into the PS Booster and then the PS where they are accelerated up to 10 GeV, and subsequently fed into the Super Proton Synchrotron in order to achieve a kinetic energy of 450 GeV. Finally they are finally injected into the LHC where half of the particles will travel clockwise and the other half will travel in the counter clockwise direction. They are then accelerated up to an energy of 7 TeV. The most important parameter for particle physics experiments is the center of mass (CM) energy. With a stationary target the CM energy scales as the square root of the energy but in a collider where the colliding objects are moving in opposite directions the CM energy scales linearly with the particle energy. Therefore it is vastly more favorable to conduct collider type collisions instead of extracting the beam to a stationary target.

When accelerating particles up to these energies it is important to avoid collisions with contaminating molecules/atoms in the rest gas. As such a vacuum system is employed in order to evacuate as many unwanted particles from the accelerator tubes as possible. The pressure in the LHC tube will be roughly 10^{-13} atm which corresponds to an ultra high vacuum.

In order to have the particle follow the path a lattice consisting of various types of magnets, such as dipoles and quadrupoles, are used. The magnets will also be used to focus the beam of particles so that a sufficiently good cross section between the beams can be achieved to optimize the number of collision events. In total well over 9000 various magnets are used in the LHC. Since the path of the particles is constant the maximum energy that can be achieved in a synchrotron is directly proportional to the field created by the magnetic dipoles. Therefore it is paramount that the magnets in the LHC have sufficiently high field strength. The required strength of the dipole field in the LHC is 8.3 T can not be achieved by any other means than that of super cold superconducting magnets. The magnets are cooled down to 1.9 K which enables them to conduct current without any resistance and a current of 11700 A is then used to create the magnetic field strength needed.

The acceleration in the LHC accelerator is achieved with the use of RF cavities. The RF cavities have a 400 MHz frequency and a potential drop of 2MV which corresponds to an accelerating field of 5MV/m. There are eight such cavities per beam. Not only will the RF cavities be used for acceleration, they will also create buncehes of particles which will even further increase the number of collision events when the two "beams" are set to collide.

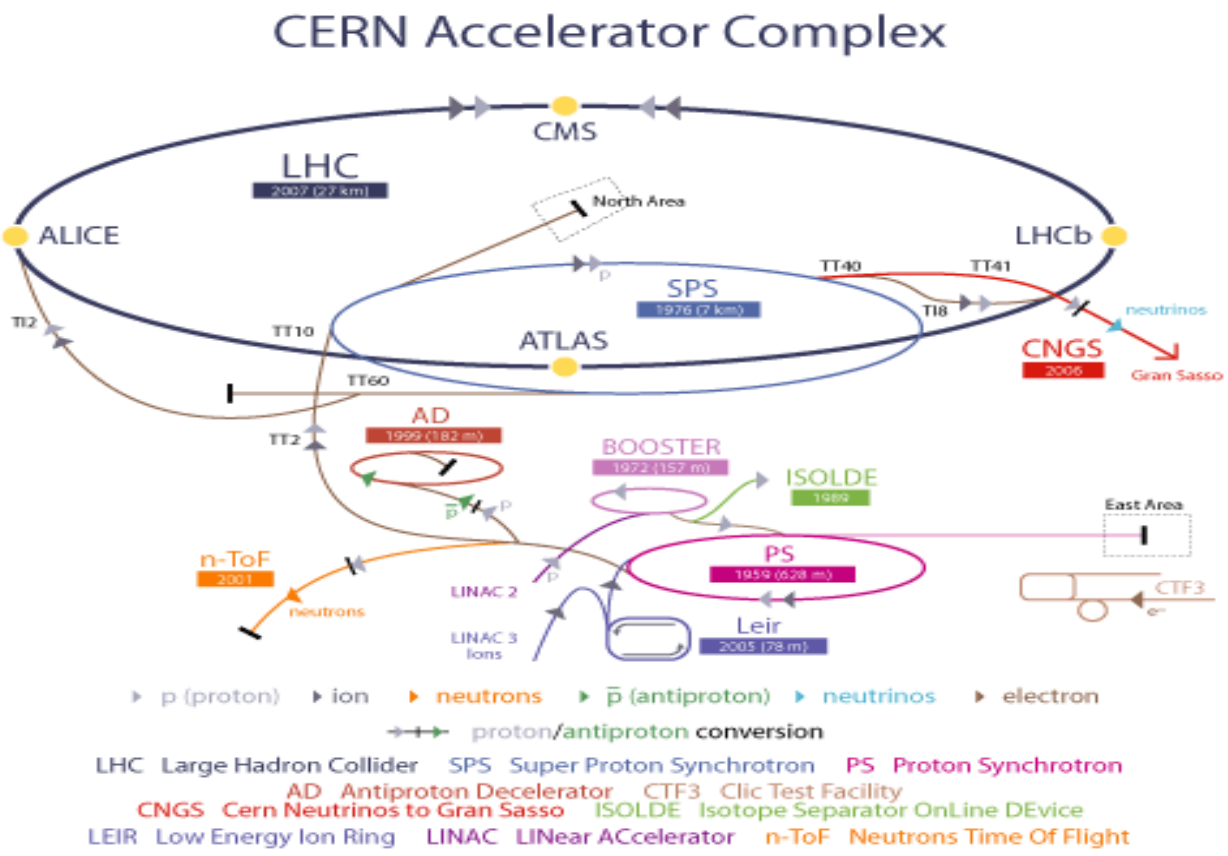

Figure 1: An extensive schematic sketch of the CERN accelerator complex [4].

3.3 What is the next step after LHC?

The field of particle physics is an ever evolving field of science. As such scientists are already planning for future colliders which can allow scientists to even further probe the SM and other theories.

In chapter 3.1 we have previously established that a heavier particle will suffer from less synchrotron radiation losses than a light particle would. We have also concluded that higher energies can possibly yield more interesting results. So why would anyone want to collide such light particles as the electron and the positron?

The key difference is that hadrons, such as the proton, are made up of quarks and gluons. The leptons, such as the electron, are not made up of any smaller constituents, they are fundamental particles. Therefore it is easier to calculate and predict the outcome of a given collision. It is also impossible to accurately predict the energy of the involved particles, often referred to as partons in a hadron collission. In such a collision one cannot know what fraction of the energy the involved quarks carried in the individual collision. For a lepton this is another matter, since it is only one particle involved it is possible to know what the energy of the involved particles are. As such it is possible to scan a range of energies in search for resonances and production thresholds. The signals from a lepton- anti lepton collision, as for instance, an electron-positron collision will not suffer from as much background noise either. Due to this it is highly beneficial to compliment hadron-hadron collision measurements with electron-positron measurements. Due to this fact the next large accelerator proposed by the scientific community will not be an even larger synchrotron collider, it will instead be a Linear Collider. The International Linear Collider (ILC) is one suggestion and the Compact Linear Collider (CLIC) another suggestion, they will be discussed in chapter 3.5.

3.4 LINACs

Just like in a circular accelerator one uses electric fields to accelerate the particles. An electron accelerated between a cathode and an anode with a potential difference of 1000 V will obtain an energy of 1 keV. At first glance it might thus be easy to think that one can simply apply a sufficiently high voltage between the anode and cathode to reach the desired energy of the particle. That is not the case; once the voltage builds up to several MV, then discharge will occur between the anode and cathode. To reach higher energies several accelerating gaps can be used. It is also possible to use rapidly alternating E-fields to avoid discharge. The rapid alternations do not provide sufficient time for sparks to build up.

The first linear accelerator was constructed by Wideröe; it consisted of several tubes charged by an alternating current. The tubes had the same magnitude of potential drop but the direction was alternating. The tubes were constructed and assembled in such a way that the time it took for a particle to traverse the distance of the tube was constant.

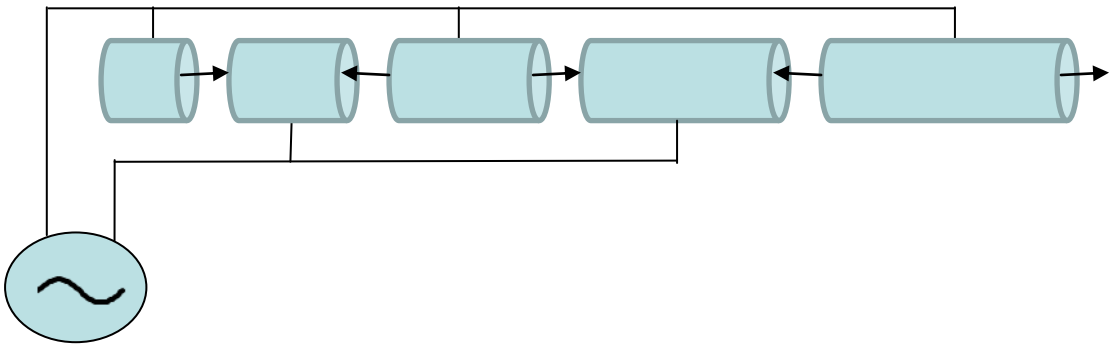

Figure 2: The schematic principle behind the Wideröe accelerator.

Further advancements to the Wideröe accelerator was done by Luis W. Alvarez in 1946 by enclosing the structure of the Wideröe accelerator into one long tube. Since an electromagnetic wave can be made to propagate or oscillate within a structure one can then make use of an electromagnetic wave which travels down the tube and builds up high electric fields in the gaps synchronous with the arrival of the particles.

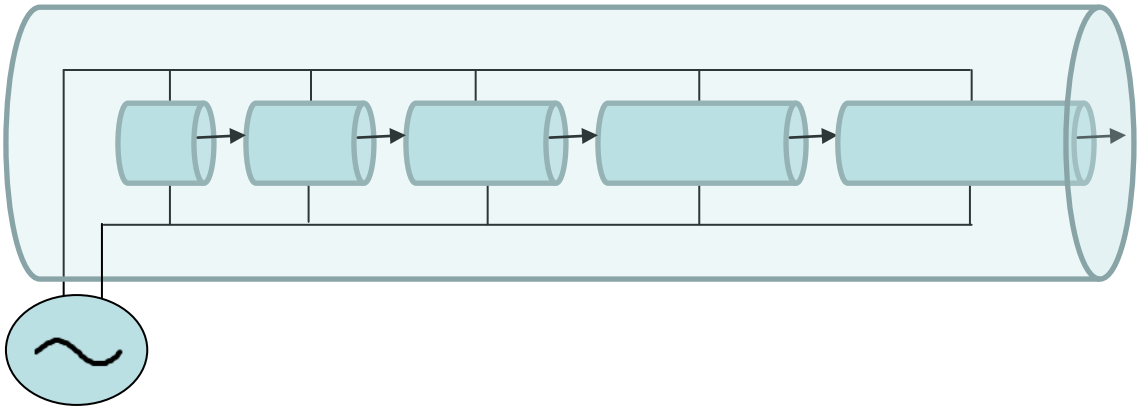

Figure 3: The Alvarez structure allows for a greater acceleration gradient to be achieved.

The Alvarez structure can handle fields of much higher frequency and magnitude than the Wideröe structure and is still used today. An accelerator can make use of both standing waves and propagating waves to accelerate the particles. A traveling wave LINAC consists of a tube with several discs placed at specific intervals. The properties of the discs are then chosen such that the propagating wave will follow the particles along the accelerator. For an electron/positron accelerator the structure and distance between the discs becomes quite straight forward as the particles becomes relativistic at roughly 5 MeV and as such will have an almost constant velocity when accelerated further [3].

3.5 The International Linear Collider

The ILC is as of yet only a proposed project and as such the predicted capabilities and constraints might not be the same as the final ones. However, it is evident that the current design should in theory be able to provide collisions which will enable extremely precise measurements assuming sufficiently good detectors.

The target luminosity, which is a measurement of how many particles there are per unit area per unit time times the opacity of the target, of the ILC will be $2 \cdot 10^{34}$ $cm^{-2}s^{-1}$ [5]. A small beam crossectional

area is of utmost importance in a LINAC since the particles will only have one chance of colliding. In a synchrotron collider the particles will have a chance to collide during the each revolution which goes on for several hours. In a LINAC that is not possible. The high luminosity will be achieved through extensive use of focusing magnets to focus the beams down to nanometer extension. This is far from trivial considering that the bunch, which consists of particles with the same charge, will defocus it self due to the repulsive Coulomb force. Before entering the LINACS, bunches of particles will be prepared in the storage rings so called damping rings to minimize the bunches in phase space. This will allow for further focusing of the bunches by draining the particles of energy trough synchrotron radiation emitted when the bunches undergo acceleration. They will then be accelerated in the linear accelerator. Since the bunches will be loosing momentum in all directions whereas at the same time only be accelerated in the direction of the beam path this will lead to even more tightly packed bunches.

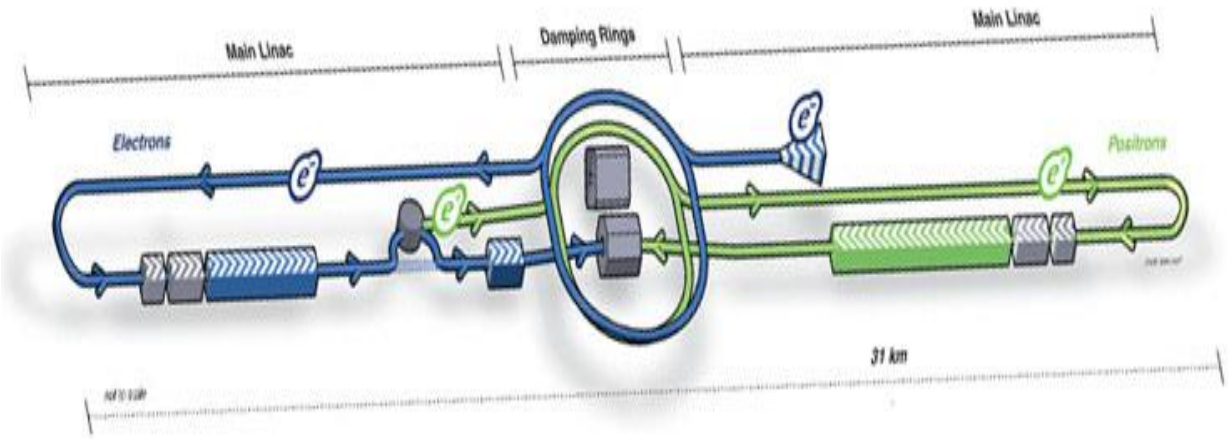

Figure 4: The proposed outline of the ILC [6].

The CM energy of the ILC should be in the order of 0.5 TeV with a possibility to upgrade the facility to produce 1 TeV CM energy collisions. However, the energy range is not yet set in stone. The final decision awaits results from LHC about e.g. the mass of the Higgs boson. To achieve these unprecedented levels of energy for a LINAC novel RF cavities are being developed specifically for the ILC. These superconducting RF cavities will be able to accelerate the leptons with 31.5 MV/m. Even with these state of the art RF cavities the length of each LINAC will need to be roughly 11 km [5].

The extreme precision of the ILC must be matched with highly precise detectors. So not only does this new proposed facility require further development of the accelerator technique used to achieve the collisions, refined detector types are also paramount. One of the proposed detectors is the International Linear Detector (ILD) , whose tracking is planned to use a Time Projection Chamber, a detector with a 3D spatial resolution. This detector is under development by the LCTPC collaboration.

Another LINAC collider concept that is being developed is the Compact Linear Collider (CLIC). This electron positron collider is being developed at CERN and aims to achieve a center of mass energy of up to 5 TeV. This will require even higher acceleration gradients than what is being proposed for the ILC, as high acceleration gradients as 100 MV/m is aimed for.

4. The Time Projection Chamber

The first Time Projection Chamber (TPC) was developed in 1974 by David Nygren at the Lawrence Berkeley Laboratory. Its first major application was in the PEP-4 detector, which studied 29 GeV electron-positron collisions at the PEP storage ring at Stanford Linear ACcelerator (SLAC), the TPC has since then been extensively used in various accelerator based experiments. It is capable of performing 3D detection of the path traveled by the charged particles created in the collision. It is also used for particle identification and momentum measurements.

4.1 General Properties of a TPC

Currently the TPC is in principle a combination of a Multi Wire Proportional Chamber (MWPC) and a drift chamber. The fundamental idea of the TPC is to replace the many MWPC planes used for conventional tracking with a large volume of gas. By applying a constant homogenous electric field in this volume of gas electrons released trough ionization drift in the direction of the electric field onto a single MWPC. A constant and homogenous magnetic field is also applied. The magnetic and electric fields, which have to be parallel, then interact with particles according to the Lorentz force (eq 7), the magnetic field then causes the charged particles to move in circular paths which due to the energy loss will become spiraling paths. The electrons released trough ionization will drift parallel to the electric field, and therefore also parallel to the magnetic field. While the diffusion of the electron cloud will try and force the electrons off their straight path the magnetic field will in turn bend the electrons back into the a parallel path of the electric field thus reducing the effects of diffusion.

$$\vec{F} = q(\vec{E} + \vec{v} \times \vec{B}) \qquad (7)$$

Depending on the particles electrical charge and momentum the path of the particles will follow paths of different bending radii. One coordinate is then given by the anode wire and a second coordinate is obtained by the rows of cathode pads along the anode wires. Since the drift velocity is known in the volume of gas, measurements of the drift time will give information of the z coordinate. The density of ionization along the path depends on momentum and type of particle that induce the ionization of the gas. Since all the ionized electrons will drift towards the endcap each anode wire over which the particle trajectory crosses will sample that portion of the track, thus making the TPC able to provide a truly 3-dimensional trajectory path of every single particle. This is of utmost importance in heavy ion collisions when vast amounts of particles are emitted, a 2-dimensional detector would not be able to distinguish between overlying paths to nearly the same degree.

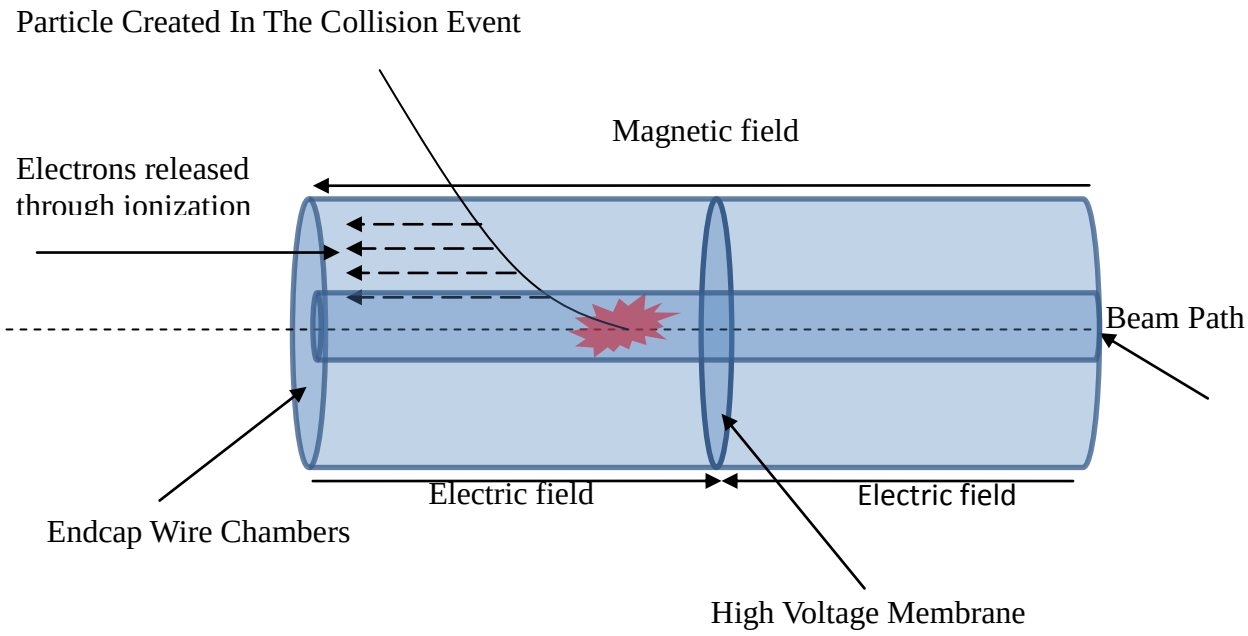

Figure 5: The principle of a TPC used in a collider.

As can be seen in **figure 5** a TPC used as a detector in an accelerator can be made to cover almost the full solid angle of a collision event. This is one of many advantages with a TPC detector. It is also compatible with other energy measurements, for instance calorimeters, thanks to the low energy deposited in the TPC itself. Since the momentum measurements, particle tracking and energy loss measurements are done simultaneously it is also possible to perform particle identification when using a TPC. The TPC measures a large number of high resolution coordinates at each track. Thus it has the ability of high momentum resolution.

4.2 The principles of the readout system

The readout system of a TPC normally consists of wire chambers read out with pads of various sizes which are etched into the cathode board material. The anode wires are used to amplify the signal coming from the primary electrons. The electrons released in the gas are usually in the order of a few tens per cm. This is too low to provide a sufficient signal for electronic readout. However, when the electrons drift towards the anode wires they will experience an increased electric field E which around a current conducting wire is given by

$$\vec{E}(r) = \frac{\lambda}{2\pi\varepsilon_0 r} \qquad (8)$$

Here λ is the charge per unit length of the wire, ε_0 the permittivity in vacuum and r the distance from the wire. It should be noted that this is only valid when r is much smaller than the length of the wire. Thus the electric field strength increases as the electrons drift closer to the wire. This causes the electrons to accelerate and with the increase in kinetic energy the electrons may begin to ionize more gas atoms. These electrons will themselves be accelerated and will often reach high enough energies to ionize yet more atoms, an avalanche of electrons is thus created, and the signal from this can be detected. As the electrons are released, the atoms will become positively charged ions. These ions will then drift in the opposite direction and this will end up on the cathode pads located behind the wires. The detected signal on a pad will provide one spatial coordinate determined by the pad location.

It is important that the electric field from the wire is uniform so that the amplification for each electron is the same no matter where it is detected. The electrostatic and gravitational forces cause the wires to sag, which in turn will lead to a non uniform electric field being produced by the wire. How much sag the gravitational force will give rise to depends on the density of the material of which the wires are produced and the tension of the wire. The sag caused by the electrostatic force scales with the square of the length and the inverse of the stretching force [7]. For this reason it is important that the wires are produced in such a material that they can withstand the stretching forces needed to mitigate the effects from the electrostatic force. For this reason tungsten is used.

Since the ions are much heavier than the electrons their drift velocity will be much slower, and will thus take a longer time to reach the cathode pads. This will lead to a buildup of positively charged particles in the gas. This will in turn lead to the formation of a non-uniform electric field. In order to mitigate this effect gating wires are implemented in the MWPC design. The gating grid is placed in front of wires with a perpendicular direction with respect to the drift velocity. As such it can be used to further manipulate the electric field so that electrons will be unable to reach the detection system unless the field from the gate is turned off, the gating grid is then turned on or off depending on whether or not a trigger signal is detected. Due to this the gating grid is not suitable for an experiment where the time between trigger events are too short.

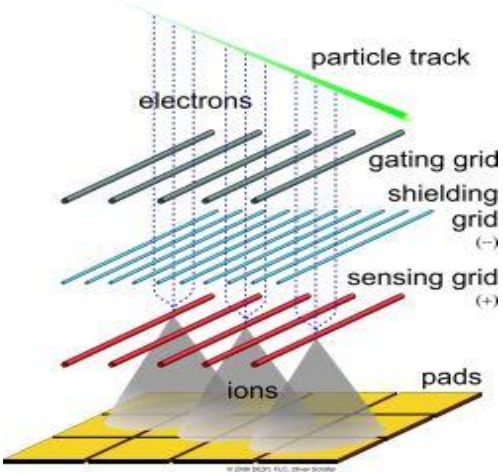

Figure 6: Schematic illustration of MWPC type of TPC readout [].

Since the detected signal is proportional to the number of primary electrons released it is paramount that it is only the primary electrons from one particle that is detected. For this reason it is a fundamental requirement of a TPC that the resolution is good enough to determine whether or not it is one or two particles that is causing the ionization, if not the ionization event will have to be discarded.

4.3 The Drift

The TPC is, as mentioned, essentially a combination of a drift volume and a readout system similar to the MWPC. The basic principle behind a drift is that an energetic particle will ionize the gas in the drift region. The size of a drift volume can be in the order of a few meters in length. It is also called a field cage and it usually consists of a cathode plane and two anode planes, placed symmetrically on

each side of the cathode. Therefore the electrons released trough the ionization, called primary electrons, will drift towards the anode plane where they will be detected. Sometimes a TPC only consist of a single cathode plane and a single anode plane.

4.3.1 The Energy Loss

The mean energy loss in a gas is related to the number of ionized atoms per unit length. So if one can understand the mechanism behind the ionization process then much information of the incident particle can be gathered by measuring the signal of the collected primary electrons. The energy transferred in such a process is given by the Bethe Bloch formula:

$$-\frac{dE}{dx} = 2\pi N_a r_e^2 m_e c^2 \rho \frac{Z}{A}\frac{z^2}{\beta^2}\left[\ln\left(\frac{2m_e\gamma^2\upsilon^2 W_{\max}}{I^2}\right) - 2\beta^2 - \delta - 2\frac{C}{Z}\right] \tag{9}$$

where r_e is the classical electron radius, m_e is the electron mass, N_a is Avogadro's number, I is the mean excitation potential, Z is the atomic number of the absorber material, A is the atomic weight of the absorber material, ρ is the density of the absorber material, z is the charge of the incident particle in units of elementary charge, β is the velocity of the incident particle in fractions of c, γ is the gamma factor of the particle, W_{max} is the maximum energy transfer in a single collision. C is the so called shell correction which is important for highly relativistic particles, δ is the so called density correction which is important at low velocities [8].

Eq 9 is usually considered valid when $0.1 < \beta\gamma < 1000$. Above the limit the energy losses due to radiation becomes more important. This is a problem for electrons at even lower values of $\beta\gamma$ than 1000. Below the limit the assumption that the shell electrons are stationary compared to the incoming particle is not valid.

The version of the Bethe Bloch formula given in eq 9 is valid when the ionizing particle remains on the same path after the collision. For a light particle such as the electron this will not be the case, the electron will instead be deflected upon collision. Eq 9 also fails to take into account that the incident electron and the primary ionization electron are indistinguishable. As such eq 9 is not valid for electrons but instead must be modified.

$$-\frac{dE}{dx} = 2\pi N_a r_e^2 m_e c^2 \rho \frac{Z}{A}\frac{1}{\beta^2}\left[\ln\frac{\tau^2(\tau^2+2)}{2(I/m_e c^2)^2} + F(\tau) - \delta - 2\frac{C}{Z}\right] \tag{10}$$

Here τ is the kinetic energy of the particle given by $m_e c^2$. $F(\tau)$ for an electron is given by

$$F(\tau) = 1 - \beta^2 + \frac{\frac{\tau^2}{8}(2r+1)\ln 2}{(\tau+1)^2} \tag{11}$$

As mentioned before the energy loss due to radiation, called Bremsstrahlung, is a competing process for light particles such as the electron and positron even at relatively low energies, and at a few hundreds of MeV they are the only particles that exhibit this behavior. The emission probability varies as

$$\sigma \propto r_e^2 = \left(\frac{e^2}{mc^2} \right)^2 \tag{12}$$

As can be seen in eq 12 the radiation loss from a muon, which has a mass of ~ 106MeV, compared to the mass of an electron 0.511 MeV, will be roughly 40000 times less. The energy released through Bremsstrahlung per unit length is given by

$$-\left(\frac{dE}{dx} \right) = N \int_0^{v_0} h\nu \frac{d\sigma}{d\nu}(E_0, \nu) d\nu \tag{13}$$

The complete loss of energy per unit length for an electron with an energy above a few MeVs is thus very much a combined function of eq 10 and eq 13. The relation between the two processes is shown in **figure 6**.

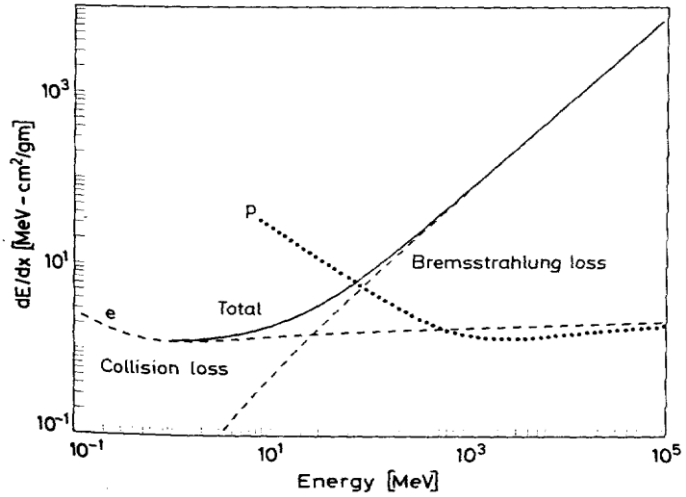

Figure 7: The radiation loss vs. collision loss for electrons in copper, the dotted line is the energy loss for protons[8].

Equations 9-13 can be found in [8].

4.3.2 Particle identification

The knowledge of the energy loss of a particle is not interesting in itself. However, when related to some other parameter, such as the momentum, it can be used to determine what particle caused the ionization. While particle identification is straightforward at low momentum it is a challenge at larger momentum. The most interesting region of a plot showing the momentum related to the mean energy loss is called the relativistic rise region. Over this relatively wide momentum range the steady increase of *dE/dx* can be used to separate particles with the same momentum but different masses from each other. However, the differences between particles of varying mass can be small and the resolution of the *dE/dx* measurements must then be sufficiently good in order to distinguish between the different particles. Currently a TPC is the only detector that comes close to providing a good enough *dE/dx* resolution for particle identification on the relativistic rise

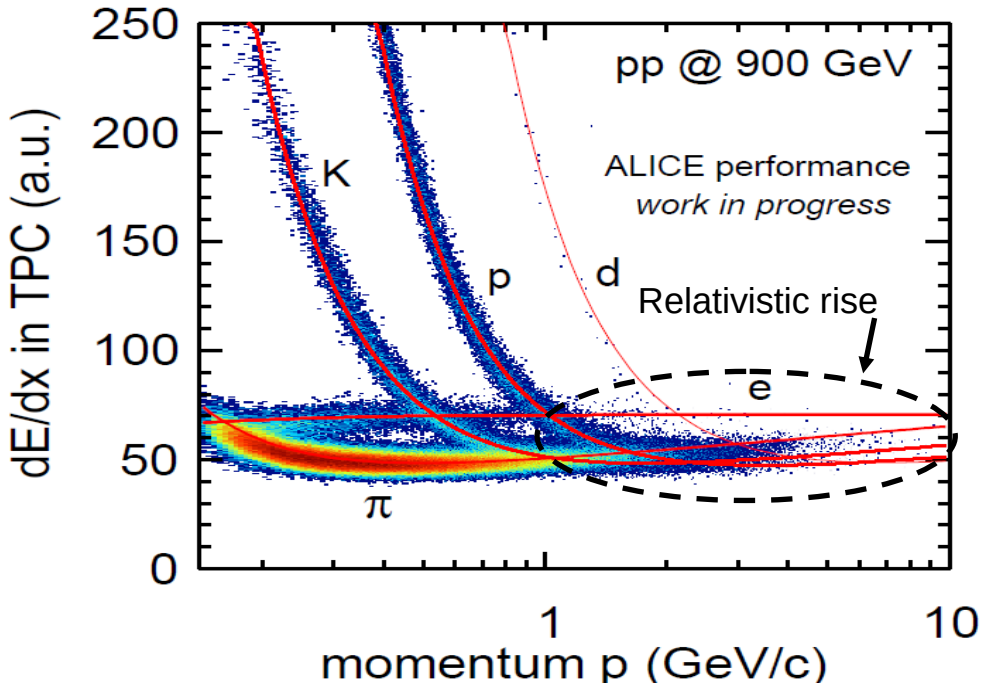

Figure 8: Particle identification through dE/dx vs. momentum measurements.

As can be seen in **Figure 8** the *dE/dx* resolution is very important for particle identification in the relativistic rise region. Unless the resolution is very good the various particle identities might be indistinguishable from each other in this region. In order to be able to characterize the different particles the *dE/dx* resolution must be improved.

4.3.3 The Truncated mean

The energy loss distribution for a particle traversing a gas will not be a Gaussian distribution. The distribution will instead be biased towards higher energy losses. This will make it impossible to estimate the average energy loss with good resolution since the measurements will only provide a finite number of samples. Another aspect of the *dE/dx* measurements is that it is not one specific ionization event that determines the energy loss but it is the integrated sum over the particle track. The energy loss distribution is essentially described by a Landau distribution. To be able to provide an optimized resolution it is important that one can determine the average *dE/dx* value in a track. This can be done by using the truncated mean of the Landau distribution. Since the number of electrons released trough ionization, and thus the *dE/dx* value, is proportional to the detected signal the truncated mean can be obtained by discarding a certain percentage of samples with the highest signal in the track and then taking the average value of the remaining values a good estimation of the average value for a track is obtained. The most commonly used limit for current TPCs is 60%. Whether or not this value is the best value for every TPC design is far from certain, the optimal value might depend on the size of the read out pads.

4.4 The composition of the gas

In order to derive useful information from the previously mentioned equations it is of paramount importance to have full knowledge of the properties and behavior of the gas. While the composition of the gas can vary it is almost always composed of some noble gas and a quencher gas.

The advantage of the noble gas is that it is far less reactive and as such does not capture drifting electrons. If an electronegative gas is present it will capture the primary electrons preventing the detection of them. An impurity of the drift gas must thus be kept to an absolute minimum. The constraints on the purity of the gas depend on the drift length of the primary electrons. Noble gases also require the lowest electric field intensities which makes them ideally suitable since the working voltage should be kept to a minimum [8]. However, it is not possible to achieve sufficiently high amplification of the signal through avalanche processes in a readout chamber containing only noble gases.

The addition of a second type of gas, commonly called quencher gas, can be used to allow an increase of the amplification in a wire chamber. The quencher gas absorbs photons created in the avalanche process before they reach the metallic surfaces like the cathode. There a photon would have had a large probability to knock out an electron which would drift to the anode, experience an avalanche effect. This could lead to an escalation of avalanche processes which could in turn lead to a spark. The quencher gas deexcites through emission of low energy photons reducing the flux of secondary electrons. With the addition of a quencher gas such methane (CH_4) the drift velocity can be increased thanks to that fact that electrons can interact with these molecules and inelastically scatter thus increasing their velocity. An increase in drift velocity will serve to decrease the dead time which is important if the detector is meant to be operated at a high count rates. However, if it is more important to have a better spatial resolution then a quencher gas such as carbon dioxide (CO_2) can be used since it will serve to decrease the drift velocity. Unlike methane carbon dioxide is not explosive.

The gas is contained at slight over pressure. Over pressure is also used to decrease diffusion into the chamber from the surrounding environment in order not to contaminate the gas.

Even when considering all the previously mentioned aspects of the gas, small variations of the temperature and pressure gradients may cause the drift velocity to deviate from the calculated value so a continuous measurement of the drift velocity can sometimes be performed during times of data acquisition. These measurements are usually performed with laser beams trough the gas [9].

4.4.4 Diffusion

One of the most pressing concerns during the drift based experiment is the diffusion of the primary electrons. The primary electron can cause more ionization events, releasing secondary electrons, the electrons will drift towards the anode plane due to the electric field. However, near elastic collisions with the gas molecules will scatter the electrons as they drift. These collision events will more or less spread out the electrons in a uniform way, and will thus affect the spatial resolution in all three dimensions. The spread of the electron cloud, σ, is dependent on the drift length since a longer drift length will lead to more collisions. With a uniform drift velocity it is given by:

$$\sigma = \sqrt{\frac{2Dz}{\mu E}} \qquad (14)$$

Here the D is the diffusion coefficient, E the electric field strength, μ the mobility of the charge and z is the drift length [8]. This is however only valid for the case of a drift in a chamber without a magnetic field parallel to the electric field. It should be noted that diffusion is not always an unwanted effect; a moderate diffusion will actually be able to increase the spatial resolution in the read out. By spreading out the electrons the signal will be shared by several read out pads. The relative charge difference, which will usually have a Gaussian distribution, will then give a more accurate position than if only a single pad detected the electron cloud.

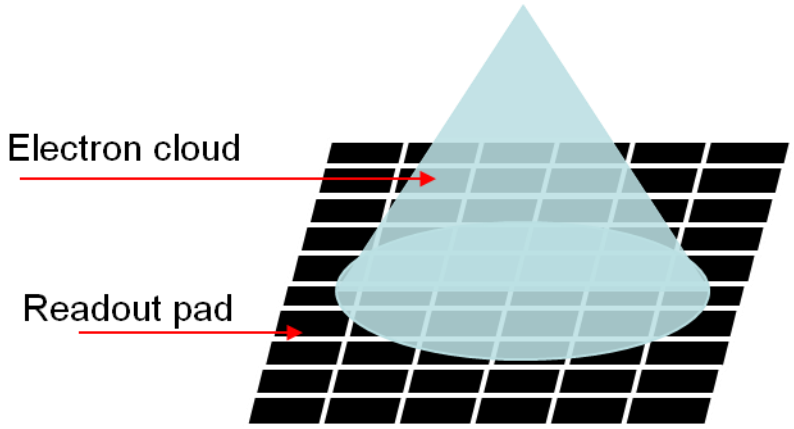

Figure 9: A basic sketch showing why diffusion sometimes can be a good thing in a detector.

A signal that is detected only by a single pad will have a maximum resolution no better than the size of the pad itself whereas the resolution of a diffused electron cloud hitting several pads will provide a resolution not limited by the size of the individual pads. However, for an electron cloud which has undergone much diffusion the signal to noise ratio might be too low for it to be accurately detected at all. Due to this a smaller pad size is still very much beneficial for the resolution of the TPC as long as the diffusion is random in space the centroid of the cloud represents the position of the ionization event.

4.5 The Electric and Magnetic Fields

Due to the collisions in the gas the motion of the primary electrons would amount to nothing more than Brownian motion, a highly stochastic motion, if they were not affected by some force which can make this movement biased towards some direction. Detecting any ionizing event would thus be very difficult. For this reason an electric field is applied over the drift chamber. The electric field must be uniform, or as close to uniform as possible, over the whole drift length. This is achieved by the use of a field cage where conducting strips are placed at the appropriate distances with the correspondingly appropriate voltages. A more thorough description of a field cage is given in chapter 7.

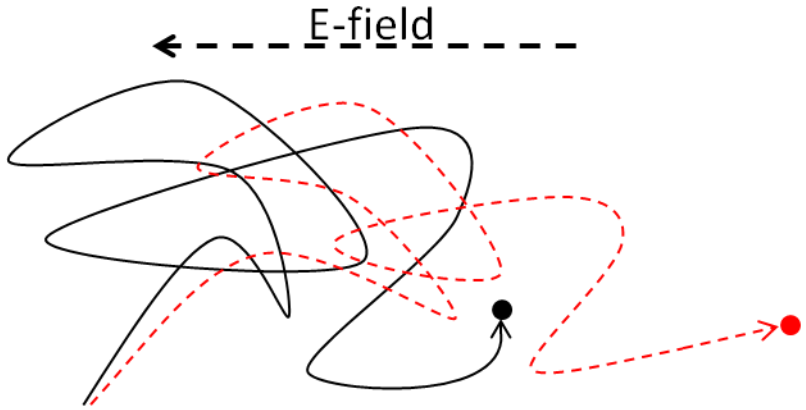

Figure 10: A conceptual figure where the solid line suggests the random movement of a primary electron without an applied electric field and the dashed line suggests the motion of a primary electron with an applied electric field.

While the Lorentz Force (eq 7) describes the force on a charged particle in vacuum it is not the whole truth when it comes to a charged particle in a medium. In a medium the charged particle will undergo stochastic collisions and that will lead to a behavior resembling Brownian motion that must be accounted for. In a medium eq 7 therefore transforms into:

$$\vec{F} = q(\vec{E} + \vec{v} \times \vec{B}) - \frac{m\vec{v}}{\tau} \qquad (15)$$

Here m is the mass of the particle, v the velocity of the particle and τ the average time between the collisions events. As it turns out these repeated collisions will give rise to a constant drift velocity of the particle. Since the mass of the particle is constant the average force on the particle can be said to be zero since

$$\vec{F} = m\vec{a} = m\frac{d\vec{v}}{dt} = 0 \qquad (16)$$

For that reason eq 15 can be reduced to

$$q(\vec{E} + \vec{v} \times \vec{B}) = \frac{m\vec{v}}{\tau} \qquad (17)$$

The magnetic field in a TPC is of utmost importance and the magnetic field strength is usually in the order of Tesla. It is the magnetic field that makes it possible to achieve momentum measurements and thus also particle identification. However, it is paramount that the magnetic field does not bend the path of primary electrons released in the ionization event. Doing so would seriously degrade the spatial resolution of the TPC.

As can be seen in eq 14 it is the perpendicular component of the magnetic field with respect to the velocity vector of the particle that will exercise a force on the charged particle and consequently bend the path of the primary electrons. In order to avoid such a distortion, often called **E×B** effects, it is necessary to have the magnetic field parallel to the electric field. While this is manageable in the drift volume it is most often a problem close to the wires in the MWPCs when the E-field is relative to the wires. For a magnetic field parallel to the electric field the drift velocity is independent of the magnetic field and eq 14 can be rewritten as

$$\vec{v} = \frac{q\vec{E}\tau}{m} \qquad (18)$$

It can be seen from eq 18 that the drift velocity will decrease as the average time between the collision events $\boldsymbol{\tau}$ will decrease and as the average time between collisions is dependent on the electric field, ***E,*** an increase of the electric field strength will not always lead to an increased drift velocity ***v***.

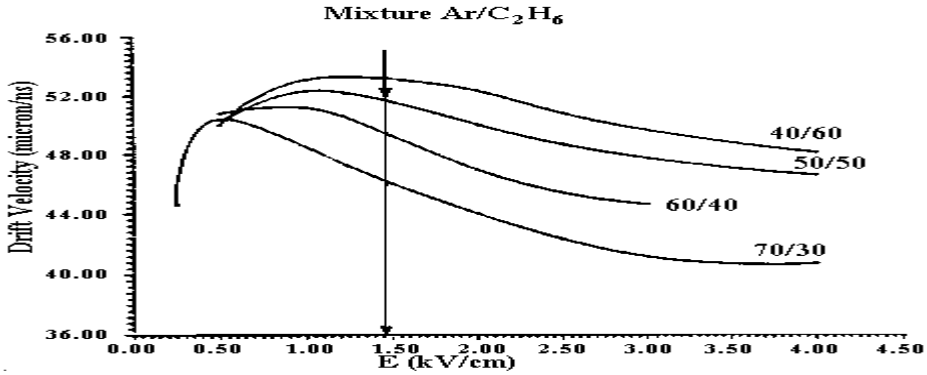

Figure 11: An example of how the drift velocity depends on the electric field [10].

The function that the magnetic field serves in a TPC is not only that of bending the path of the charged particle, it also serves to minimize the effect of diffusion. The electrons scattered outwards with a velocity vector not in the direction of the electric field will be bent by the magnetic field that is no longer parallel to the velocity vector of the particle. As such the magnetic field will exercise a force upon the particle which confines the primary electrons to helical trajectories.

5 The LCTPC

The requirements on any detector are based on what you want to study. The scientific objectives of the ILC put unprecedented requirements on the TPC that is proposed. In order to accurately estimate the mass of a possible Higgs boson, with a margin of error no larger than 150 MeV, the momentum resolution of the TPC must be in the order of $9 \cdot 10^{-5}$ GeV^{-1} and the momentum resolution for the whole detector system a momentum resolution of $2 \cdot 10^{-5}$ GeV^{-1} should be achieved in order to extract enough information from the experiments [11]. In order to achieve such a high momentum resolution a strong magnet with a magnetic field strength of 3.5 T will be used. A comprehensive table of the requirements can be seen below in table 5. Among other things these requirements have more than one order of magnitude better momentum resolution than the best TPCs to date. As such further development of the TPC is needed.

Size	ϕ = 3.6 m, L = 4.3 m
Momentum resolution for the TPC (3.5 T)	$9 \cdot 10^{-5}$ GeV^{-1}
Momentum resolution for all systems (3.5 T)	$2 \cdot 10^{-5}$ GeV^{-1}
TPC Material budget	~0.04 X_0 to outer fieldcage in r ~0.15 X_0 for readout endcaps in z
Number of Pads/Timebucket	~$1 \cdot 10^6$/1000 per endcap
Pad Size/no.padrows	~1 mm x 4-6 mm/~200 (standard readout)
σ_{point} in $r\phi$	>100μm (average over $L_{sensitive,}$ modulo track ϕ angle)
σ_{point} in rz	~0.5 mm (modulo track θ angle)
2-hit resolution in $r\phi$	~2 mm (modulo track angles)
2-hit resolution in rz	~6 mm (modulo track angles)
dE/dx resolution	~5%
Performance	> 97% efficiency for TPC only (p_t>1 GeV) >99% efficiency for all tracking (p_t>1 GeV)
Background robustness	Full efficiency with 1% occupancy
Background safety factor	Chamber will be prepared for 10 times worse backgrounds at start up of the linear collider

Table 5: A Comprehensive overview of the necessary requirements of the LCTPC with standard electronics [12].

6. Future Developments of the TPC

One of the proposed improvements of the TPC is the replacement of the MWPCs at the end plates. As previously mentioned they suffer from **E**×**B** effects and ionic build up. As such other methods of amplification are investigated, most notably the Micro Pattern gas detectors, Micromegas and Gas Electron Multipliers (GEMs). This thesis will focus solely on the GEMs.

6.1 The GEMs

The GEMs consist of an insulator and two foils of conducting material. In this study a thin, 50 μm, Kapton foil clad with 5 μm thick copper layers on both sides were used. The GEM is then perforated with uniformly placed holes with a hole density of 50-100 holes/mm^2. The diameters of the holes are in the order of 70μm. By applying a potential difference, usually ranging between 150 V up to 400 V, between the two layers of foil an avalanche process is started when a free electron enters the hole where the field strenght is high. The amplification is in the order of a 100 but this can be varied depending on the chosen voltage between the foils. This amplification might at first glance seem like a minimal and unsatisfactory amplification but one of the advantages of the GEMs is that the amplification of several GEMs behaves almost linearly, so using two planes of GEMs will provide a total amplification of 10^4 and consequently three planes could roughly provide an amplification of 10^6.

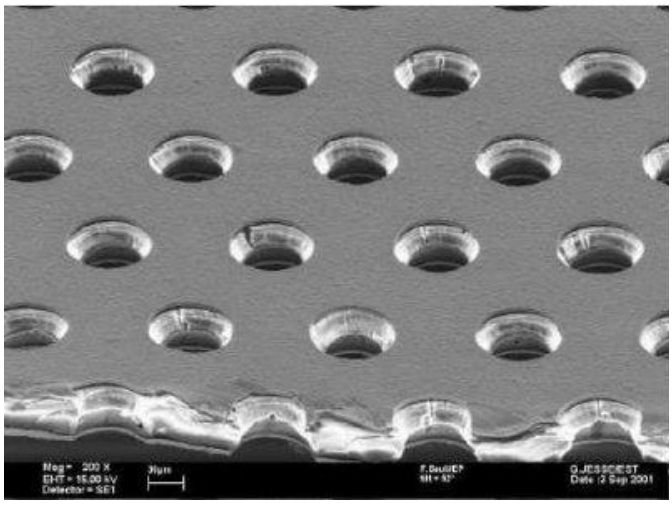

Figure 12: A 200:1 magnified picture of a GEM taken with an electron microscope [13].

The holes are generally produced in an equilateral triangle pattern. As can be seen in figure 10 the individual holes are not uniform throughout but instead take the shape of a dual cone; this is due to the etching process used when the holes are produced. As the primary electrons drift towards the holes the experienced electric force will increase and inside the holes the electron will be accelerated with, assuming a 250 V potential, up to 500 kV/cm in the hole.

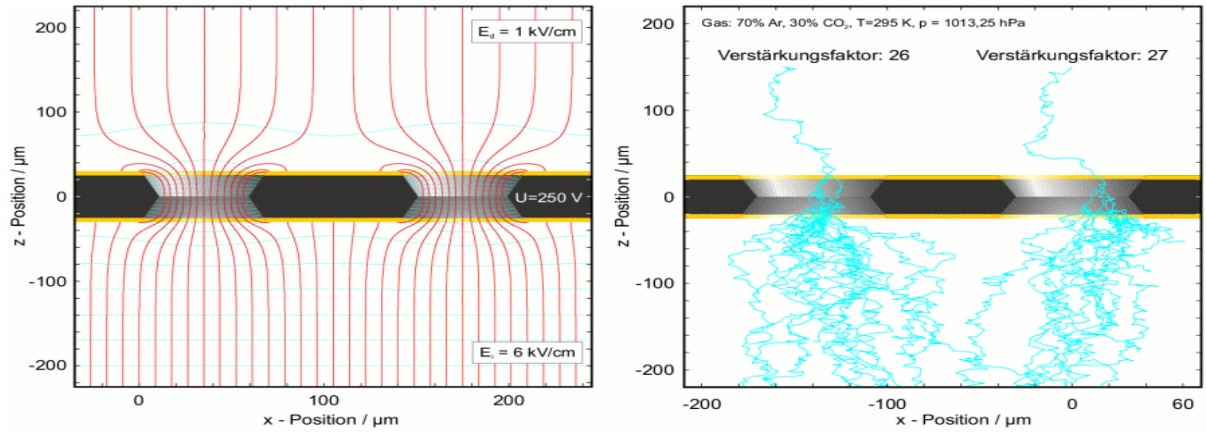

Figure 13: A conceptual sketch of the working principle of a GEM. The left hand side shows the suggested electric field lines and the right hand side shows an example of two avalanche events [13] .

Thanks to the possibility of using several layered GEMs the voltage in each individual GEM can be kept at low enough gain to make sure that there are no sparks created. This is but one of the advantages with the GEMs, unlike the MWPC a GEM will not suffer from the same problems with **E**$^{\times}$**B** since the anode of the drift field is the flat GEM surface, perpendicular to the E-field. Furthermore the GEMs can be used to almost eliminate the effects of ionic back drift. By applying a lower voltage in front of the GEM than behind will make it possible to remove the back drift ions. Having the electric fields configured in such a way will lead to a situation where a large part of the gradient of the electric field in front of the GEM will be directed into the upper copper foil. This is shown graphically in the left hand side of **Figure 13.** This will lead to ions being collected by the copper foil where as the electrons will continue straight trough onto yet another GEM for even higher amplification or onto the pads for read out. Another advantage of the GEMs is that by removing the MWPCs one thus also removes size restrictions of the cathode pads. It is possible to use much smaller pads than with the traditional setup if the B-field is high enough. One of the drawbacks of the GEMs are that a GEM will provide no better amplification than allowed by its worst hole. It is therefore reliant on the methods of production being very precise, this was previously not the case and this is a reason for why the GEMs were deemed inferior to wires in the ALICE TPC at the time of the design. Now the GEM fabrication technology is mature enough to allow construction of large detectors.

6.2 New read out electronics

The GEMs will make use of novel electronics in order to take full advantage of the possibility to use smaller anode pads. Using GEMs will decrease the charge image for each ionization event. Thus the pads must be smaller which will in turn provide a better position resolution. It is estimated that the pad size will be in the order of 6 mm^2 [13]. The goal is to have all of the required front end electronics integrated into the same chip. A prototype setup is currently being developed, in particular for studying parameters which are of interest for the design of the final readout electronics. This setup and the results from the measurements is the main focus of this thesis and it will be discussed in the next chapters.

7 General Layout of the Data Acquisition System for the Prototype TPC

The anode pads used in this study are only 5.1 mm^2, using a pad size is thought to be optimal for the present magnetic field. The electronics of this prototype is based on the electronics used in the ALICE TPC but some fundamental modifications have been done in order to allow GEM readout. While the goal of a future TPC is to have all the electronics integrated on the pad plane it was not possible in this study since the Front End Cards (FECs) have a much larger area per channel than the pads themselves. For this reason long Kapton cables have been used to connect the FECs to the smaller pads. Below is a schematic figure of the whole Data AcQuisition system (DAQ).

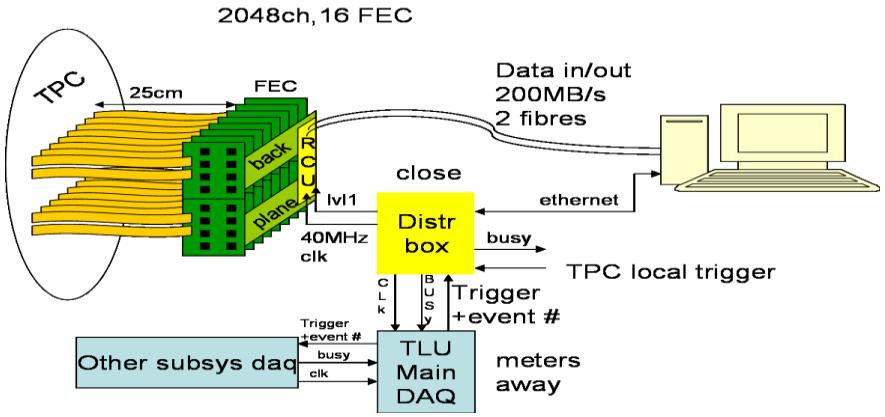

Figure 14: A General overview of the DAQ [14].

7.1 The Pad modules

The individual pads have the dimension of 1x5.1 mm and are etched on a so called pad module. The module accommodates up to roughly 4600 individual pads arranged with roughly 170 pads in the 1 mm direction and 27 pads in the 5.1 mm direction of the pads. The long edge of the pads will be in the direction of the radial component of the recorded track in a real ILC experiment. This is chosen to optimize the momentum resolution of the high momentum tracks, which are almost straight and radial. The spacing between each pad is 0.1 mm. The prototype end plate has room for 7 pad modules as shown in **Figure 14**. The end plate will be discussed in more detail in chapter 8.3.

The signal from each individual pad is then integrated with a multi pin connector mounted directly on the back side of the pad circuit-board. Since the pad has the dimensions 1x5.1 mm a very high-density connector is used. It has the dimension 13.9x4.7 mm, and contains 40 pins. A total of 32 pins are connected to the pads and 8 pins are used for grounding. While one ground pin per channel would be ideal the distance between each pad is so small that 8 pins evenly spread out will provide sufficiently good ground reference. Using 32 pins as connectors adheres to the modularity of 16 channels per chip on the FEC.

In order to systematically study the performance of such a GEM system readout of pads as described above a system of 10000 channels was developed. This allows full instrumentation of one pad module or partial instrumentation of three modules. Such partial coverage is acceptable as long as the incoming particles can be directed into a specific area where the read out electronics are located.

As mentioned above a pad size puts certain constraints on the possible electronics used. While the

belief is that the pad sizes can increase somewhat while maintaining a good momentum resolution further studies are needed to confirm this.

7.2 The Front End Electronics

Each of the FECs contains the charge to voltage preamplifier, the shaping amplifier and the digitizing functions of 128 channels. The charge to voltage amplifier/shaper is a newly developed programmable charge amplifier called PCA16 and the digitizing is done by the so called ALice Tpc Read Out (ALTRO) Application Specific Integrated Circuit (ASIC). Both of these ASICs will be dealt with in the forthcoming subchapters.

As previously mentioned the spatial dimensions of the FECs and the pads are far from compatible and for this reason the FECs have to be connected to the high-density connectors by long flat Kapton cables. While using Kapton cables will increase the noise, the noise levels are quite low because of the low input capacitance. Thus the noise levels as a whole will be acceptable assuming sufficiently short Kapton cables are used. In the prototype TPC Kapton cables with a length of 25 cm were used. This length is too long for optimal noise behavior.

The readout electronics used in the prototype have more rigorous design criteria than the demands on the performance than that of a final detector. While this might seem strange at first the reason for this is to make it possible to study which aspects of the electronics that can be optimized with respect to power consumption and cost while still maintaining a sufficiently good resolution required by the goals mentioned in chapter 4. Using less advanced electronics can vastly reduce the cost and power consumption of the final version detector and this work has been the main purpose of this thesis.

7.2.1 The PCA 16 ASIC

The programmable PCA16 is a charge preamplifier ASIC. It has, as the name suggests, 16 channels. The first tests of the performance were done on a non-programmable 12 channel version. This was done in order to determine whether or not the chip was up to the specifications for all the required parameters so that it could be used in the prototype experiment. The 12 channel chip had a fixed rise time of 100 ns and was produced on 130nm Complementary Metal Oxide Semiconductor (CMOS). The results from the tests are shown in **Table 6.**

Parameter	**Specification**	**Simulation**	**Prototype Samples**
Noise	*<500 e*	*300e (10 pF)*	*270e (10 pF)*
Conversion gain	*10 mV/fC*	*10 mV/fC*	*9.5 mV/fC*
Peaking time (Default)	*100 ns*	*100 ns*	*100 ns*
Non linearity	*<1%*	*0.35%*	*<0.3%*
Cross talk	*<1%*	*0.4%*	*<0.3%*
Dynamic range	*>2000*	*3300*	*4600*
Power consumption/channel	*<20 mW*	*10 mW*	*10 mW*

Table 6: Comparison between specifications, simulations and the test of the 12 channel non/programmable version of PCA16 [14].

The results of the tests show that the chip was up to specifications and in some cases, like for the dynamic range, well beyond the specifications.

The current version of the PCA16 boasts even better characteristics than the prototype chip. The chip is fabricated in a 0.13 μm CMOS process. The power consumption is 8 mW or less per channel. This power is supplied by a 1.5 V source. The peaking time is programmable in four steps ranging from 30 ns to 120 ns. The gain can be chosen in four steps, namely 12, 15, 19 and 27 mV/fC. The noise is kept low with a mere 300 electrons at 10 pF. The preamplifier output is single ended while the output amplifier is fully differential. On top of this both positive and negative input signal polarities can be selected.

The PCA 16 chip carries 94 pins in total. 9 out of these 94 pins are used to set the programmable parameters of the card. 16 pins are input pins and 32 pins are output pins for the differential signals. The remaining 39 pins are used for grounding and voltage supply.

The control for the chip uses the Board Controller (FPGA) which is used to set an octal Digital to Analog Converter (DAC) which is used to define the decay time of the pulse. An 8-bit shift register is used to set the rise time, the gain, the polarity and the ability to bypass the shaping function of the PCA 16 chip

7.2.2 The ALTRO Chip

The ALice TPC Read Out chip (ALTRO) was first developed specifically for the Alice TPC, hence the name. However, it was soon realized that its programmability and architecture would make it ideal for several other detectors as well. Each ALTRO Chip has the ability to digitize the analog signals from 16 channels. In addition to this the digitized data is simultaneously compressed and stored in a multi-acquisition memory. The chip has the dimensions 7.7 x 8.35 mm^2 and contains 6 million transistors. The embedded memory is 800 kbit and the supply voltage is 2.5 V.

The data transfer from the PCA16 for digitization in the ALTRO ASIC, is differential but it is internally converted to single ended analogue signals. The various grounding pins of the ALTRO chip will be used to provide the separation of the analogue and digital grounds.

Incorporating the 10 bit ADC onto the chip imposed some constraints as to how the other layout and the pin outs could be placed. The reason for this is that non-optimized placement of the ADCs would cause more noise than necessary. It could also pose some problems as to how effective the conversion from analog to digital signal would be. For this reason the ALTRO chip contains 8 ADCs on each long side of the rectangular ALTRO chip and the pedestal memories are placed in close proximity to the ADCs.

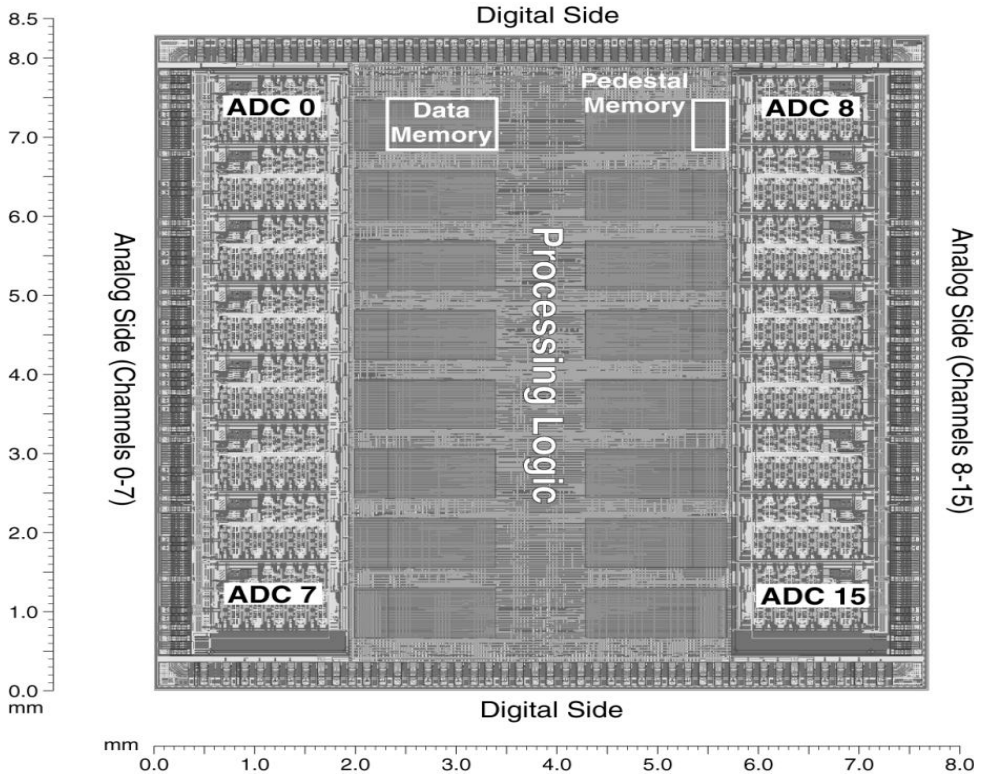

Figure 16: The layout of the ALTRO chip, note that the scale in the x and y direction are different [15].

As can be seen in **figure 16** the digital pads have been placed on the short edges of the ALTRO chip, this was done to minimize the noise.

The ADC is fully differential and it allows up to 2 V differential swing. Since the accuracy of the ALTRO Chip is 1 ‰ the Least Significant Bit corresponds to 2 mV. The bandwidth, and consequently the power consumption, of the ADC is defined by a polarization current which is provided for each channel by an internal resistor. It is possible to optimize the bandwidth and power consumption by changing a single metal layer. The ALTRO chip has been produced with two different ADCs, one with a maximum rate of 25 Million Samples Per Second (MSPS) and a power consumption of 12.5 mW and another chip with a maximum rate of 40 MSPS and a power consumption of 43 mW [15].

7.2.2.1 Baseline Correction

Once the signal waveform has been digitized, many manipulations of the raw pulse can be performed on the digital level. The ALTRO has several built in functions for signal processing.

The ALTRO chip is able to provide several ways of baseline corrections. The baseline corrections are performed in two different stages. In the first stage such operations as baseline corrections as channel to channel gain equalization, nonlinearity correction, baseline drift compensation and offset removal are preformed. The first stage can also be used to change the polarity of the signal as well as to subtract systematic signals originating from false sources. The removal of these signals is possible by using a pedestal pattern stored in the dedicated memory. The second stage in turn removes signal perturbations created by nonsystematic effects such as pickup noise.

The first stage of the baseline correction part of the ALTRO chip consists of a self calibration circuit and a pattern memory. The self calibration circuit continuously tracks the signal outside of acquisition time while at the same time computing the cumulative average of the signal. By using the last value

from the first trigger level as a self calibrated offset this can be subtracted from all the samples of the acquisition time and thus one can correct slow baseline perturbations, such as the perturbations arising from temperature drifts. The pattern memory on the other hand can be used to subtract the input signal from every value stored during each acquisition. This will allow for the removal of systematic perturbations. However, it can also be used as a specific Look Up Table (LUT) which will enable dynamic conversions alternatively it can be used to equalize the signal over different channels. On top of this the memory can be used to inject a pattern in the processing chain that can be used to test all the subsequent circuits.

The second stage of the baseline correction, which is used to remove nonsystematic effects, operates by assigning a baseline signal with an upper limited threshold thr_{hi} as well as a lower level threshold thr_{lo}. The baseline is then continuously updated based on the last eight samples which lay between the two thresholds. If on the other hand there is an abrupt change of the signal that puts it over or under the allowed threshold window then the signal is excluded from the baseline calculation. The value of the signal is then corrected by removing the last value of the moving average filter and as such the signal would be sitting on zero. The principle behind this is shown in figure 15.

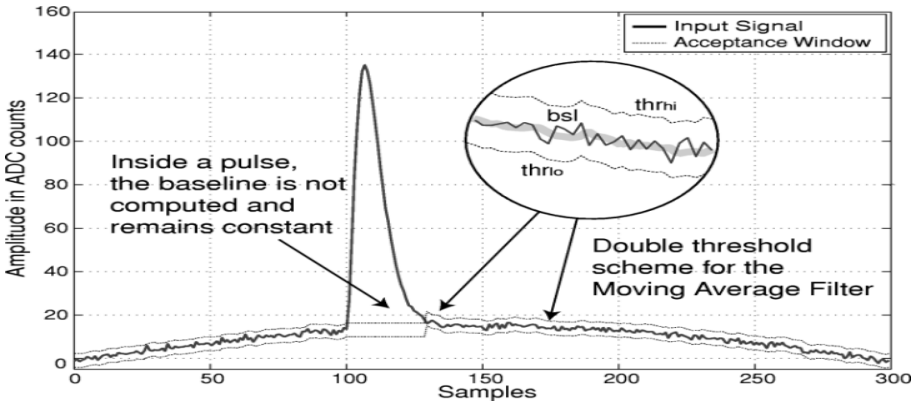

Figure 17: The principle behind the removal of nonsystematic effects [15].

7.2.2.2 The Tail Cancelation Filter

The signal coming for the pads has a quite characteristic behavior. The signal has a very short rise time, often in the order of 1 ns or less. This short rise time is then followed by a long and quite complex tail generated by the moving positive charges in a MWPC. The shape of the tail is dependent on the geometry of the pads and details of the chamber it self. The long tail can cause pile up effects when the rate of interaction is high. This is what sets the most pressing constraints on the track density which the detector can be exposed to. The ALTRO is outfitted with an 18 bit fixed point Tail Cancelation Filter (TCF) which can suppress this tail within 1 as after the peak. This is done with an accuracy of 1 ‰ which is, in this case, also equivalent to the LSB. It is important to note that while the shape of the signal arising from a pad is often characterized as previously mentioned, the TFC is programmable and can be used to suppress a wide range of signal shapes.

As has been mentioned before the GEMs greatly reduce the tail of a pulse. Nevertheless a tail cancelation filter is still used in the ALTRO.

7.2.2.3 Zero Suppression

After the baseline corrections and the tail cancelation have been performed one can apply a zero suppression function. Zero suppression implies that any signal under a given threshold is removed. If

the baseline can be assumed to be flat then threshold can be as low as the peak noise level. By removing the samples below this threshold the data compression will be enhanced. The zero suppression function of the ALTRO chip can also be used as a glitch filter; the glitch filter checks for consecutive samples above the threshold value. By doing this it can be determined whether or not a sample actually originates from a real pulse or from some source of noise. The ALTRO chip can also record pre and post samples of non zero samples. This is essential in order to be able to study the full pulse shape which in turn is necessary so that further extraction of information can be performed.

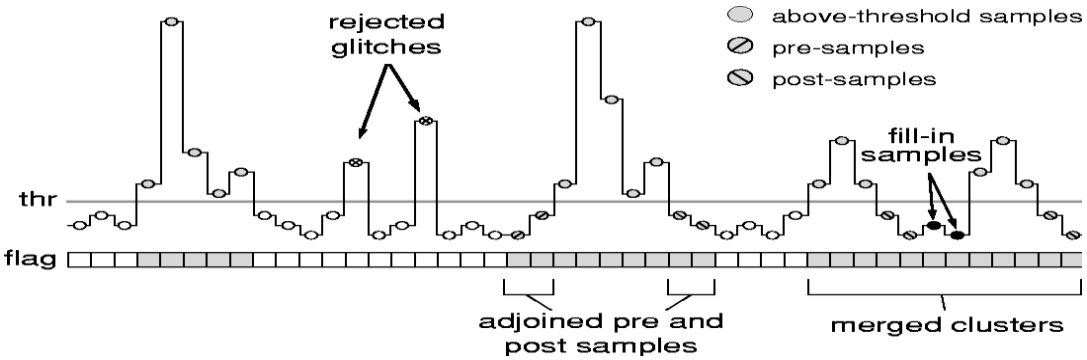

Figure 18: An example of the zero suppression scheme. [15].

The ALTRO ASIC has more functions than the ones described above, they are however nonessential for this thesis and are thus dealt with in Appendix A.

7.3 The Data Acquisition system hardware and software

Some of the Data Acquisition System is based on the DAQ used in ALICE but since the demands on LCTPC prototype, in this regard, is less than those of the ALICE system some simplifications have been made in order to simplify the DAQ for the LCTPC.

Just like in the ALICE experiment the information from the FECs is sent trough a Detector Data optical Link (DDL) and to a Detector Read Out Receiver Card (DRORC) which is a 32-bit Peripheral Component Interconnect (PCI) card located in a normal PC. The FECs themselves are controlled by a Readout Control Unit (RCU). However, while the ALICE experiment uses a Trigger and Timing Control (TTC) and the ALICE Detector Control System (DCS) to for acquisition of data these rather cumbersome and complex systems have been replaced in the LCTPC prototype by the Distribution BOX (DBOX) and a Trigger Logic Unit (TLU), see **figure 14**. With the replacement of the TTC the minor modifications to RCU have been necessary since the trigger and clock signals will be received from cables and not the TTC itself. In the LCTPC prototype the TLU works as a central trigger distribution for all the sub-detectors. While the drivers and libraries that are used for readout of the hardware are exactly the same as the ones used in the ALICE experiment a standalone system for monitoring and histogram presentation have been developed for the LCTPC prototype [14].

7.3.1 Trigger and Readout

The trigger system consisted of four scintillators. These four scintillators were placed two by two with a distance of 1 m between each pair in the path of the electron beam. If all four scintillators triggered in coincidence a no trigger signal was sent signaling the passage of a beam electron. This enables discrimination from, for instance, cosmic particles which travel non-parallel to the electron beam.

In order for the LCTPC prototype to start acquisition of data a START DAQ command must be received from the run control. The START DAQ command will open the necessary devices, setup and configure the readout and download the configurations that will be used to set all the variable setting in the PCA16 and ALTRO chip etc. After this the system will be idle until it receives a START RUN. When a START RUN command is recieved the system is ready to receive triggers. If a trigger event is detected in the DBOX it sends a signal to the RCU which in turn will distribute the signal to the FECs. This signal will then start the digitization by the ALTRO chip to which the data from the PCA-16 chip is sent. The data stored in the ALTRO chip is continuously read out by the RCU and stored directly in a file located on a local storage disk.

8 The Mechanical components and the gas mixture of the TPC prototype

The mechanical components play a vital part in determining the performance of the TPC and the individual parts will be discussed in the forthcoming subchapters.

8.1 The Field Cage

In order to reach the desired requirements on the homogeneity of the electric field in a TPC, a field cage is used. The desired homogeneity of the electric field in the LCTPC prototype is that fluctuations should be no larger than 10^{-4} of the field strength. The field cage used in the LCTPC prototype consists of several 35 μm thick copper strips placed on to a 75 μm thick Kapton foil glued to the inside of the chamber wall. They lie with decreasing negative potential from the cathode to the anode and this serves to increase the homogeneity of the electric field. However, these strips alone do not serve to make the electric field homogenous enough because they will have small gaps between them. These gaps can then lead to a so called punch through effect. When this happens the applied external field will perturb the internal field which is the opposite of what one is trying to achieve. In order to prevent this from occurring a second layer of copper strips is added on the other side of the Kapton layer, these strips are called mirror strips. The mirror strips are connected through the foil and have a potential between two neighboring strips.

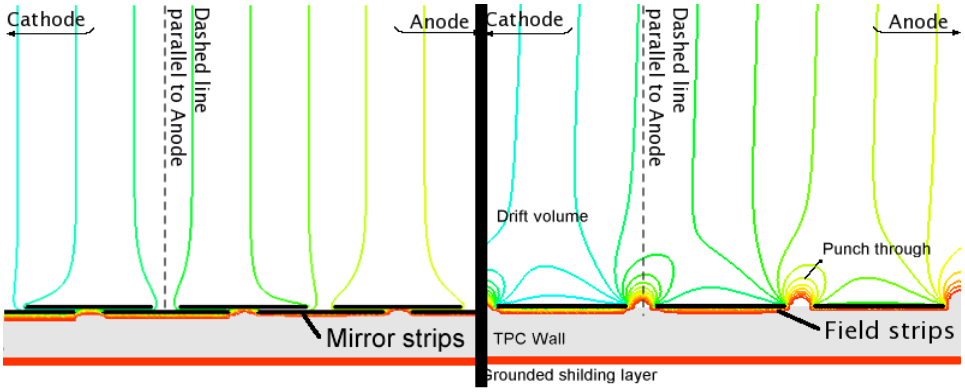

Figure 19: A sketch showing the difference between a field cage with mirror strips to the left and one without to the right [16].

The field cage must be compatible with the magnet used in the prototype. For that reason the length of the field cage used in the LCTPC prototype is 0.61 m long and has an inner diameter of 0.71 m. The outer diameter of the field cage is 0.77 m. The inner diameter of the magnet is 0.86 m and the extra distance between the field cage and the magnet is to allow the placement of a silicon strip detector between the two. However, during the test runs discussed in this thesis no silicon detector was used.

In order to achieve the desired specifications of the electric field homogeneity the mechanical accuracy of the field cage can be no less than 100 μm. At the same time the field cage should be able to withstand an overpressure of about 10 mbar. While this could prove a problem in itself it becomes even more of an issue when taking into account that a low material budget is needed in order to minimize the scattering and conversion of photons between the TPC and a planned vertex detector. While a vertex detector is not planned to be compatible to the prototype the electron beam will pass trough the chamber wall. For this reason the material budget of the LCTPC prototype must be kept close to 1% of the radiation length of the material.

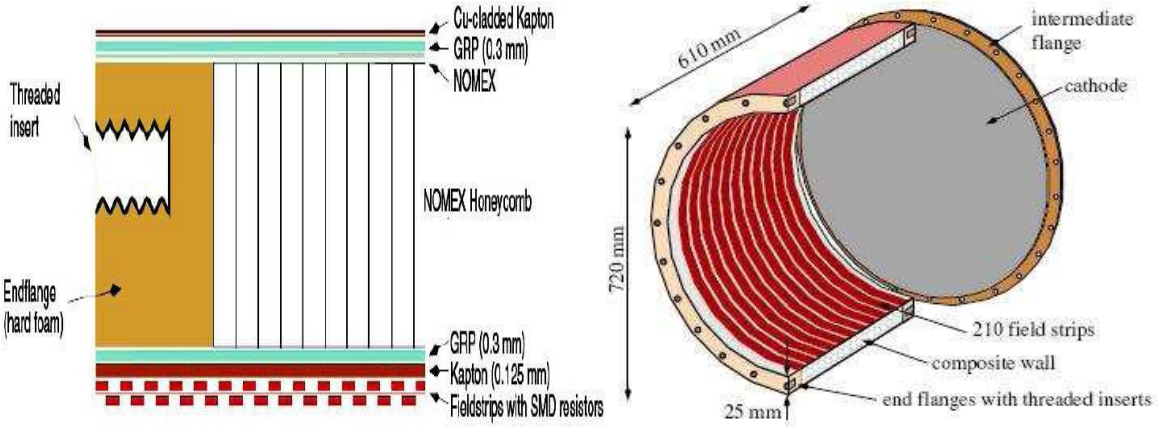

Figure 20: The left hand side shows the cross section of the chamber wall and the right hand a schematic image of the field cage [18].

The supporting walls of the field cage are made out of 23.5 mm thick layer of aramid fibre (NOMEX) with a honeycomb shaped structure. This fibre is covered with a layer of fibre glass reinforced plastic on each side and an insulating layer of polymide. The KAPTON layer is 125 μm thick and that is more than enough to prevent breakdown events at an operational voltage of 20 kV.

8.2 The Magnet

In order to generate a sufficiently high magnetic field strength a Permanent Current MAGnet (PCMAG) is used. This is a superconducting solenoid shaped magnet. The maximum current that can run through it is 520 A and this will generate a magnetic field of up to 1.2 T. The highest magnetic field strength used during the experiments in this thesis was 1 T. Since it is a superconducting magnet it must be cooled to a very low temperature, so liquid He is used.

The magnet covers the whole field cage and the bore of the magnet has a diameter of 0.85 m and a length of 1.30 m. The homogenous part of the magnet stretches 0.30 m in the forward and backward direction of the center of the magnet, which is what sets length limit of the TPC prototype.

The magnet was stationary during the measurements discussed in this thesis. For this reason the drift length of the electrons could only be altered by moving the TPC itself inside the magnet. This was not a problem since the read out electronics was fixed on the TPC and followed in the movements. The drift lengths vary between 0.070 m and 0.300 m which is within the homogenous parts of the B-field. The standard drift length in this study is 0.150 m which is safely inside the homogenous region. In experiments performed lately, the whole setup of magnet and TPC was movable relative to the beam, thus allowing measurements of different depths of the TPC under constant B-field conditions

8.3 The End Plate

The endplate used in this experiment is circular in shape and has a 0.77 m diameter. The material used is aluminum. As shown in **figure 21** the end plate has openings for seven pad modules. However, during the data taking no more than 3 modules were used at once. The end plate used in the LCTPC prototype is supposed to represent a subsection of the whole planned end plate of the ILD-TPC. The location and direction of the end plate and the modules placed within was perpendicular to the beam path so that the momentum resolution would be optimized for tracks that have very small bending radius in the ILD-TPC i.e. an optimization on the highest momentum for which the demand on position resolution are the highest. The end plate was also shaped in such a way that an electronics crate containing the FECs could be attached.

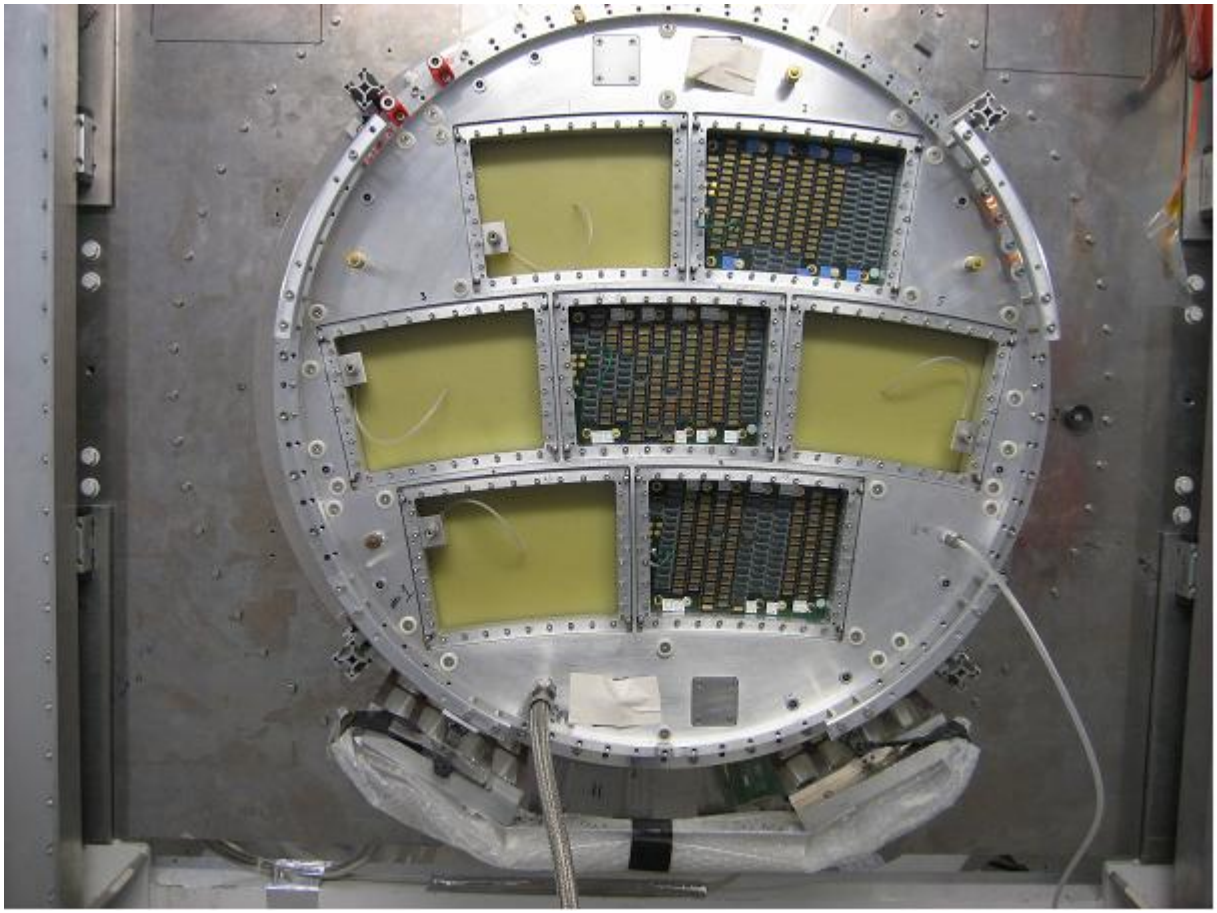

Figure 21: The end plate used in the TPC prototype with three attached pad modules [17].

8.4 The High Voltage System

The High Voltage (HV) system used to supply the voltage to the cathode used in the TPC is capable of delivering voltages up to -20 kV which was applied for the central cathode. Since the measurements performed with the LCTPC prototype were done with three pad modules the unused parts of the end plate were filled with dummy modules to mitigate the effects on the inhomogeneity of the electric field. In addition to this a second HV input was added at the 7th field strip. By connecting the 7th strip and the dummy modules to the same output the potential between the various components should be kept the same. However, due to miscalculations, distortions to the electric field near the first GEM in the stack were a source of concern in the performed measurements due to the extremely high

sensitivity of the systems for such effects.

The GEM modules had a HV source of their own and this HV source includes a mechanism which protects it from discharge by continuously monitoring the current and switching the voltage to zero in case of an event where the current exceeds a few μA for a few seconds. The voltage distribution to the GEMs was done by the use of a resistor chain as a voltage divider between the GEM surfaces.

8.5 The Cooling system

In order to keep the electronics from overheating, a cooling system has been developed for the LCTPC prototype. This is nontrivial since the electronics is inside the magnetic field where electric motors can not be used. During the measurements performed in 2009 a large fan connected to the FEC through a large aluminum tube were used. In the 2010 measurements this rather cumbersome setup had been replaced with a cooling system consisting of perforated copper tubes connected to a compressor through high pressure tubes. The copper tubes were then attached to the electronics crate used to house the FECs.

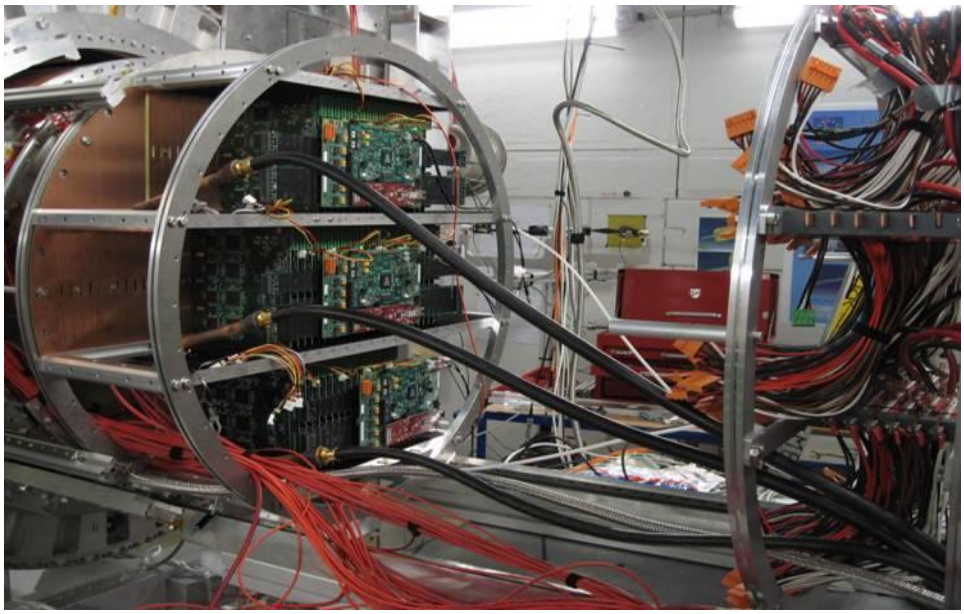

Figure 22: The cooling system used during the 2010 measurements. Black rubber tubes connect the copper tubes to the compressor [17].

Monitoring of the temperature was done continuously and automatically by sensors placed on every 4th FEC. Continuously monitoring the temperature of the electronics is important not only as a safeguard for the hardware but the pedestals also vary with temperature so even if the electronics themselves are unharmed the measurements can become void if the temperature fluctuates.

8.6 The Gas Mixture

The gas mixture called T2K, named after the Tokyo to Kamiokande neutrino experiment where it has been extensively studied, was used in the LCTPC prototype. It contains three different gases, 95% Argon, 3% Tetraflourmethane and 2% Isobutane. The T2K gas has a low diffusion coefficient so it should be possible to use in conjunction with the other equipment to provide a sufficiently good

resolution so that the goals of the ILD can be met. It has been shown that the gas provides the best overall drift performance at 250 V/cm [19].

The properties of a the gas do not only vary with the electric field strength but also with the temperature, pressure and the level of contaminating contents such as oxygen. For this reason these proprieties were monitored and noted for each run.

9 Data Analysis

The information collected in the LCTPC prototype must be properly processed in order to obtain more meaningful information and discard the superfluous and faulty information. The raw data collected for each pad contains, as described above in chapter 6, the channel number, the time information and the ADC sampled values of the pulses. The data acquired during the measurements are handled with C++ code and with the help of a library called ROOT. ROOT was developed at CERN and contains several useful tools suitable for data analysis in particle physics, such as several various ways of creating histograms as well as various fitting methods. After exporting the raw data the reconstruction of a particle path has been done in three steps by three programs; pulse reconstruction, clustering and lastly track fitting. Due to the design of ROOT where data from each step is stored as an object all the information, be it information about a single pulse or several clusters, are easily available.

These three programs which have formed the framework of which I have been working in have been written by *Martin Ljunggren* and *Phillipe Gros* and will be discussed more in detail in the next sub chapters.

9.1 Pulse reconstruction

When two pulses arrive within such a short time span that the first pulse has not fallen below the threshold, usually 4 ADC units, in the ALTRO chip this will at first appear as one single pulse. Having what is in reality two separate pulses analyzed as one large pulse will degrade the quality of the tracking. As such it is important that the pulse reconstruction can divide the two pulses into two separate pulses. This separation is done by having an algorithm check for ADC values in time sequence and comparing each value, over the threshold value, to the preceding value. The highest ADC value found in such a series of values is flagged as the peak of the pulse. The highest ADC value found in such a series of values is flagged as the peak of the pulse. However, if an ADC value is again discovered which is higher than the previous one then this value will be tagged as the peak of a new pulse if also the next value is higher than the value detected before the previous value. This new pulse will then be stored in a separate pulse object. A minimum increase of three ADC values is needed to flag a value as a new peak; this is to try and avoid false peaks originating from noise fluctuations. This algorithm does not compensate for the buildup of the second pulse caused by the first pulses' tail but most of the time the effects will be very small.

The time and total charge of every detected pulse is then calculated. By using a voltage weighted mean of five samples surrounding the peak of the pulse the arrival time can be determined and the height of the peak represents the charge.

During the measurements performed in 2010 the setup suffered from some readout channels becoming more or less inactive. Such a readout channel is called a dead channel. This can cause severe problems for the data reconstruction especially in the clustering stage. As such it is important that it is dealt with in the step preceding the clustering which is why this is done in the pulse reconstruction stage. The way this is done is by flagging a readout channel as dead if no more than 10 counts are detected during

a full run. This value is well below the value which one can expect from an active readout channel.

The final step of the pulse reconstruction is to store the data in a pulse file. This file will then contain all the information regarding time and charge for each detected pulse which is needed to perform the clustering.

9.2 Clustering

The clustering is done by adding pulses from adjacent pads into a cluster. The pulses are added pad row by pad row. Like the pulse algorithm the clustering algorithm searches for the pulse with the highest ADC value in a pad row and it then adds any neighboring pad to the cluster. If it detects an empty pad, that is a pad without a charge above the threshold, it will stop searching in that direction and then it will continue searching for pads in the opposite direction until it reaches an empty pad in that direction. When an empty pad has been detected in both directions of the pad row the clustering algorithm has identified a whole cluster. This is assuming the empty pad has not been flagged as a dead channel by the pulse algorithm in which case the cluster algorithm checks the subsequent pad. If it detects a charge in a pad on the other side of the dead channel the whole cluster is flagged as bad. While it would be possible to redeem such a cluster it is in practice unnecessary since the tracks normally have enough clusters to be well enough measured.

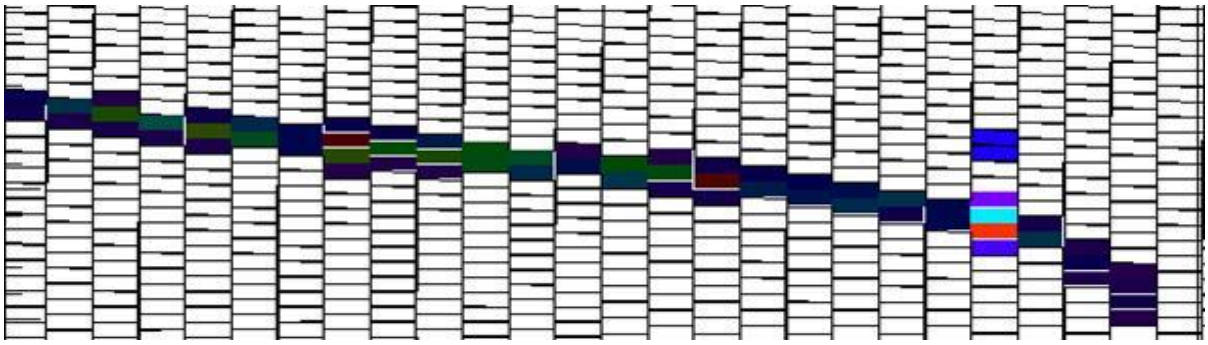

Figure 23: An example of track of a particle with row of colored pads making up a separate cluster. The fifth pad row from the right contains two separate clusters [17].

The cluster will then be used to provide a more precise position in the *x* and *z* direction. This is done by weighting the pulse charges according to eq 19.

$$x = \frac{\sum x_i Q_i}{\sum Q_i} \qquad (19)$$

Here x_i is the coordinate in the *x* direction along the pad row for the *i:th* pad and Q_i is the charge in the same pad. The total charge of a cluster is the total charge of all the included pads in the cluster. The *y* coordinate is given by the location of the pad.

Just as with the pulses two or more clusters can sometimes be located in such close proximity of each other that there are no empty pads between them. Such a cluster can be separated by the clustering algorithm in similar way as the pulse algorithm does. In the analysis performed in this thesis events with more than one track have been dismissed. However, for real data it is important that nearby tracks can be both distinguished and handled since decays of high momentum particles produce secondaries with small opening angles.

9.3 The tracking

The test measurements and the planned measurements in the ILD will be of a relatively low track density. Because of this the tracking algorithm can be relatively simple. The tracking starts by assigning a cluster in the right most pad row of the pad plane as a starting point for a track. The reason the right most cluster is used is because of the fact that the beam path is parallel to the *y*-direction and the direction of the beam is from the right to the left. When a cluster has been found in the rightmost pad row the tracking algorithm opens search windows in both the *z*-direction, which is the drift direction, as well as the *x*-direction. If a subsequent cluster is found within the predetermined window then this cluster is added to the track. However, if a cluster is not found then the algorithm will skip onto the next row window searching for yet another cluster. If this pad row turns out to be empty as well the track candidate is rejected. If a new cluster is instead found then the tracking algorithm will proceed as normal. In this tracking a track candidate must contain a certain number of clusters in order to be classified as a track. This number is usually ten per pad panel, but this can be increased with little loss of tracks. A track candidate must also not contain more than two empty pad rows or it will be discarded nor can it contain more than four separated empty pad rows. The only way a track can contain as little as the previously mentioned ten clusters is if the track leaves the instrumented region. If it traverses the entire active area, as it is supposed to, it will contain 28 or close to 28 clusters.

In order to allow for several tracks to be detected during the same event each cluster belonging to a track is flagged as belonging to a certain track. After a track has been fully determined the tracking algorithm will then search for additional clusters belonging to another track by using all other clusters as a possible starting position of a track. The ability to detect, and discriminate against, multi track events is important because most multi track events originate from γ conversion close to the TPC and as such are not tracks that one wants to study in this point of the detector development. As previously mentioned the final TPC will need to be able to resolve close laying tracks originating from decays of high momentum particles.

The measurements performed in 2010 have some noise effects which originated from the motor used to move the magnet. This gave rise to short stochastic bursts of noise which would trigger every single pad. Since the bursts were short they are rather well defined in the drift direction and as such the events where the noise is close to a track and the events where the noise is far from the track can be separated.

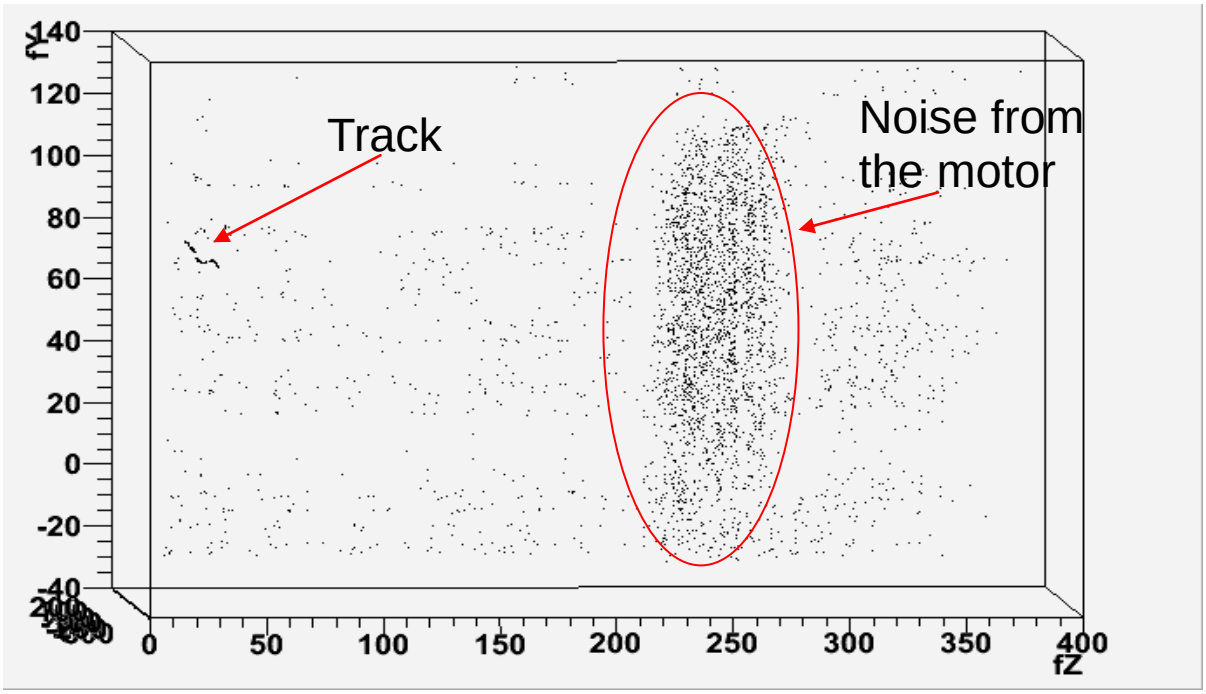

Figure 24: An example of an event where the motor noise is located far away from the track.

When all the possible tracks have been determined by the tracking algorithm the coordinates are fitted with a straight line in the case of a run without magnetic field and a second degree polynomial in the case of a run with a magnetic field.

10 Analysis done in this thesis

Various analyses have been performed on the data within the scope of this thesis but the main focus of this thesis has been to test the robustness of the LCTPC prototype data. In other words, how well within the desired limits found in **table 5:** is the current setup and is it possible to compromise on parameters of the system while still retaining a sufficiently good resolution. This has been done in several ways, such as, varying the sampling frequency and the ADC resolution.

10.1 Spatial resolution

The residual resolution is then measured by performing a Gaussian fitting to the residuals distribution. The residual is the deviation of the cluster coordinate from the track fit. While it would be optimal to have a second detector to measure the true path of the track no such detector was available during the time of the measurements. For this reason the true path of the track is chosen to be the track determined by the tracking algorithm and the fit to the track. The width of the residual distribution will be slightly worse than the true position resolution since the inaccuracy originating from the fact that the track position is represented by the fitted track will be folded out. On the other hand, inaccuracy from systematic effects from track to image on the pad plane may not show up in the analysis.

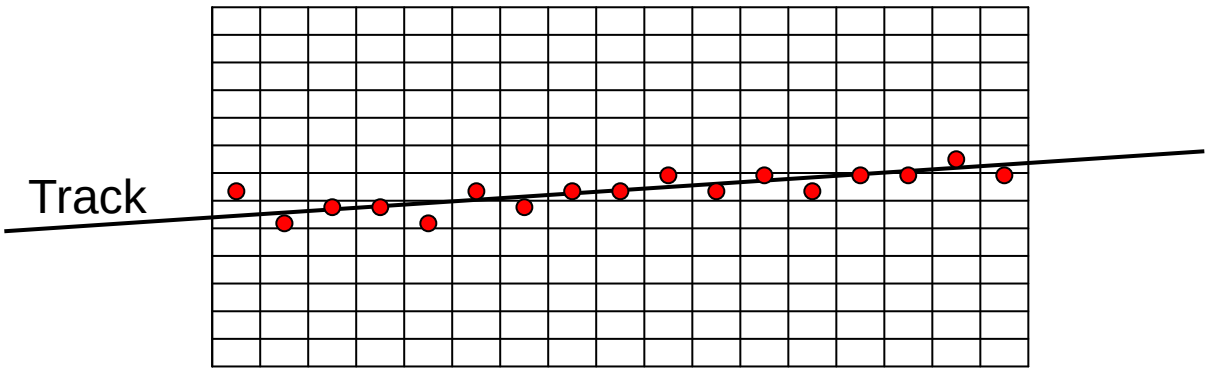

Figure 25: The concept behind the position resolution. The distance from each red dot, which represents the cluster coordinate in the pad row, to the fitted curve of the track gives the residual distribution for the run.

Due to the fact that the tracking is used to determine the true path of the particle it will give rise to some bias in the residual resolution. If one includes the clusters being investigated the perceived residual resolution will be slightly better than it really is but if the points are excluded then the perceived resolution will be worse. For this reason it is advantageous to use the geometric mean of the two methods to determine a more realistic value of the spatial resolution.

$$\sigma = \sqrt{\sigma_{Inc} \cdot \sigma_{Exc}} \qquad (20)$$

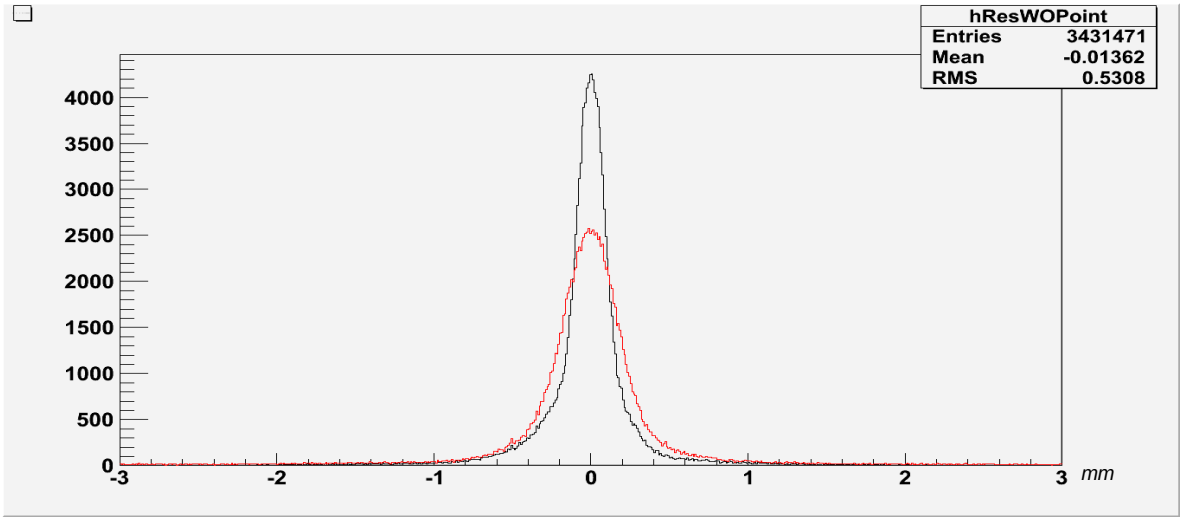

Figure 26: The residual distribution with a fitting which includes the residual value is shown in black whereas the red histogram corresponds to a fitting done while excluding the residual. The measurement was done with a B-field of 1T and a drift length of 150 mm.

While the most correct value for the residual resolution is found by taking the geometric mean the forthcoming analysis is done with the point included in the fitting. Since the analysis focuses on how the resolution is affected by for instance varying the ADC resolution whether one uses the geometric mean or simply the fitting which uses the included point is of little importance since the relative difference should be the same.

The spatial resolution of a run done with a magnetic field should be better than for a run without a magnetic field present. This is because the magnetic field limits the diffusion of the electron clouds. However, at a first glance of the data it did not appear to be the case.

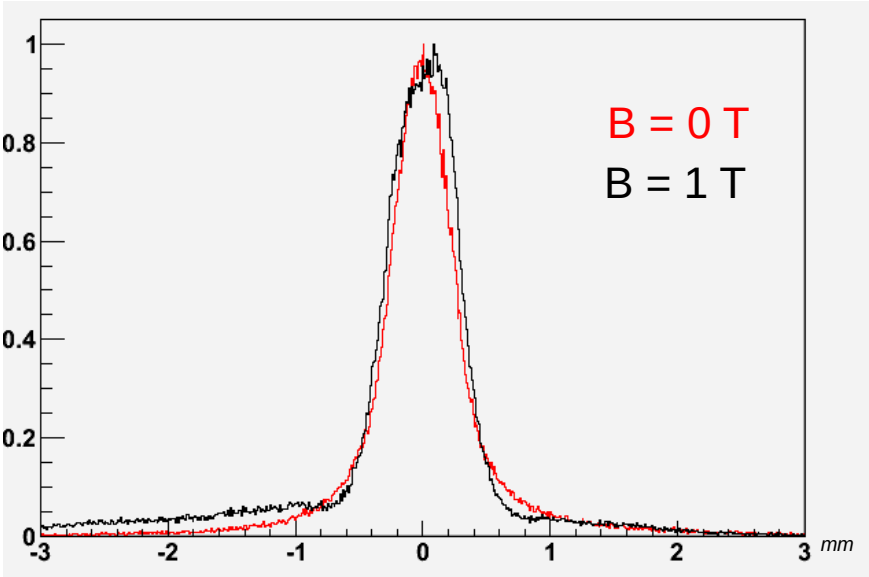

Figure 27: The residual distribution with and without a magnetic field present. The drift length of both runs were 150 mm.

Unfortunately, the measurements taken during both 2009 and 2010 suffered from distortion effects caused by an inhomogeneous electric field at the module edges. This was due to the fact that the field shaper was not properly configured. The 2010 measurements also suffer from some misalignment between the three modules. These effects are to some extent handled and corrected by the tracking algorithm.

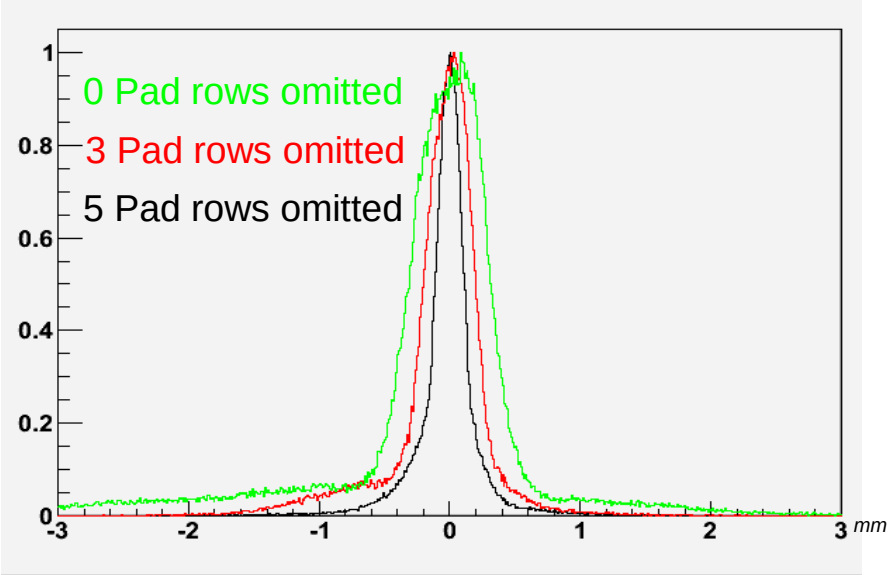

Figure 28: The residual resolution of a run with various number of pad rows omitted, starting from the module edge.

While it might seem as if omitting more and more pad rows yields a better resolution result this is not desirable since the loss of clusters will be too large. By trial and error it was determined that the best result while retaining sufficient statistics was obtained when discarding the five outermost pad rows on each side. It is worth noting that this fit is done with a second degree polynomial. If a higher degree polynomial is used the fit becomes better in the distorted region but it is not desirable from a physics viewpoint to use anything but a second degree polynomial as a fit to a run with a magnetic field.

When the outermost pad rows have been omitted from the analysis the resolution is as expected better when there is a magnetic field present during the measurements.

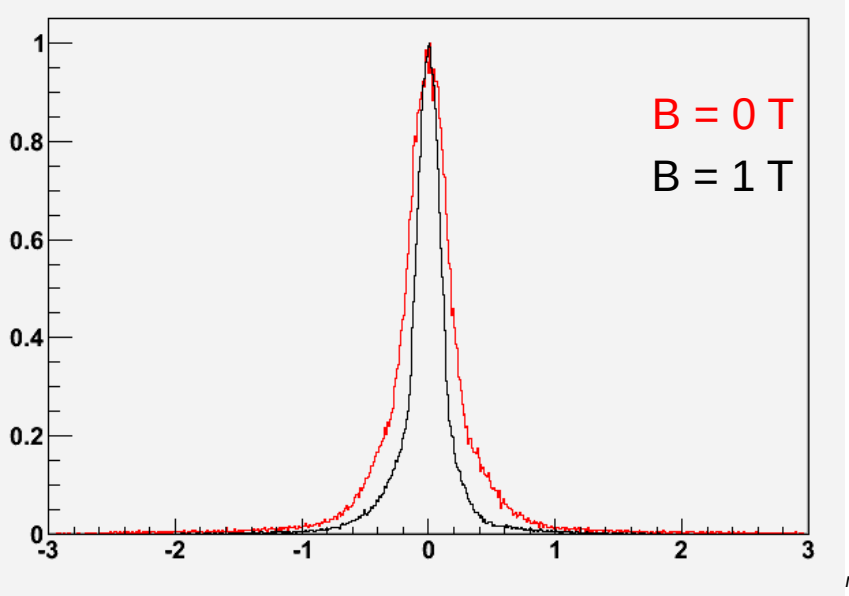

Figure 29: The residual distribution with and without magnetic field with the 5 outermost pad rows removed on each side.

Ways of optimizing the results have also been tested. Among these are tests as to which value used for truncation that yields the best *dE/dx* resolution and a new fitting method for the tracking algorithm has also been tested. All the various analyses will be dealt with in the next sub chapters.

10.2 Gain Drops

While most discrepancies such as merging clusters are handled in the steps mentioned above the measurements suffered from one additional distortion. The amplification of the GEMs would suddenly drop for a short time. This will result in pulses with much lower ADC values than one would expect for a particle with that energy loss. While it did not happen often it was frequent enough to affect the pulse amplitudes. For this reason a program was developed to automatically detect and remove events happening during these gain drops.

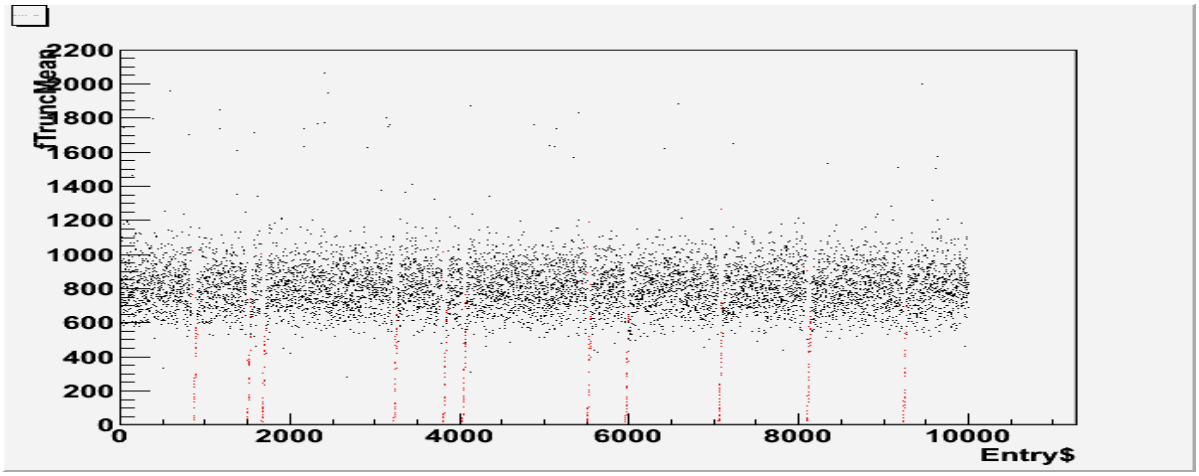

Figure 30: The gain drops marked in red are clearly visible. The red dots are flagged as incorrect and later removed

The program searches trough each consecutive value and detects if two consecutive entries have truncated means which are below a certain set limit.

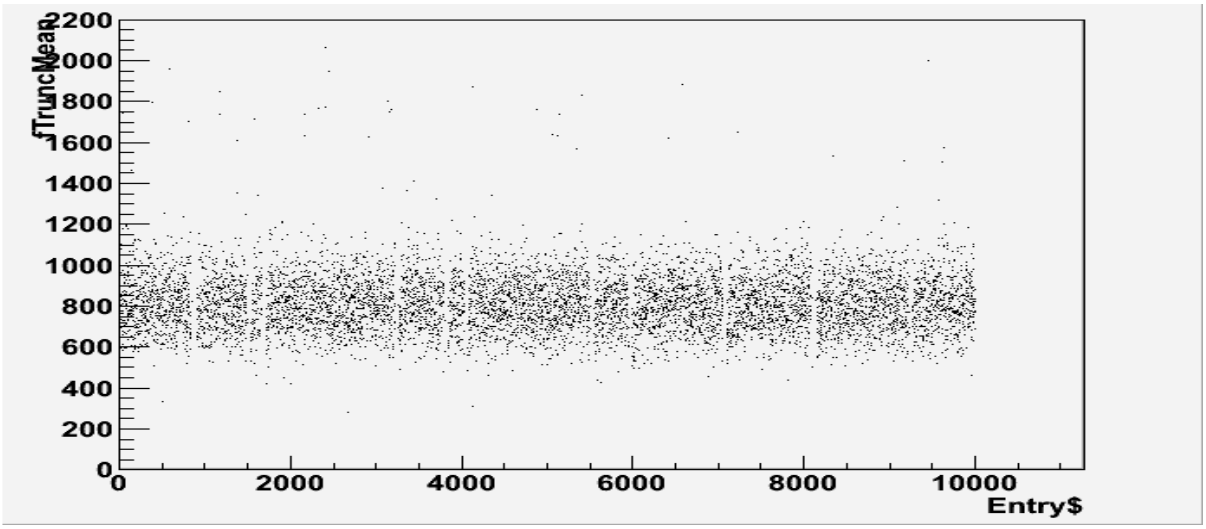

Figure 31: The gain drops previously visible around entries 2300, 4600 and 6000 have now been removed. Here the x-axis indicate the event number.

10.3 Residual distribution depending on ADC resolution

Using an ADC with fewer bits would be less costly not only in production cost but it would also have lower power consumption. If it is possible to keep the residual distribution for 6-bit ADC at the same level as a 10-bit ADC it would be advantageous to use the 6-bit ADC in a final design.

The data acquired during both the 2009 as well as the 2010 measurements where all taken with the setup described in chapter 6 and 7. As such the resolution of the ALTRO ADC was 10 bits. To study whether or not the number of bits can be decreased while retaining a sufficiently good residual distribution the collected data had to be modified. This was done by implementing an option where the range of the sample was kept constant but the size of the ADC bins were increased in factors of two.

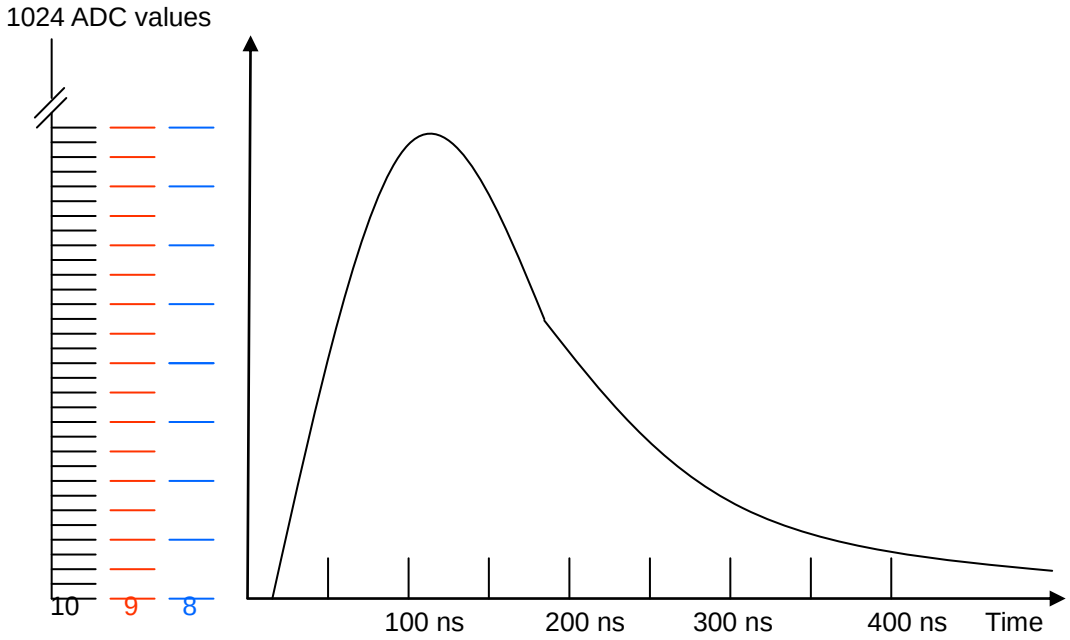

Figure 32: A conceptual sketch of how a bit reduction from 10 bits to 9 and 8 bits is done.

After the ADC resolution has been set to the desired value each of steps mentioned in chapter 9 are performed and the residual distribution is determined as described in chapter 10.1.

The histograms of the various ADC resolutions for run 7415 are presented in **figure 33** and **figure 34** whereas the residual resolution vs. ADC resolution is presented in **figure 35.**

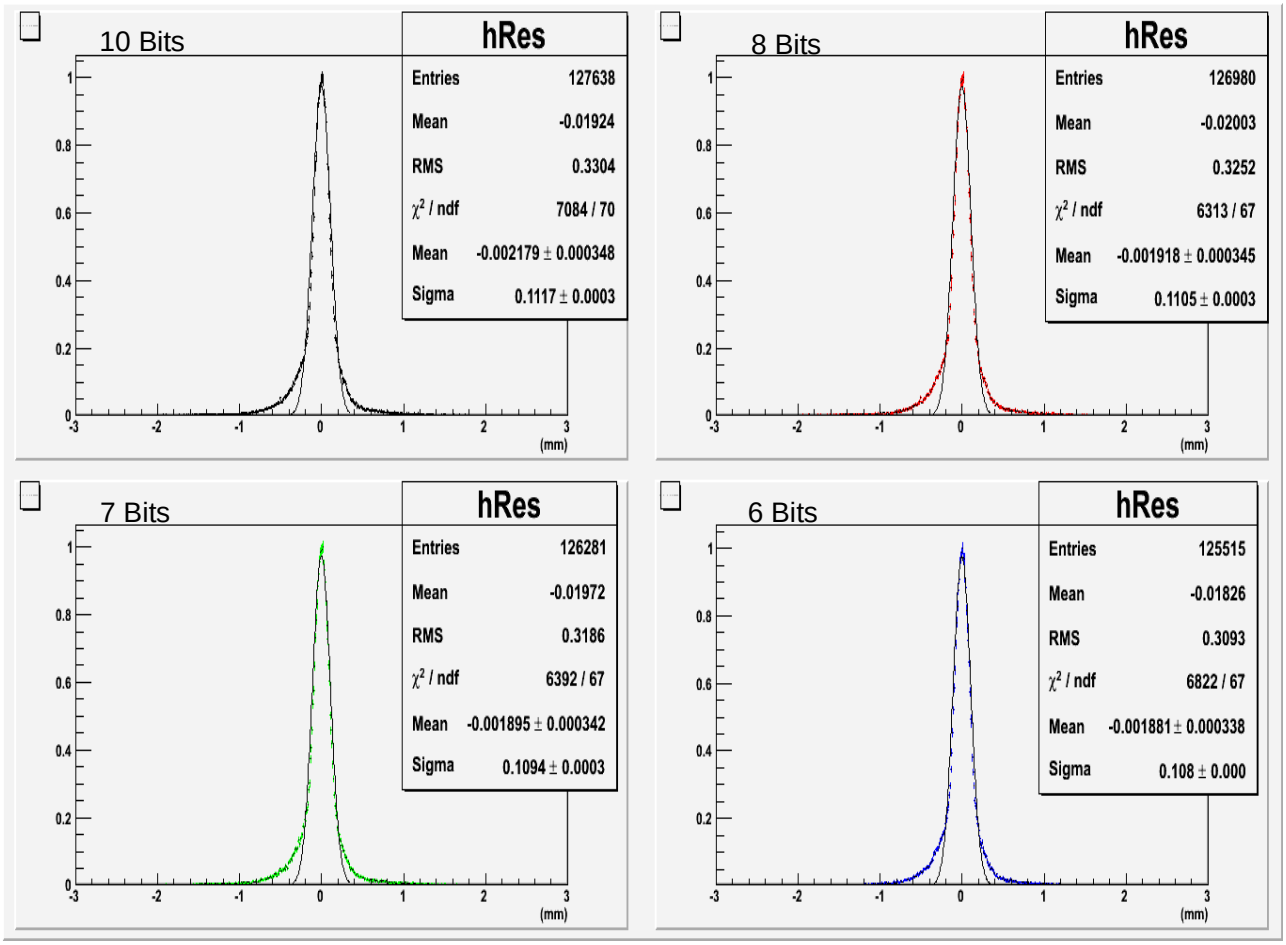

Figure 33: The residual distribution of run 7415, with a drift length of 150mm and a magnetic field of 1 T. The value of sigma indicates the resolution in mm.

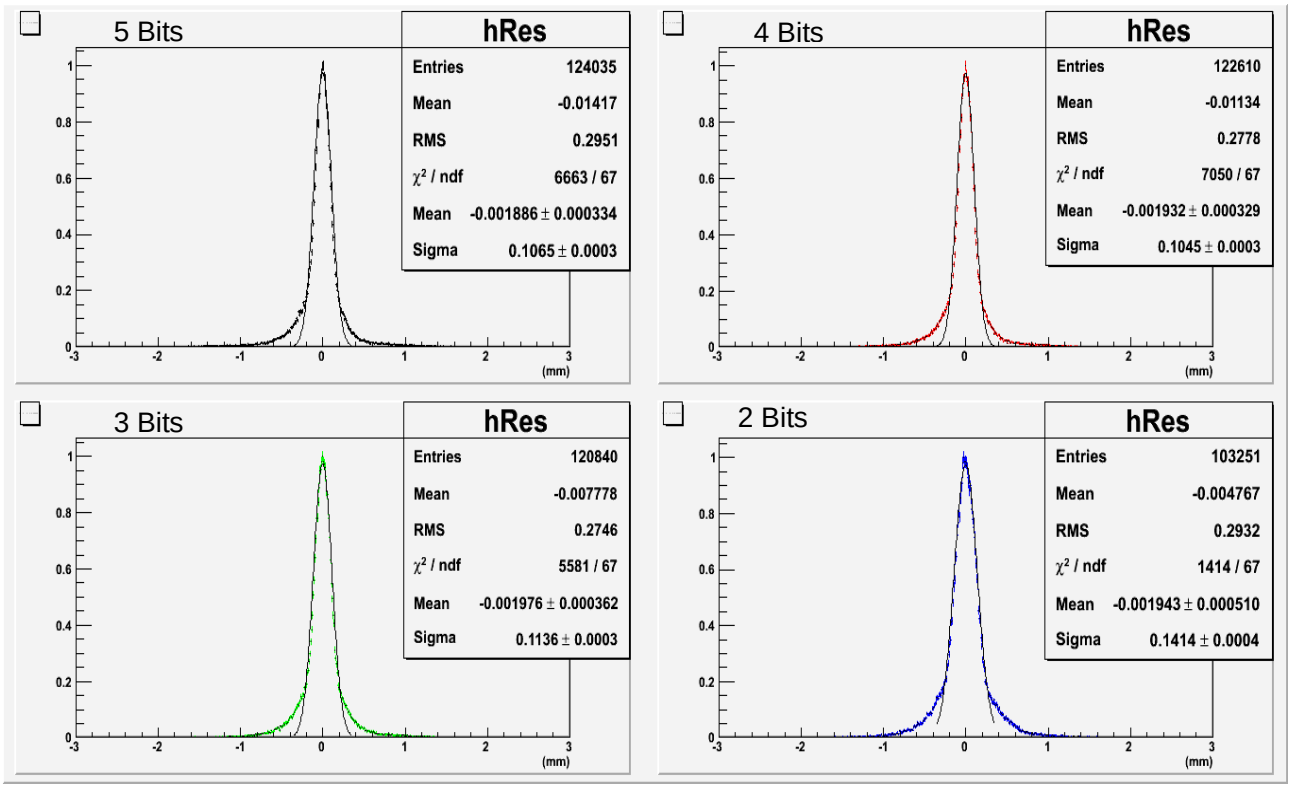

Figure 34: The residual distribution of run 7415, with a drift length of 150mm, a gain of 27mV/fC and a magnetic field of 1 T.

As can be seen in the above figures the resolution is largely unaffected for ADC values from 10 down to 4 bits. The residual resolution is actually improving, albeit minimally, with decreasing ADC resolution down to an optimal resolution at 4 ADC bits. This can possibly be because a majority of the relatively few clusters that do disappear due to the reduction in ADC bits are clusters with weak signal arising from perturbations and not the real track. In order to determine whether or not this is the case more in depth studies are needed. What is apparent is that after 4 bits the real and good clusters are starting to be affected as well.

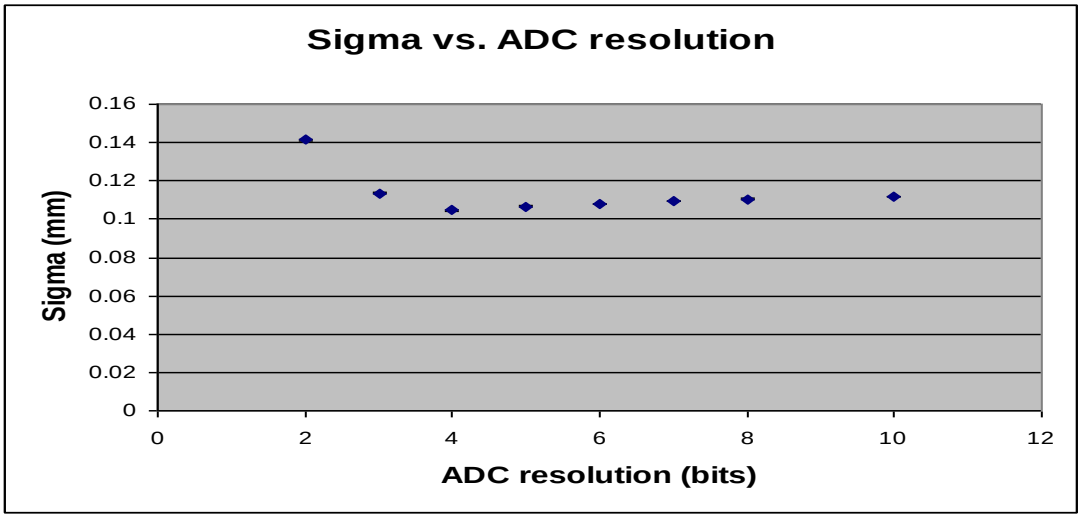

Figure 35: The residual resolution with respect to the ADC resolution. The magnetic field was 1T and the drift length 150mm whereas the gain was set to 27 mV/fC.

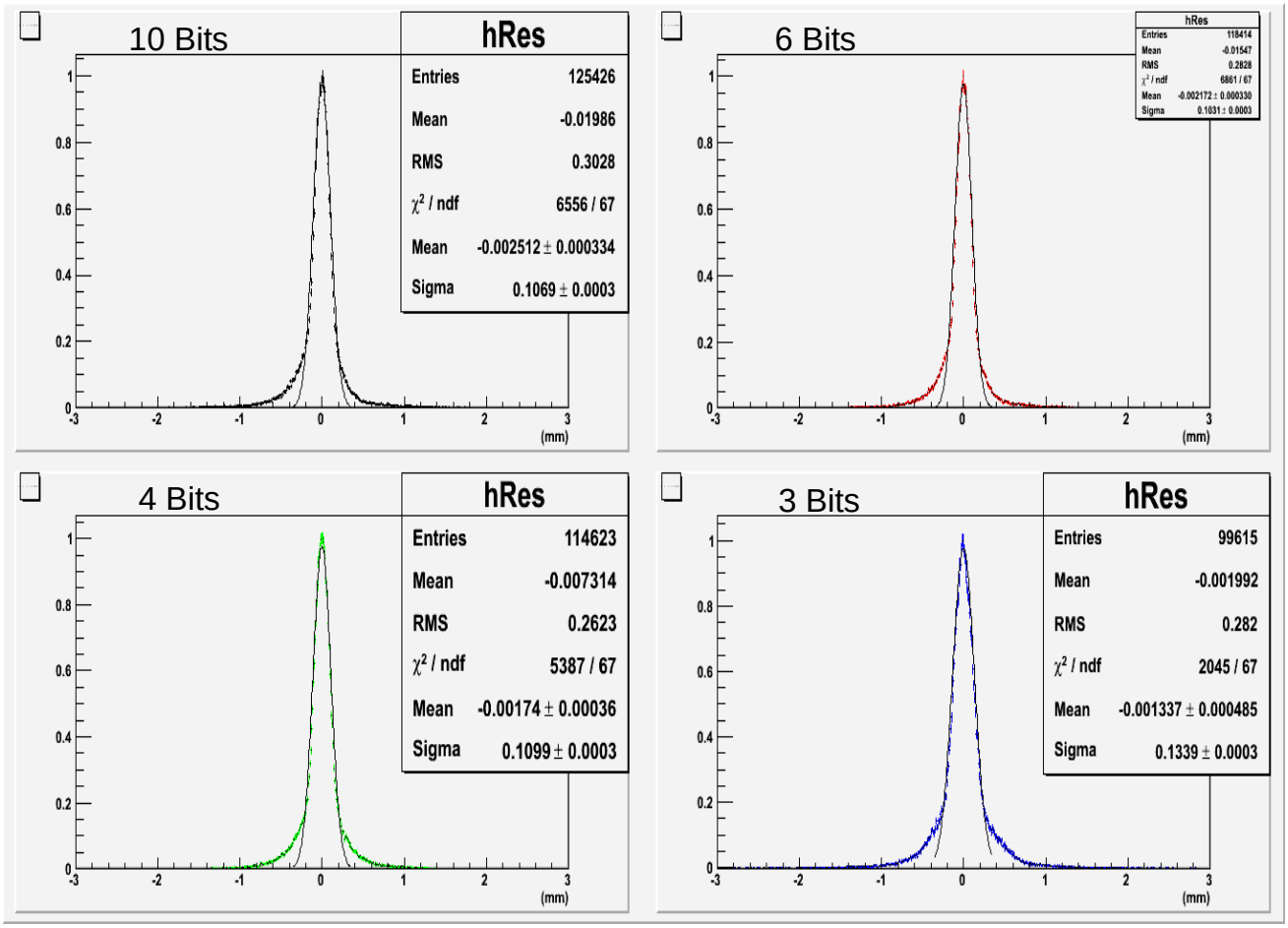

Figure 36: The residual distribution of run 7399, with a drift length of 150mm, a gain of 12.5 mV/fC and a magnetic field of 1 T. The value of sigma indicate the resolution in mm.

A similar pattern is appearing in run 7399, the reduction in residual resolution is however apparent already after a reduction in the ADC resolution to 6-bit. The amplification of the both runs is the only parameter which is different, so it is possible that the amplification plays an intricate role in how prominent the effect on the residual resolution that the reduced ADC resolution has.

10.4 Residual distribution depending on the number of pads used in a cluster

The electric noise can have a large effect on pads with low ADC values. For this reason it might be beneficial only to include a given number of pads, limiting the number of low signal pads included in the analysis. By modifying the cluster script to allow for only a given number of pads, symmetrically chosen around the pad with highest charge to be included in each cluster, this can be tested.

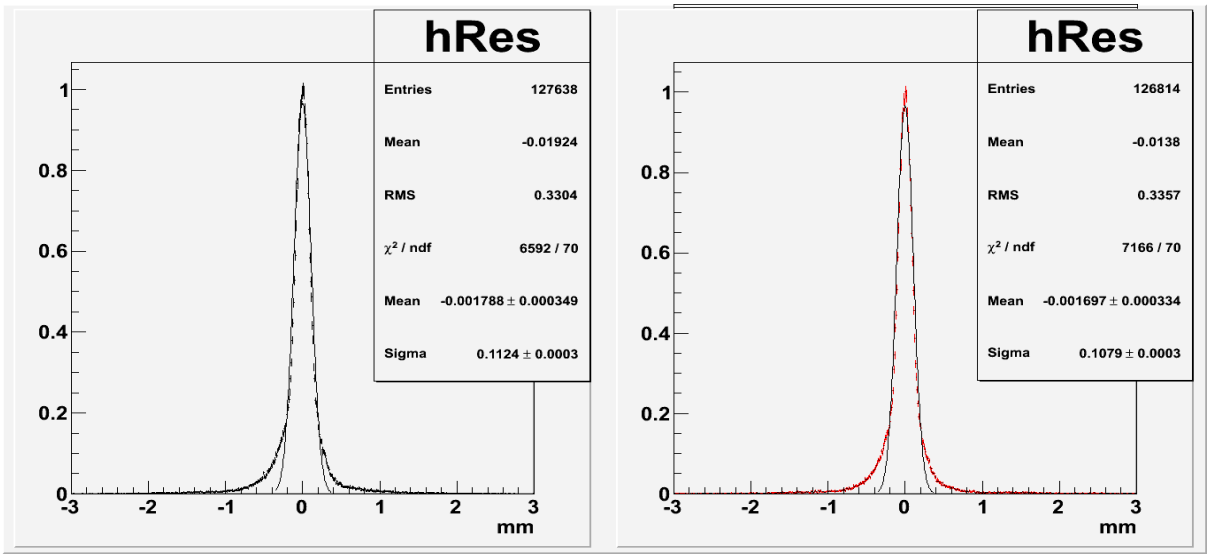

Figure 37: The residual distribution of a normal analysis compared to the same run but when only 3 pads per cluster were used. These measurements were performed with a drift length of 150mm, a magnetic field of 1 T and a gain of 27 mV/fC.

As can be seen in the above figure the spatial resolution is largely unaffected by the limitation of only using the three central pads in each cluster. In this run the resolution of the three pad limited fitting is slightly better than when all the pads are used in the fitting. This is however most likely due to statistical fluctuations but the fact that the outermost pads are neglected can help since it is possible that the relative uncertainty of the actual charge in a pad with low charge is higher due to a worse signal to noise ratio. While setting the limitation of only using three pads in each cluster might reduce the data to some degree the most useful aspect of these results is that by using only three pads in each cluster it will be made easier to differentiate between two close tracks.

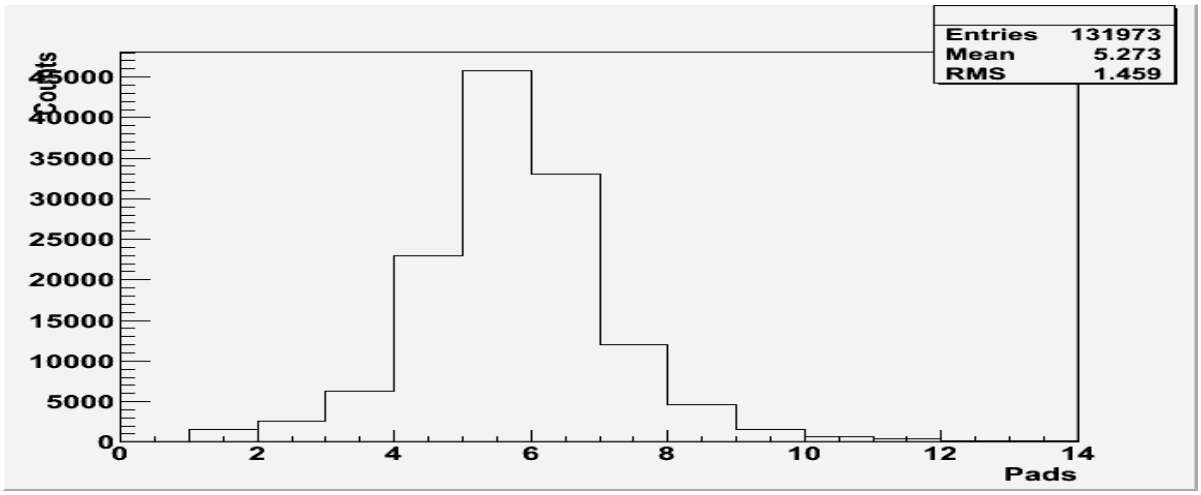

Figure 38: The number of clusters containing a certain number of pads. This measurement was with a drift length of 150mm, a magnetic field of 1 T and a gain of 27 mV/fC.

10.5 The residual distribution depending on sampling frequency

It is also possible to reduce the amount of data by reducing the sampling frequency of the ALTRO chip. The normal sampling frequency is 20 MHz and if a sampling frequency of 10 MHz can be used instead then the volume of data would be halved. This in turn would lead to further benefits such as a reduction in power consumption and thus need for less cooling needed for the system. A reduced sampling rate was constructed by disregarding every second sample.

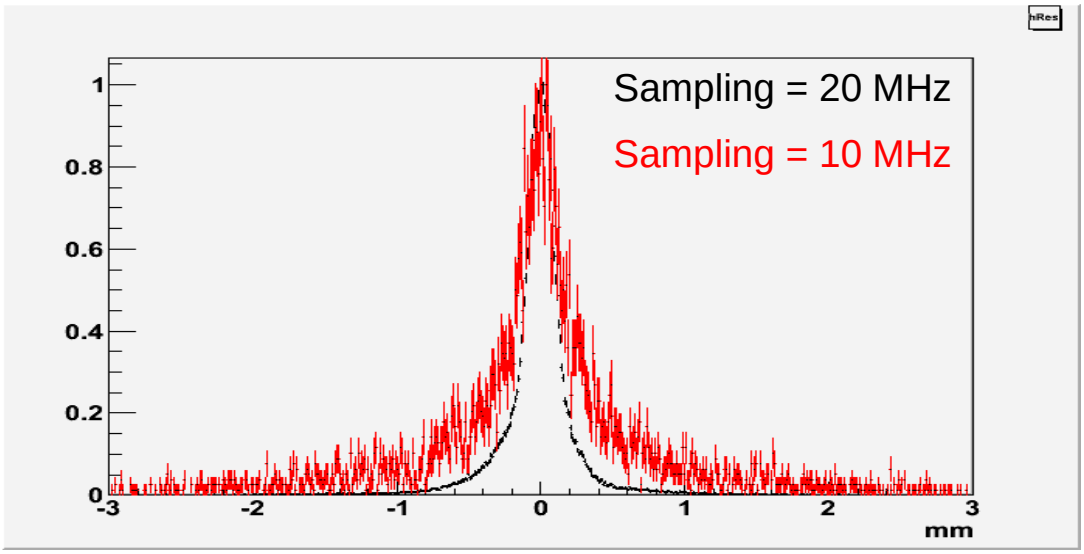

Figure 39: The residual distribution for a sampling frequency of 20 MHz (black) and 10 MHz (Red) with a pulse rise time of 120 ns, a drift length of 150mm,gain of 27 mV/fC, and a magnetic field of 1 T.

The resolution is severely hampered for a pulse with a rise time of 120 ns. With a sampling frequency that barely matches the peaking time of the pulse it is evident that half the number of samples drastically reduces the spatial resolution. If the peaking time is only measured by one sample instead of two or three samples it becomes impossible to accurately deduct any information from the pulse and thus the resolution becomes much worse. The jagged shape of the 10 MHz curve is due to the fact that many tracks are missed due to the low number of clusters which leads to a situation with less than desired statistics, the number of good clusters are in the area of a few thousands whereas the run analyzed with a sampling frequency of 20 MHz usually has more than 100 000 good clusters, 127638 in this case.

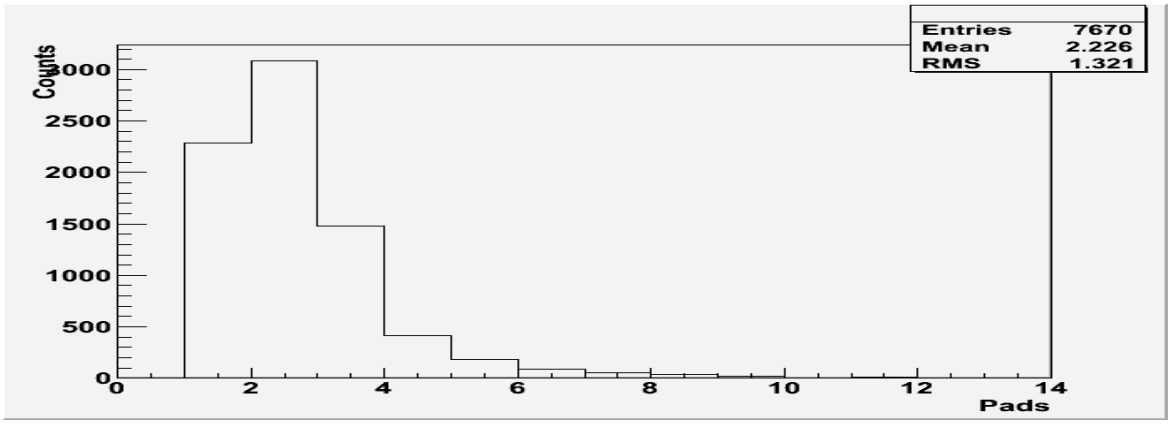

Figure 40: The number of clusters containing a certain number of pads in the case with a 10 MHz sampling frequency. This measurement was with a drift length of 150mm and a magnetic field of 1 T.

One can see that by comparing **figure 40** to **figure 38**, not only do we have a larger fraction of one pad clusters for which the residual resolution is limited by the pad size, even more importantly we have lost a huge number of clusters, 131973 clusters with the 20 MHz sampling rate compared to 7670 clusters with a 10 MHz sampling rate.

One could think of using a shaping time longer than 120ns and a sampling rate of 10 MHz. This will however lead to a worse resolution in *z as* has been shown by M. Ljunggren [17].

10.6 The residual distribution depending on pad threshold

The threshold for which a pad value is accepted can affect the resolution in two ways; if the threshold is too low then noise may spoil the resolution, if on the other hand the threshold is set too high then the resolution may be hampered since fewer pad values contribute. The ALTRO provides a zero suppression function which is used to set a threshold value for when a pad value is used as a pulse. If there are two consecutive pad values above the threshold value then it will be declared as a pulse.

There were no runs performed without the ALTROs' zero suppression active and as such new measurements must be performed to determine how a removal of the zero suppression will affect the resolution of the LCTPC but by using runs with the lowest set value of the zero suppression it is possible to determine whether or not a higher threshold yields a better resolution.

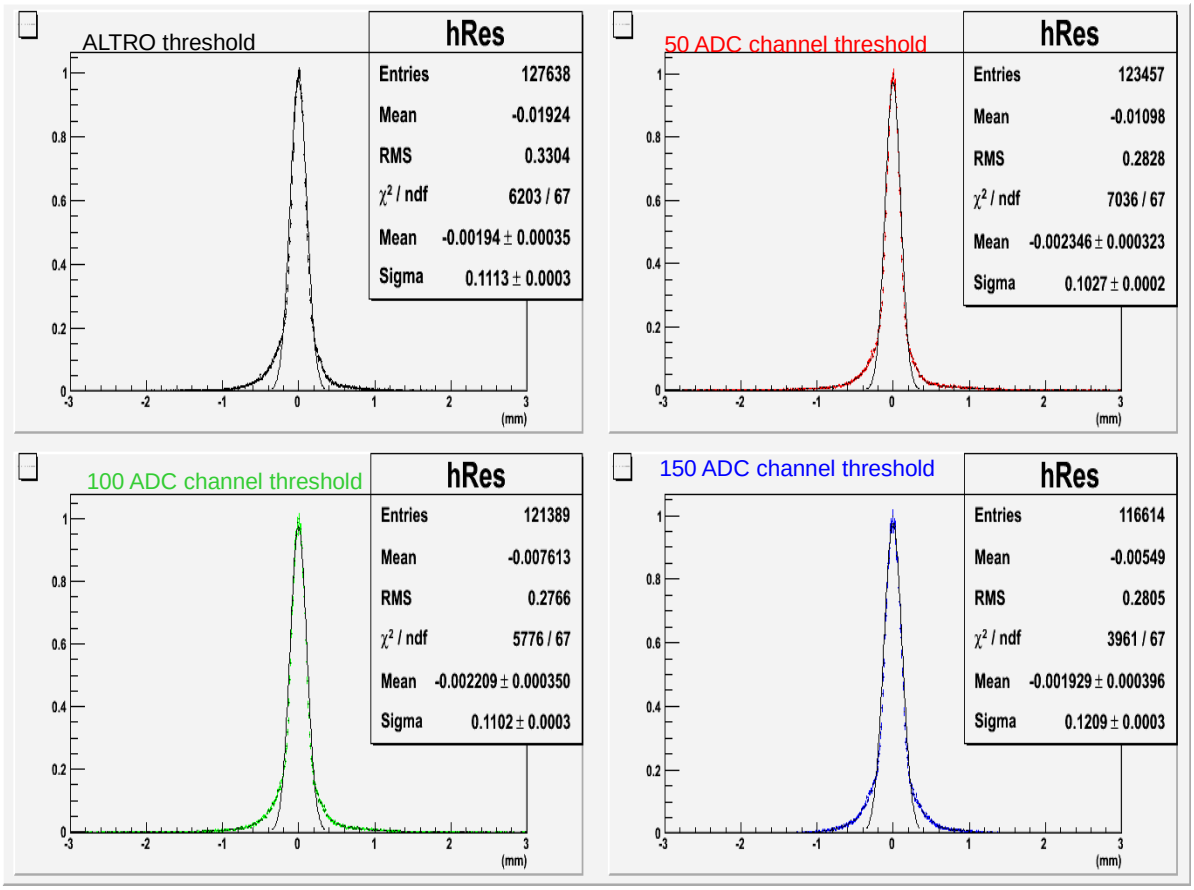

Figure 41:Residual distribution depending on the threshold set for the pads for run 7415 with a B-field of 1 T and a drift length of 150mm. The gain of the PCA16 was 27mV/fC.

A slight increase in resolution is achieved while increasing the ADC threshold to 100 but the most noticeable change of the residual distribution appears to be at a threshold value of 50 ADC channels. This suggests that there is a nonlinear dependence between the residual distribution and the threshold value of the ADC values. While the effects are relatively small there certainly appear to be a trend.

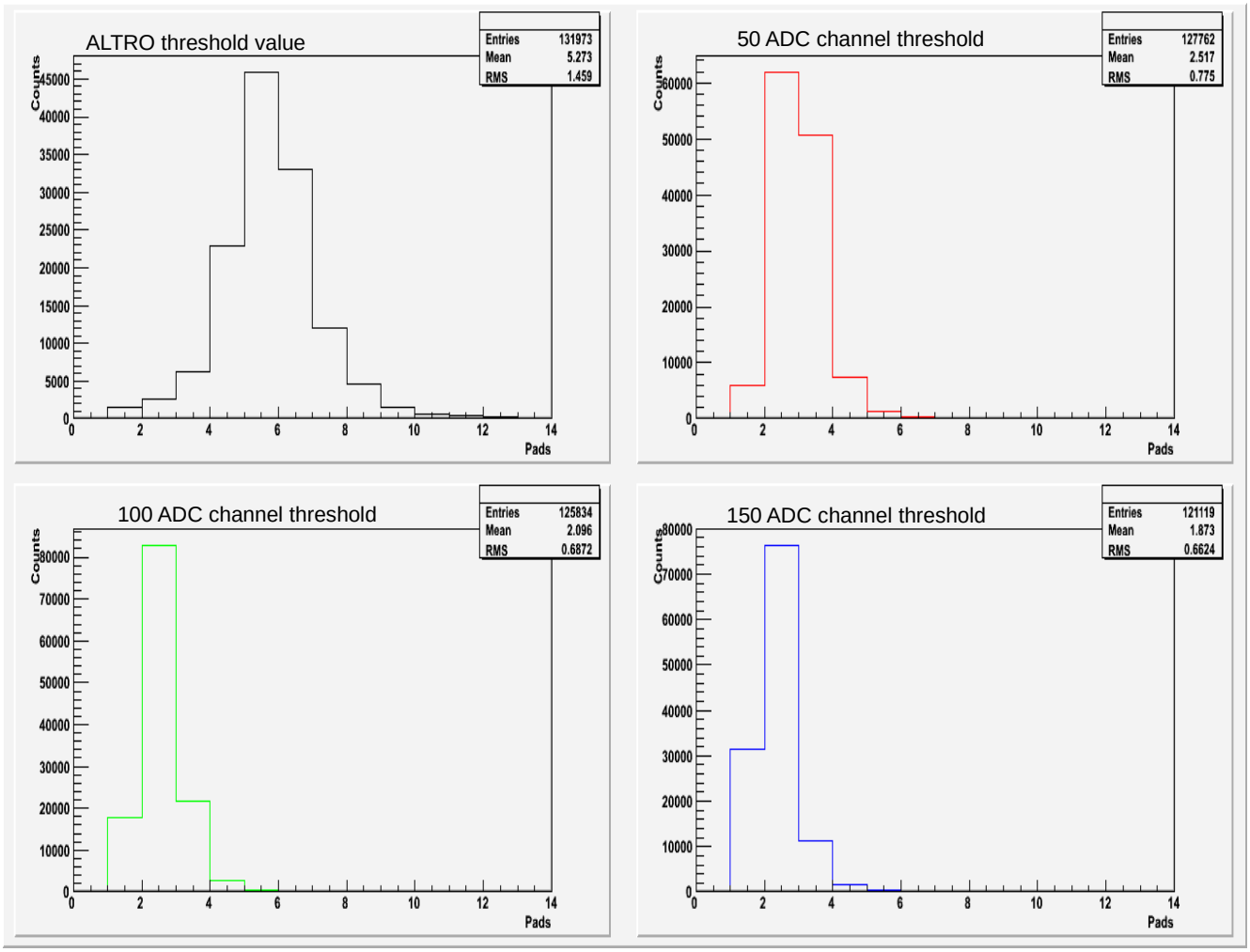

Figure 43: The number of clusters containing a certain number of pads. This measurement was with a gain of 27mv/fC, a drift length of 150mm and a magnetic field of 1 T

Here it is apparent that a lot of pads with very low ADC values are lost by increasing the ADC value threshold. While increasing it too much will create lots of one pad clusters which will give a poor residual resolution, having many pads with low ADC values contributing to the clusters is apparently not wanted either. An optimal value of the ADC threshold should be found in order to obtain the best residual resolution.

The difference between the number of entries in **figure 41** and **42**, arises due to the fact that the residual fitting is done after the tracking algorithm is performed whereas the number of pads in each cluster is found after the clustering algorithm is performed. The residual fitting disregards tracks that contain less than 15 clusters and these clusters make the difference.

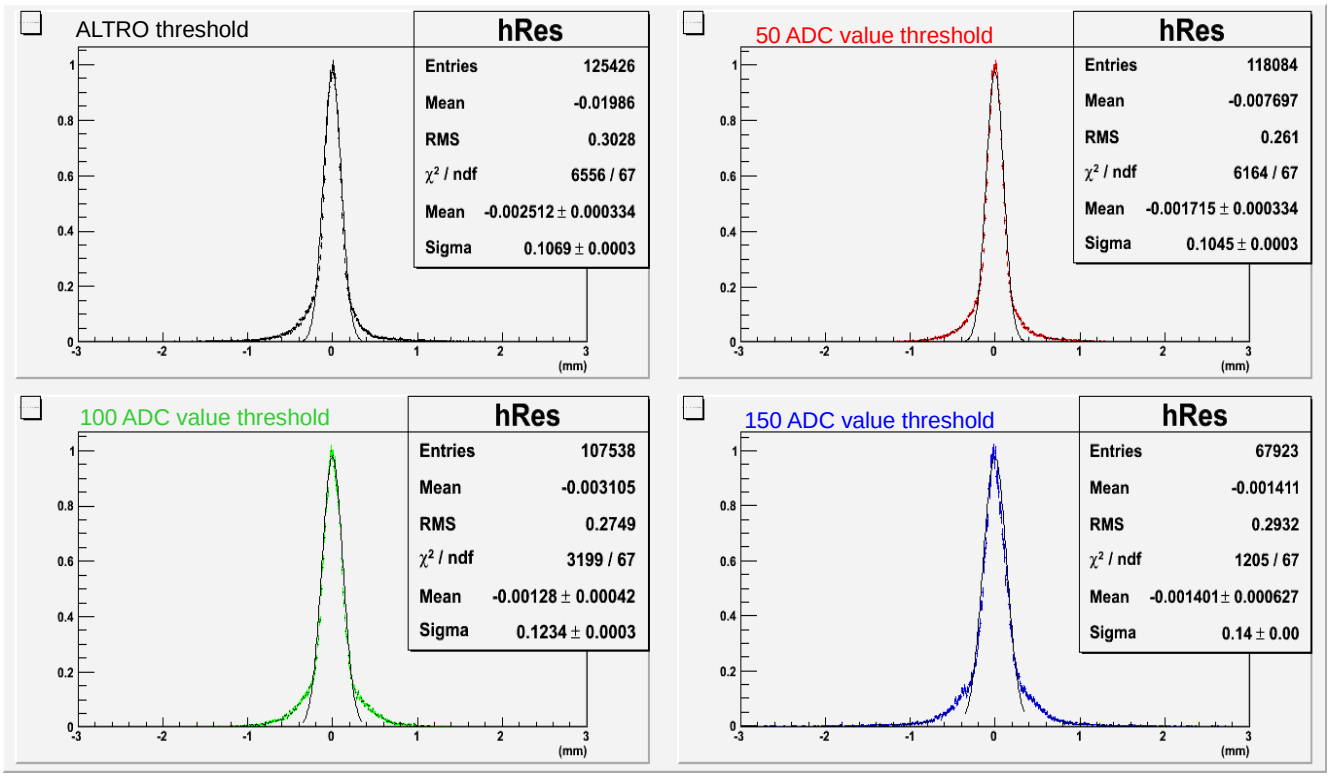

Figure 44:Residual distribution depending on the threshold set for the pads for run 7399 with a B-field of 1 T and a drift length of 150mm. The gain of the PCA16 was 12mV/fC.

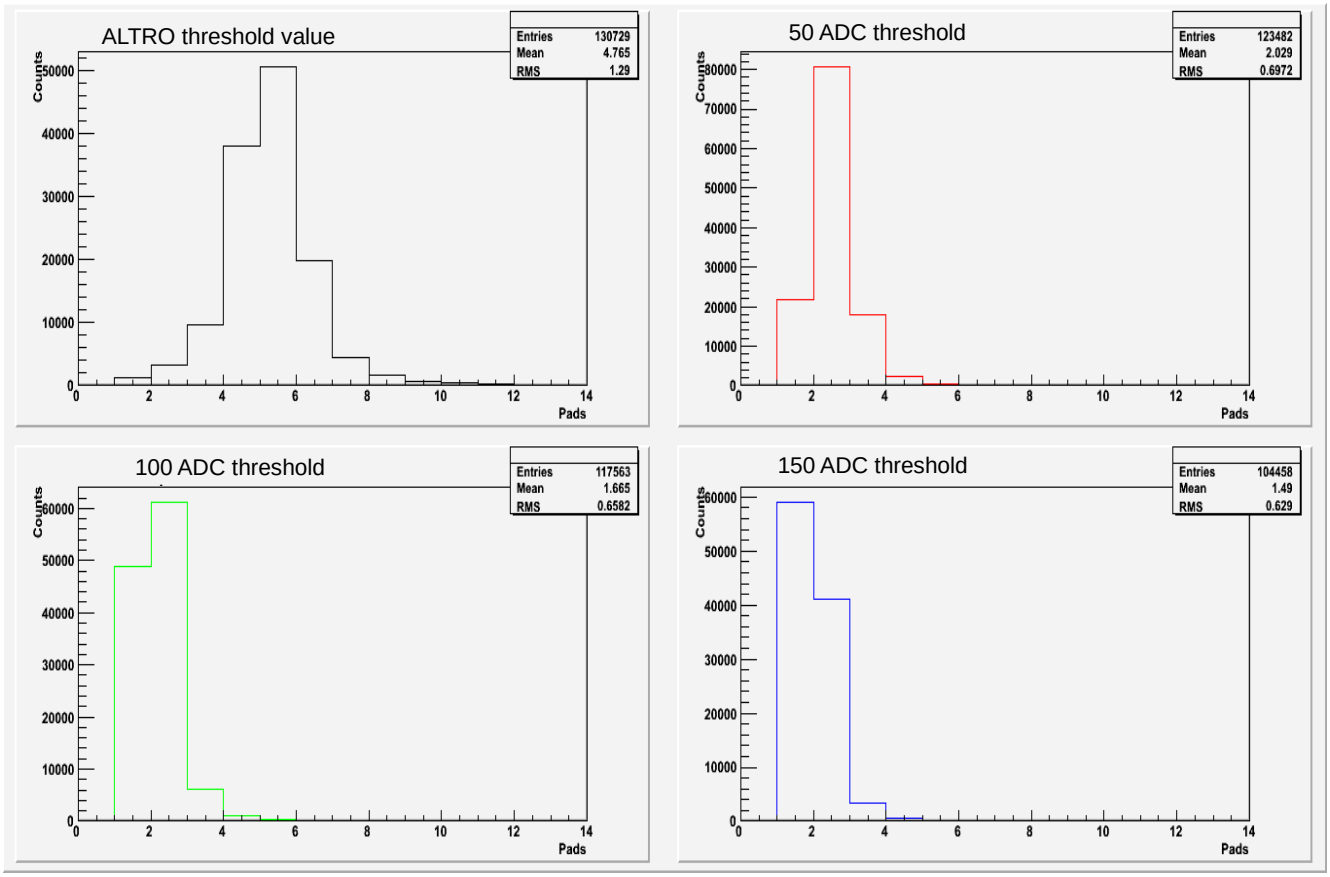

Figure 45: The number of clusters containing a certain number of pads. This measurement was with a gain of 12mv/fC, a drift length of 150mm and a magnetic field of 1 T.

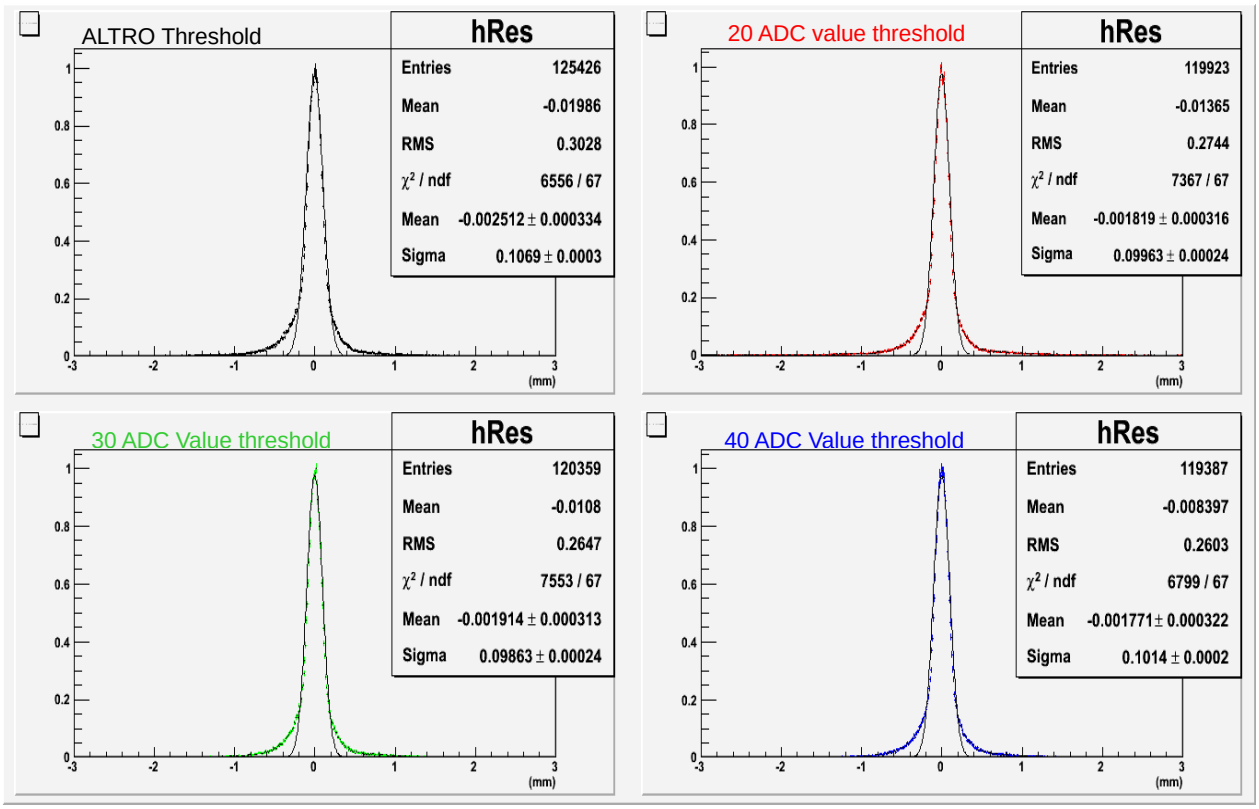

Figure 46: Residual distribution depending on the threshold set for the pads for run 7399 with a B-field of 1 T and a drift length of 150mm. The gain of the PCA16 was 12mV/fC.

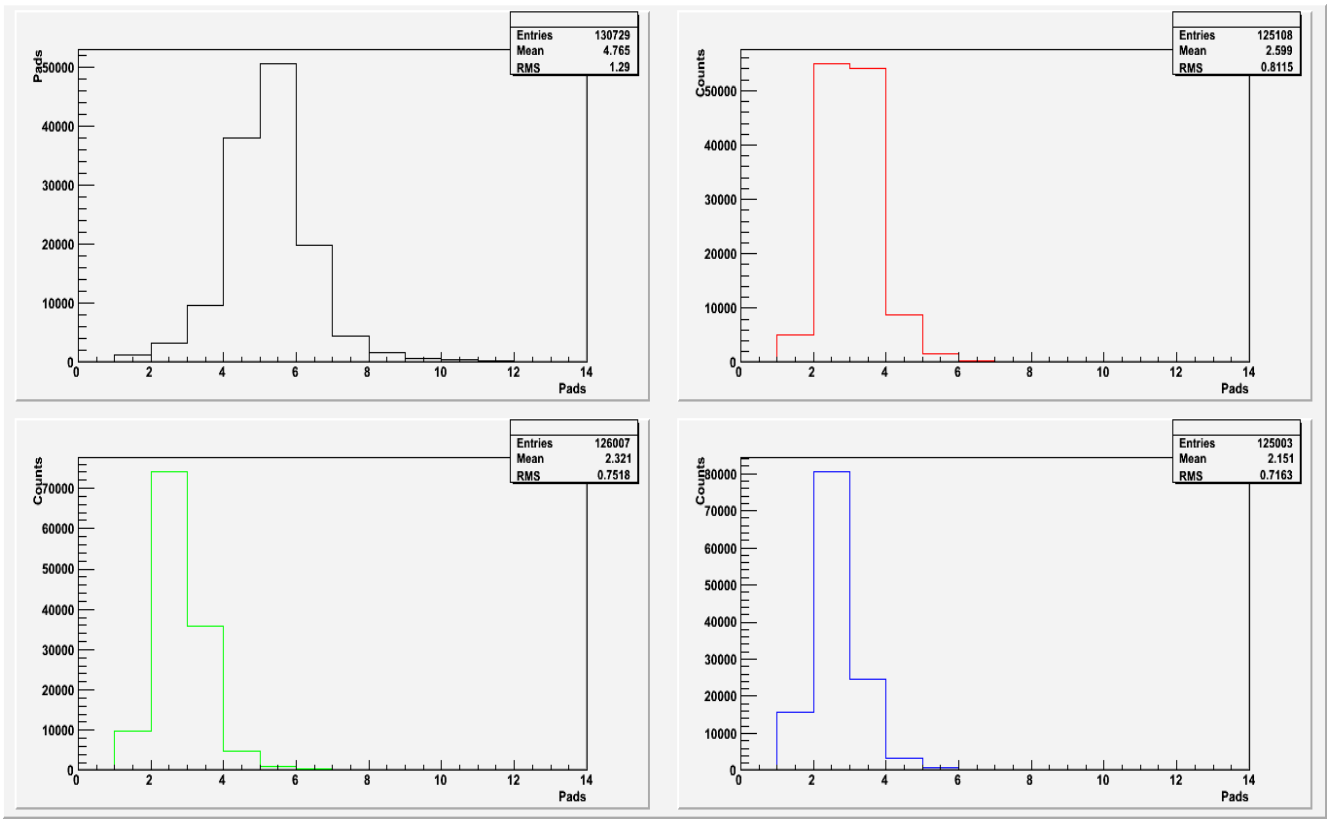

Figure 47: The number of clusters containing a certain number of pads. This measurement was with a gain of 12mv/fC, a drift length of 150mm and a magnetic field of 1 T.

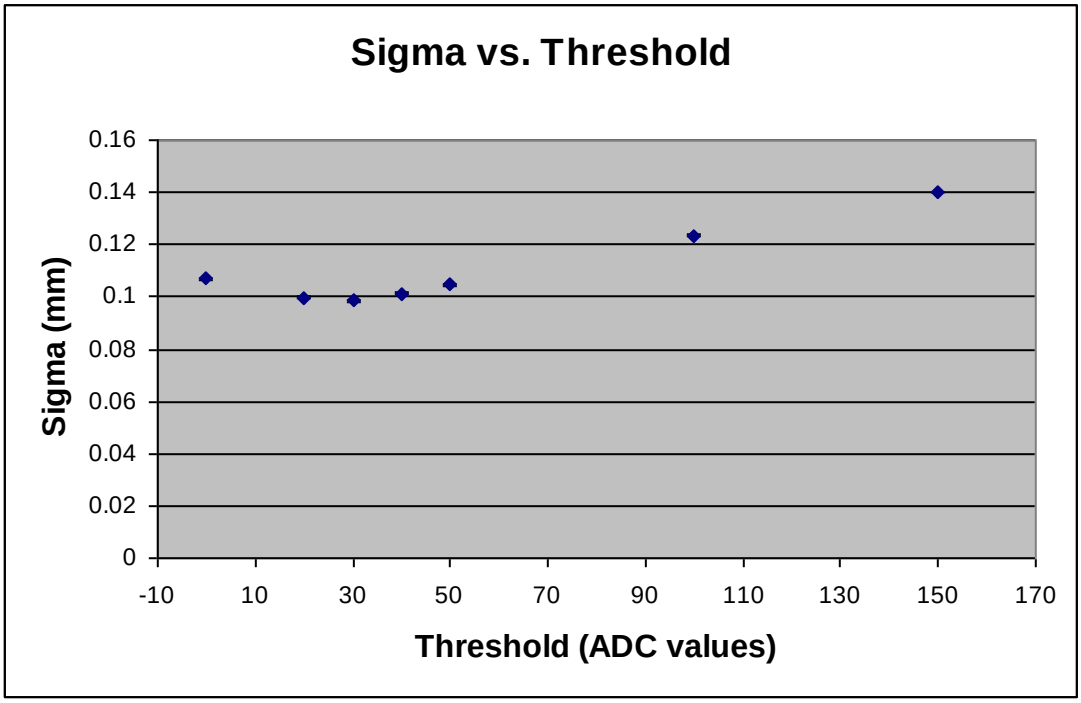

Figure 48: The residual distribution of a run with the gain of the PCA16 set to 12mV/fC as a function of the ADC threshold.

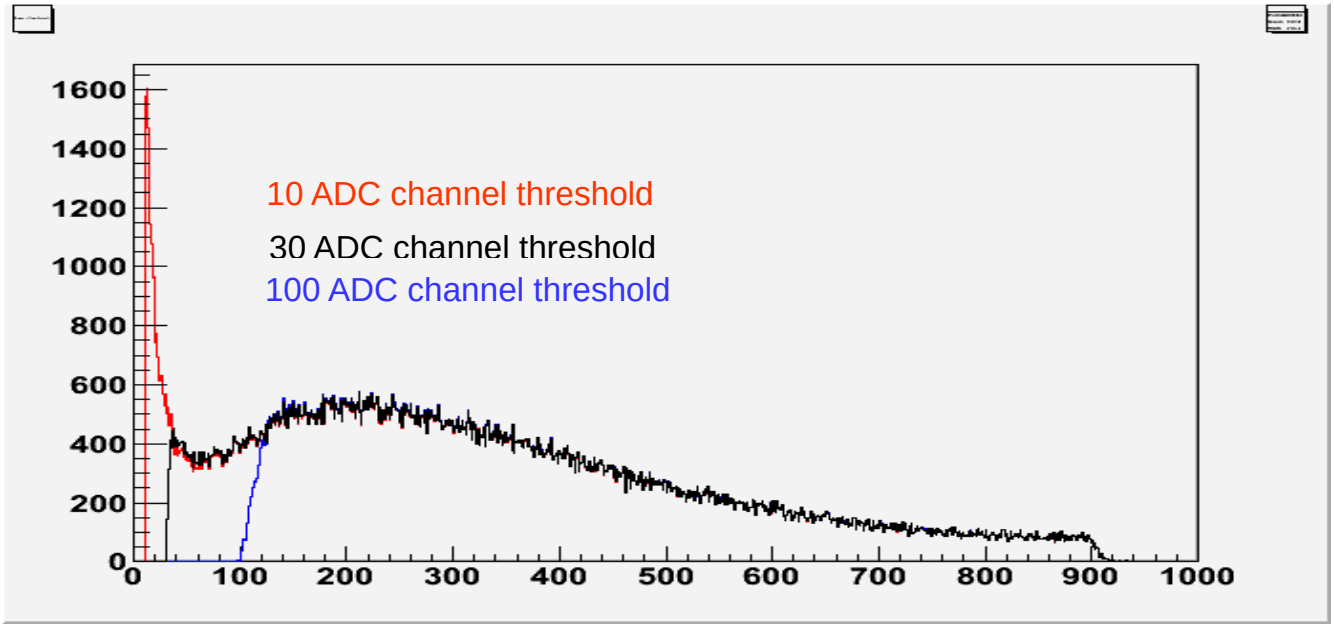

Figure 49: The max sample in each pad for run for run 7399 with a B-field of 1 T and a drift length of 150mm. The gain of the PCA16 was 12mV/fC.

There appears to be a large number of pads with a low charge. These pads will widen the residual distribution of a run if they are included since they are very likely be affected by noise or some other effect. Removing values that belong to the rise of the Landau distribution will in turn also decrease the residual distribution of a run. Possibly the most important aspect is that the optimal residual distribution is not achieved by using the local minima between ADC values 30 and 100 as one could have suspected. It is likely that this is due to the fact that a lot of "real" data is removed as well. An

optimal residual distribution is likely to depend on the amount of noise and the amplification of the PCA16. With a higher maximum of the Landau distribution a higher threshold value can be chosen.

10.7 The dE/dx resolution depending on number of ADC bits

While the spatial resolution of the TPC is important for the momentum measurment it is only one of the properties used to determine which particles that are detected. The energy loss of the particle is obtained by determining the charge released in the gas by a whole track. As previously mentioned in chapter 4.3.3 the truncated mean is used to determine the *dE/dx* value of a track.

By limiting the ADC resolution just as in **10.2** the *dE/dx* resolution has been tested for various different values of ADC bits.

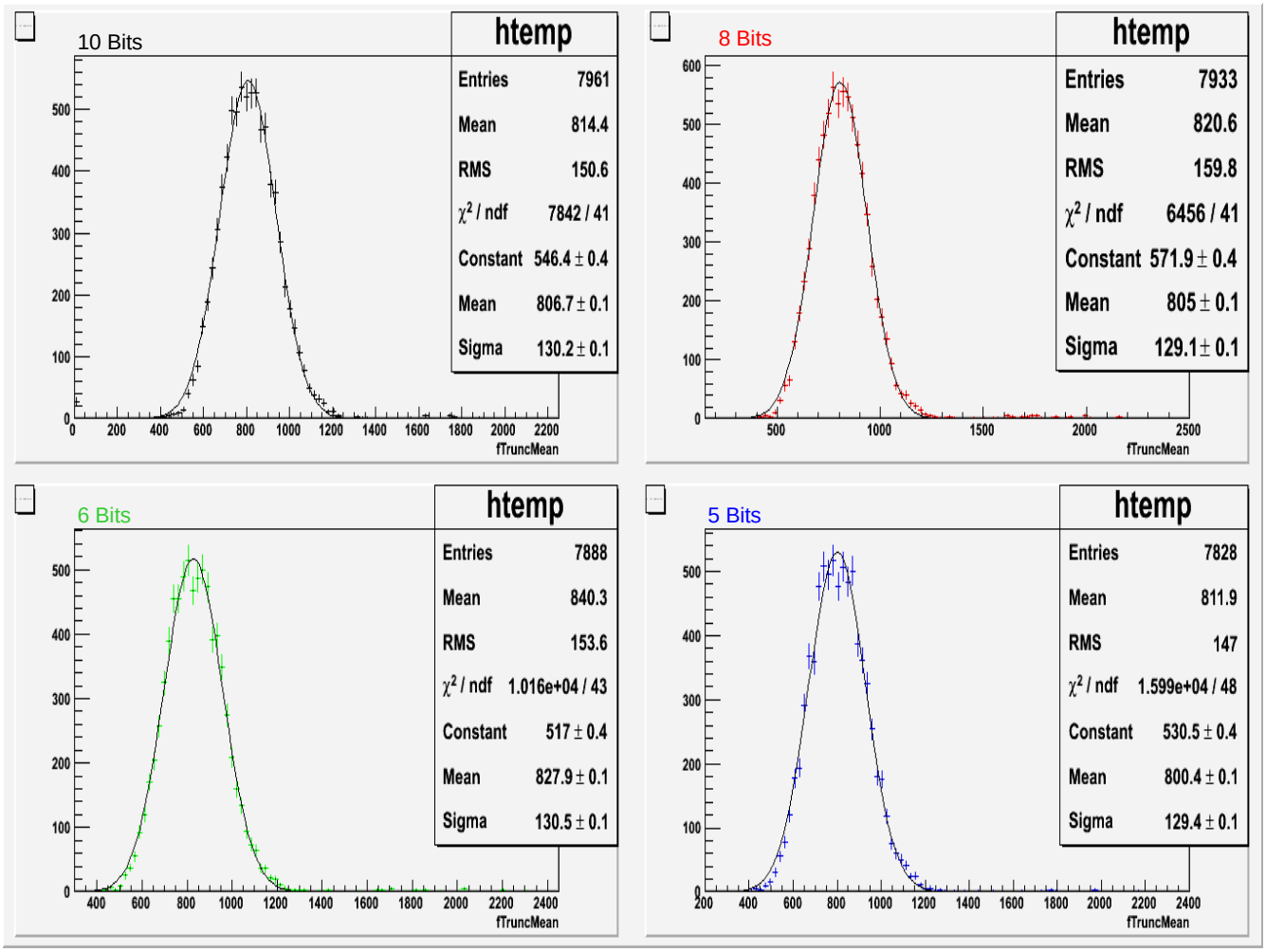

Figure 50: The truncated mean of run 7415 with various ADC resolutions, a B-field of 1 T and a drift length of 150mm.

Just like with the residual distribution it appears as if a reduction in ADC resolution has a minimal effect on the *dE/dx* resolution. The resolution is nearly constant from 10 ADC bits resolution down to 5 ADC bits resolution. The mean value of the *dE/dx* remains fairly constant and that is also a good indication that despite the fact that a few tracks, noted as entries in **figure 50** have disappeared it does not appear to affect the general performance of the TPC.

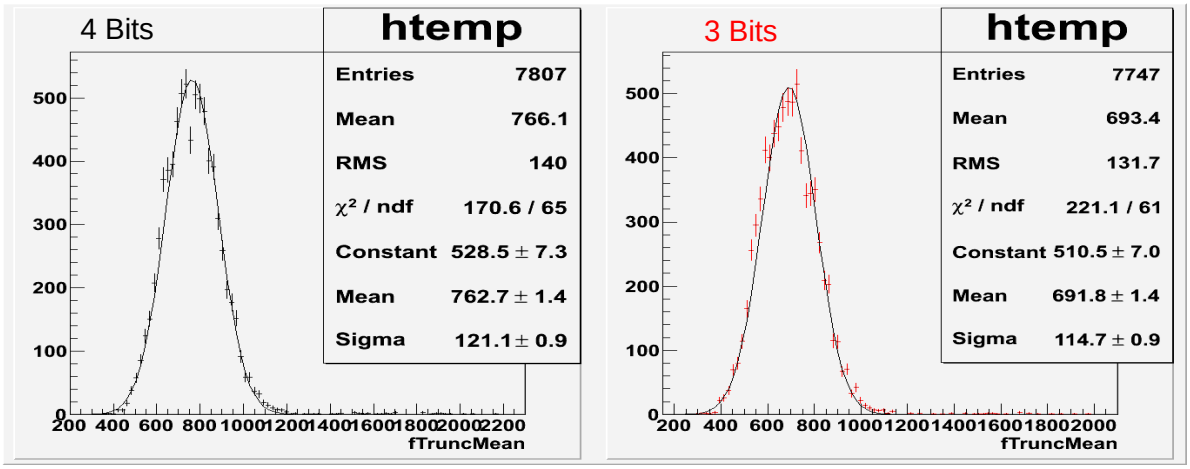

Figure 51: The truncated mean of run 7415 with various ADC resolutions, a B-field of 1 T and a drift length of 150mm.

A further reduction of the ADC resolution down to 4 bits appears to affect the resolution somewhat. Here the mean value of the truncated mean starts to steadily decrease and the *dE/dx* resolution starts to decrease as well. It would appear as if the *dE/dx* is becoming quite unreliable with only an ADC resolution of 4 bits and below. With a 2 bit resolution there are only 4 discrete values of energy which can be assigned to each pad. This leads to situations where certain *dE/dx* values are nigh impossible to reach and as such the distribution of *dE/dx* values behave almost in a stochastically manner making the measurements useless.

10.8 The dE/dx resolution depending on truncation limit

The truncation limit is most often set to 60%, that is, the 40% highest *dE/dx* values are discarded when the average *dE/dx* is calculated. This might seem as quite a low limit and as such it is important to know that it is not set too low so that many important samples are discarded. The limit comes from TPCs with substantially larger pad sizes and thus it is of interest to determine whether the same truncation limit is also optimal for this pad size. It is also valuable to know whether or not the resolution will increase if some of the lowest values are discarded as well.

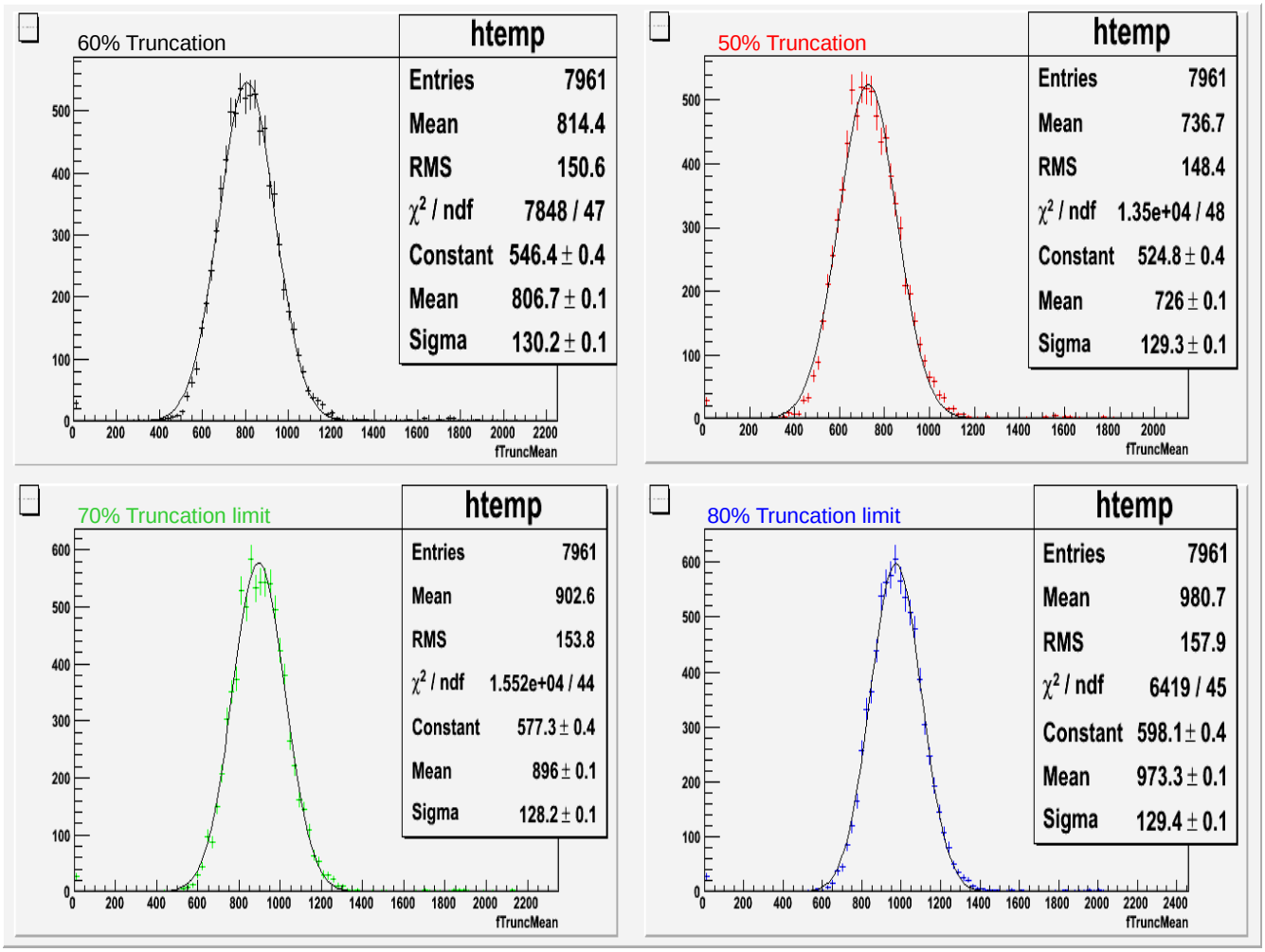

Figure 52: The truncated mean of run 7415 with various truncation limits, a 1 T B-field and a drift length of 150 mm.

While the *dE/dx* resolution remains largely unaffected and the shape of the curve remains Gaussian for all truncation limits it appears as if the 80% truncation limit is slightly better than the lower truncation limits.

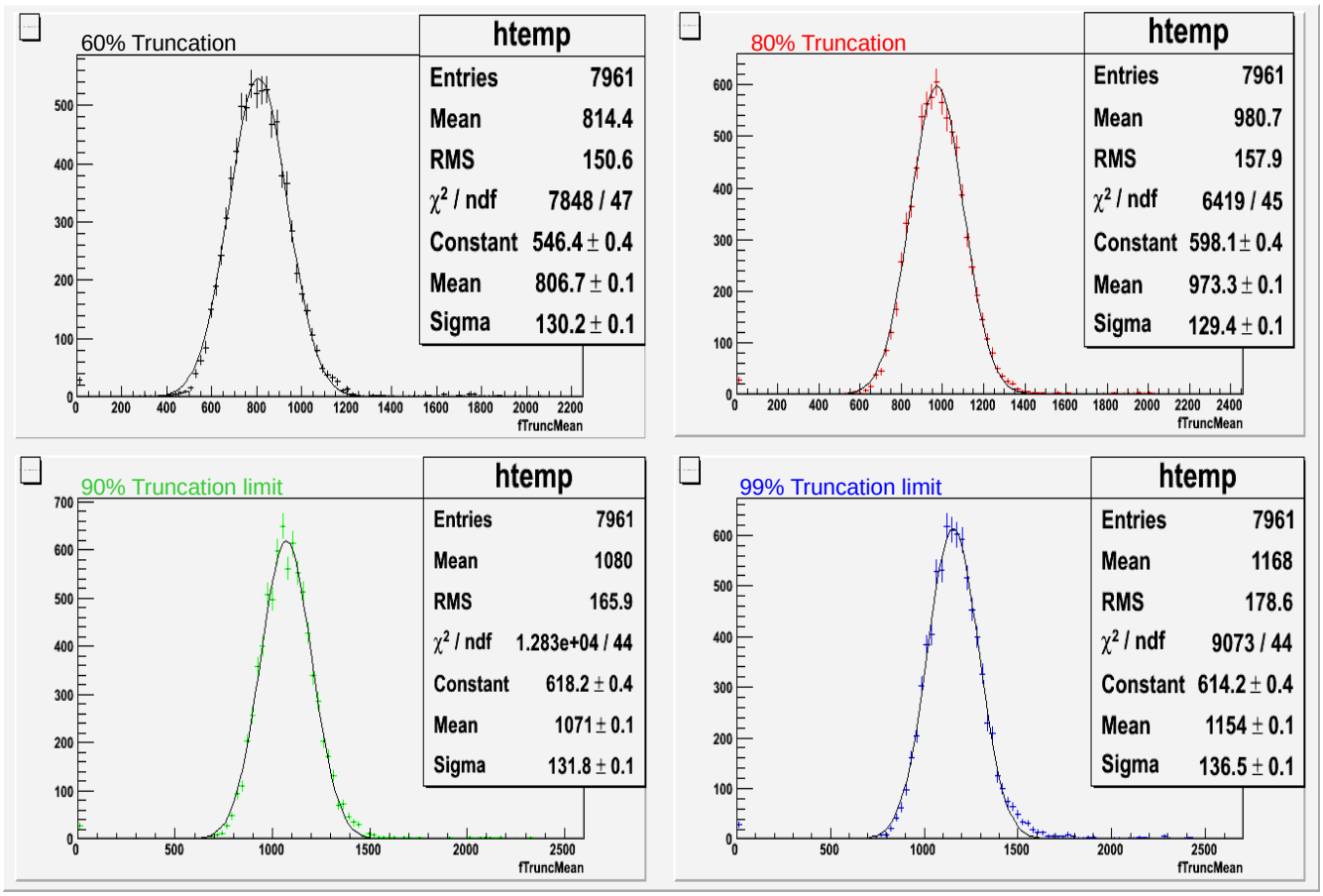

Figure 53: The truncated mean of run 7415 with various truncation limits, a 1 T B-field and a drift length of 150 mm.

In **figure 53** it appears as if the overall performance is still adequate but in the cases of a 90% and to an even greater extent the 99% case a bias towards higher values are noticeable. While the higher *dE/dx* values appear to leave the Gaussian fit largely unaffected or even better it is apparent that the *dE/dx* values around 1500 fits are poorly described by the Gaussian fit.

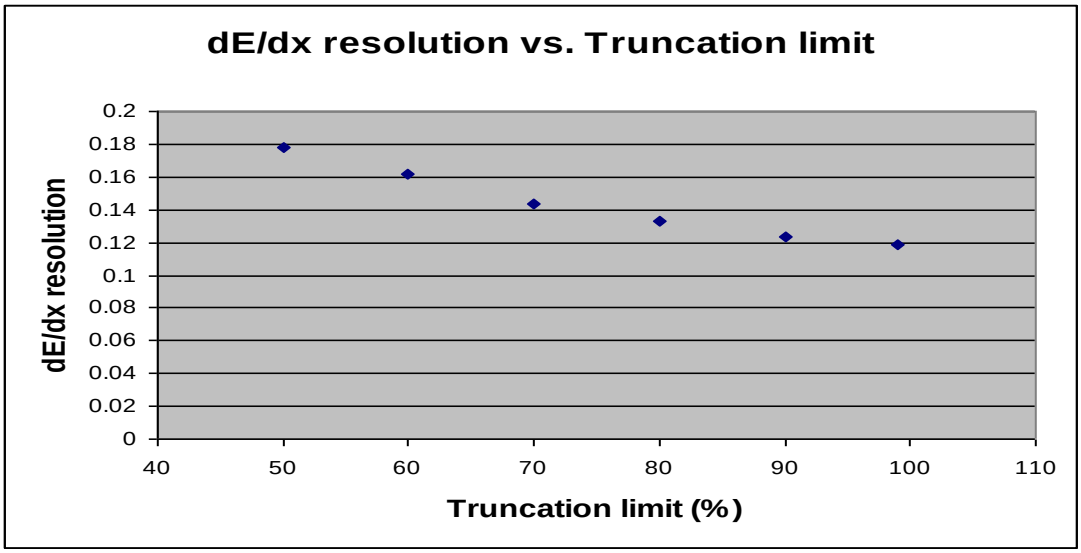

Figure 54: The dE/dx resolution with respect to the truncation limit. The magnetic field was 1T, the drift length 1T and the gain 27 mV/fC.

11 Summary

A novel technique which can possibly be used for signal amplification in a future ILD TPC has been tested. The technique called GEM produces the avalanche effect. The readout electronics have also been tested in order to try to determine the optimal cost vs. resolution setup.

The measurements were performed in both 2009 and 2010 at DESY 2. During the 2009 measurements the prototype TPC suffered from distortions to the E-field caused by the exposure of a support structure for a non-present GEM which made the information obtained from the outermost pad rows distorted. In the 2010 measurements this was supposed to be mitigated by a newly installed field shaper. However, the erroneous calculations, and subsequent settings, of the field shaper further increased the distortions. For that reason 2009 data was used for the vast majority of analysis in this thesis.

During the 2009 and 2010 measurements there were cases of gain drops in every studied run. Data taken during these gain drops were removed before any further analysis of the data was performed.

The residual distribution in the bend plane was tested with varying ADC resolution. It was determined that a sufficiently good resolution can be obtained while decreasing the ADC resolution from 10 bits down to 6 bits without any apparent risk of reducing the resolution at all.

A modification to the clustering algorithm was performed. This was done in order to test if having a maximum of three pads included in the weighted mean would decrease the residual resolution. The result showed that the resolution remained unaffected with this restriction. This can be helpful when trying to distinguish between two close laying particle tracks.

The residual distribution with a 10 MHz sampling frequency was compared to the normal sampling frequency of 20 MHz at the longest shaping time of 120 ns. Here the resolution greatly deteriorated but most importantly the lowering of the sampling frequency caused massive amounts of clusters to be lost due to poor digitization of the pulse

An extra threshold and its effect on the residual distribution was also analyzed. This revealed that the maximum resolution was achieved with a threshold value of around 30 ADC channels; the exact value varying somewhat depending on the amplification used in the PCA16.

The *dE/dx* resolution was also tested with varying ADC resolution. The results were similar as for the case with residual distribution. A reduction of the ADC resolution down to 6 bits appears to be possible while still retaining an unaffected *dE/dx* resolution.

The truncation limit used in order to determine the average *dE/dx* was tested and compared to the conventional limit of 60%. It appears as if this limit can be increased to at least 80%. This is likely to be due to the fact that the pads used for read out are much smaller than conventional pads and as such, ionization of delta electrons will not deposit as much charge in each pad as it otherwise would.

Acknowledgments

First of all I would like to thank everyone at the division for Experimental Particle Physics for providing an excellent working atmosphere. In particular I would want to thank my supervisor Anders Oskarsson for his endless patience with me as well as his invaluable help with the execution of the thesis. I would also like to thank Leif Jönsson for taking care of me in Hamburg, as well as his input into this thesis.

Without the vast amounts of help with the programming that I received from both Philippe Gros and Martin Ljunggren none of this would have been possible. I would also like to thank Peter Christensen for his help with the programming and general ideas.

I would like to thank Ulf Mjörnmark for his help and company in Hamburg as well as his help with various computer related issues in Lund.

References:

[1] S.F Novaes "*Standard Model:An Introduction" 2000* http://arxiv.org/abs/hep-ph/0001283v1

[2] Demina, R. "*Measurement of the forward-backward charge asymmetry in top quark production in collisions at 1.96TeV* Presented at Europhysics Conference on High-Energy" Physics 2011

[3] Accelerator Technique Edition 2.5 (Sverker Werin)

[4] http://public.web.cern.ch/public/en/research/AccelComplex-en.html

[5] *INTERNATIONAL LINEAR COLLIDER REFERENCE DESIGN REPORT 2007 Vol 3*

[6] http://www.adams-institute.ac.uk/l4a/laserwire.html

[7] *"ALICE technical design report of the Time Projection Chamber"*

[8] W.R Leo "*Techniques for Nuclear and Particle physics Experiments"*

[9] Vincent Lepeltier *"Review on TPCs:* 3rd Symposium on large TPCs for low energy rare event detection."

[10] http://www.phenix.bnl.gov/WWW/tracking/dc/experts/dr_vel.gif

[11] *INTERNATIONAL LINEAR COLLIDER REFERENCE DESIGN REPORT 2007 Vol 4*

[12] ILD Concept Group – *The International Large Detector, letter of intent*

[13] A. Oskarsson et.al. *"A General Purpose Electronic readout system for tests of Time Projections Chambers, equipped with different avalanche multiplication systems." 2008*

[14] Leif Jönsson, Ulf Mjörnmark. "*Front-End electronics and the Data Acquisition for the LCTPC*." *2008*

[15] R.Esteve et al. "*The ALTRO Chip: A 16-channel A/D converter and Digital Processor for Gas Detectors"* 2003

[16] L. Hallermann and P. Schade, *In the Proceedings of 2007 International Linear Collider Workshop*
(LCWS07 and ILC07), Hamburg, Germany, 30 May - 3 Jun 2007, pp TRK29.

[17] M. Ljunggren *High Momentum Resolution in a Linear Collider Experiment; Test results from a Prototype TPC" 2011*

[18] P. Christiansen et al. *"Particle tracking and energy loss measurements with the LCTPC:A comparison to simulation models"2010*

[19] K. Ackermann et al., *Nucl. Instrum. Meth. A 623, 141 (2010) [arXiv:0905.2655 [physics.ins-det]]*

Appendix A

A.1 Data Format

In the data format stage two operations are performed, the cluster labeling and the data packing. The cluster labeling, which assigns each cluster with a time stamp and its size, is done so that it is possible to reconstruct the acquisition afterwards. The information in the time stamp is found from the time stamp last sample in the pulse and the size is determined by how many 10-bit words the pulse contains. These words include the words for the time stamp and data samples. The data packing is done in order to make sure that the recorded data has the same format as the read out bus, which is 40-bit wide. As such it might be necessary to add additional information to the recorded data in order to provide a 40-bit word, this is called stuffing. After all 40-bit words have been constructed from an event another 40-bit word is added, a so called trailer word. This is done to enable unpacking of the 10-bit words and it contains all the necessary information such as the total number of 10-bit words as well as the address of the chip as well as the channel which recorded the signal [15].

A.2 Multi Event Memory

The memory of the ALTRO chip can be partitioned in two different ways, either with four buffers or with eight. With four buffers it can store four complete 1000 sample events with non-zero suppressed data. In order to use eight buffers it can not store more than 511 acquisition samples. The writing of the memory fills a 40 bit word per four sampling clock cycles. The major reason for this is the previously mentioned conversion from 10-bit words into 40-bit words done in the previous stage. However, the readout is performed at a four times higher pace. For this reason a central memory manager handles the storing and readout of the memories. In order to reduce the noise as well as the dead time of the circuit it is designed in such a way as all of the buses should be inactive during acquisition time and as such no readout is done during an acquisition event but it will resumed instantly after the acquisition has ended and when all of the buffers are filled a full signal is generated and any further triggers are ignored. The ALTRO chip also contains a trigger manager which generates a temporal window during which time data can be recorded [15].

A.3 Protection of Finite Machines from Single Event Upsets

Electromagnetic radiation as well as ions and electrons can impact onto or close to an electronic device and deposit a relatively large amount of energy into the material. This can cause ionization of the material which leads to a situation with lots of free charge surrounding the electronic device. If this happens near or in a crucial logical component this can cause a change of state in the component. The change of state can cause various errors, the severity of the error which depends on what logical circuit that is affected, can cause anything from faulty readout of a single event up to such severe situation as one where the state of the memory allocation is switched thus voiding whole acquisition runs. Such events as mentioned are, with a common name, called Single Event Upsets (SEU) and it might be important to take the necessary precautions to avoid or correct such events, especially if it is deemed that they will be frequent [15].

A possible control mechanism that can be used to correct the data from these SEUs is called Hamming encoding. With the use of Hamming encoding errors of up to two bits can be detected and one bit errors can be corrected. Hamming codes are class of linear binary codes that can be used for a data word with any length and it satisfies the following two relations

$$n = 2^r - 1 \quad (21) \qquad \text{and} \qquad k = 2^r - r - 1 \quad (22)$$

Where n is the block length or the maximum number of bits, k is the message length of the data word and r is the number of check bits and must have an integer value ≥ 2. It is important to remember that any positive integer can be represented with base 2 as shown in **Table 7**, which shows the representation for any positive integer up to 15 with base 2, this is the equivalent of 4 bits.

	$\mathbf{2^3}$	$\mathbf{2^2}$	$\mathbf{2^1}$	$\mathbf{2^0}$
1	0	0	0	1
2	0	0	1	0
3	0	0	1	1
4	0	1	0	0
5	0	1	0	1
6	0	1	1	0
7	0	1	1	1
8	1	0	0	0
9	1	0	0	1
10	1	0	1	0
11	1	0	1	1
12	1	1	0	0
13	1	1	0	1
14	1	1	1	0
15	1	1	1	1

Table 7: Shows the binary representation of the base 10 numbers 1-15

By using each bit position that is a power of two in the data word as a so called check bit it is possible to code the data word in such a way that it is also possible to determine the exact location of a faulty bit in the data word, if such an error would arise. Assuming a 10 bit data word is transferred one would then need 14 bits in total to accurately describe this data word using Hamming code. The number and position of the bits checked by the check bits are determined by the check bits position. The check bits always starts by checking itself and then the consecutive bits until the number of checked bits are equal to *r*, it skips *r* consecutive bits and so on until all the end of the data word, after all the bits have been checked the value assigned to the check bit is set to 1 if the parity is odd and 0 if it is even. Below is an example of how the 10 bit data word 1001001001 would be represented with Hamming code.

1	**2**	3	**4**	5	6	7	**8**	9	10
		1		0	0	1		0	0

Table 8: A representation of the data word 1001001001 with the check bits, in bold, unassigned.

Check bit 1 would be given the value: 1+0+1+0+1+0 = 1
Check bit 2 would be given the value: 1+0+1+0+1+1 = 0
Check bit 4 would be given the value: 0+0+1+0+0+1 = 0
Check bit 8 would be given the value: 0+0+1+0+0+1 = 0

1	**2**	3	**4**	5	6	7	**8**	9	10
1	**0**	1	**0**	0	0	1	**0**	0	0

Table 9: A representation of the data word 1001001001 with the check bits, in bold, calculated.

So the full 14 bit data word sent would be **10**1**0**001**0**001001. However, if the data word received was **10****0**001**0**001001 the check bits would return 0, 1, 0, 0 and a comparison between the check bits of the sent data word and the newly calculated check bits can be compared to uniquely determine the location of the switched bit.

	2^0	2^1	2^2	2^3
Sent check bits	1	0	0	0
Received check bits	0	1	0	0
Exclusive Or	1	1	0	0

Table 10: A correction matrix for a data word sent with Hamming encoding.

If the Exclusive Or (XOR) statement returns anything but 0 then a bit flip have occurred. By comparing the XOR statement to **Table 7** it is determined that the bit flip occurred in bit 3 and thus it can be corrected. While the use of Hamming encoding will increase the size of the data word the relative increase will vastly decrease as the data word increase in length. The 10 bit word mentioned above will give rise to a 40% increase in size, a 40 bit word on the other hand will only suffer a 15% increase and a 512 bit word will end up with less than a 2% increase.

A Hamming encoded circuit can be in three defined states, namely, coding state which is free from errors, derived state which contains errors but they are recoverable and invalid state where the error is detected but it can not be corrected.